TRANSIENT RESPONSE OF WIRE ANTENNAS AND SCATTERERS

by

Edward Paul Sayre

May, 1969

TECHNICAL REPORT TR-69-4

Approved by Dr. Roger Harrington
ELECTRICAL ENGINEERING DEPARTMENT
SYRACUSE UNIVERSITY
SYRACUSE, NEW YORK 13210

This work was supported in part by

NATIONAL SCIENCE FOUNDATION
under Grant Number GK-1233
and GK-4227

ABSTRACT

Direct time domain solutions for radiation from and scattering by thin conducting wires are considered. The problem is formulated in terms of two coupled integrodifferential equations obtained from the retarded potentials, the continuity equation, and the boundary conditions for the wire. Application of the method of moments reduces these equations to a set of simultaneous matrix equations in terms of currents, charges, and potentials. A time domain reciprocity theorem is developed which demonstrates the relationship between reciprocity and the adjoint operator for the problem.

Two moment solutions are presented for straight wires: (1) a point tested solution and (2) a pulse tested solution. The pulse tested solutions are extended to arbitrarily bent wires and applied to radiation and scattering by a conducting circular wire loop. The radiation field is found for both straight and curved wires by a direct application of the reciprocity theorem. All solutions are presented as algorithms suitable for digital computation. The algorithms are iterative by nature, and inexpensive in terms of computer time.

Illustrative computations are given for the straight wire antenna excited by a unit step voltage applied at an arbitrary driving point. Further results are presented for the straight wire scatterer excited by a plane wave with unit step time dependence. Similar results are presented for the loop as an antenna and a scatterer. In all cases, the wire may be loaded with arbitrary resistive loads. Fourier transform methods are used to obtain frequency domain information.

ACKNOWLEDGMENT

The author is greatly indebted to Dr. Roger F. Harrington for his encouragement, suggestions and assistance. He is also indebted to Dr. Joseph Mautz and Mr. Barry Spielman for numerous stimulating discussions.

Special thanks are also due Dr. Theodore Bickart for many helpful suggestions concerning the manuscript, and Dr. Joseph Murdock of the University of New Hampshire, and Mrs. Louise Capra for her patience and suggestions during typing.

The work was supported in part by the National Science Foundation under Grant Number GK-1233, and by the Electrical Engineering Department of Syracuse University.

CONTENTS

LIST OF FIGURES

LIST OF TABLES

DEDICATION

To my wife Vivien and my children, Kathleen and Edward, without whose love, patience, and encouragement this work could not have been completed.

Chapter 1

INTRODUCTION

This dissertation examines direct time domain solutions for thin wires utilizing methods similar to those proposed by Harrington[1] in the frequency domain. The time-dependent integrodifferential operators are approximated by matrix operators which incorporate the initial and boundary conditions within the formulation. The proposed solutions are presented as algorithms suitable for digital computation. The algorithms are iterative by nature and hence inexpensive in terms of computation time.

Direct time domain solutions have some interesting aspects when presented in the language of linear spaces and the method of moments. Because the time domain operator is not self-adjoint, the adjoint space must be used in evaluations by the method of moments. The relationship between time domain reciprocity and the method of moments is presented with emphasis placed on the equivalence of the reciprocity theorem and the definition of the time domain adjoint operator.

Numerical results are presented for the current and charge induced on a straight wire scatterer excited at arbitrary incidence angles by a plane wave unit step electric field. Further results are presented for a dipole excited by a localized unit step voltage. The driving point and transfer indicial admittances, and the normalized radiation field are evaluated. The proposed method is extended to wires of arbitrary shape through the use of the pulse tested method of moments. Results are presented for the wire loop as a scatterer and as an antenna to provide a demonstration of the moments solution.

1.1. Background

Solutions of electromagnetic problems for general time dependent excitations have been of interest for many years. Manneback's paper[2] written in 1923 is typical. Two major approaches have been used on time dependent electromagnetic problems of the thin wire type: transform methods[3,4,5,6,7,8] and transmission line theory[9,10,11]. A relatively few papers have examined the thin wire antenna analytically in the time domain. Of those few, only one[12] has direct import to this dissertation. Reciprocity theorems have been derived for the general time dependent electromagnetic system. Two authors in particular[13,14] have presented alternate forms of the reciprocity integrals and have derived variational principles for scattering problems from these integrals. As in the frequency domain[1,15] these integrals can be interpreted as functionals useful in the evaluation of near and far field quantities.

1.2. The General Formulation in the Time Domain for the Response of Wire Obstacles

The electromagnetic field due to current and charge on perfectly conducting bodies is described in the time domain by the following equations.

$$\underset{\sim}{E} = -\frac{\partial \underset{\sim}{A}}{\partial t} - \nabla\Phi + \underset{\sim}{E}^{i} \tag{1}$$

$$\underset{\sim}{A}(t,r) = \frac{\mu}{4\pi} \oint\!\!\oint_{S} \frac{\underset{\sim}{J}(t-\tau,r')}{R(r,r')}\, ds' \tag{2}$$

$$\Phi(t,r) = \frac{1}{4\pi\epsilon} \oint\!\!\oint_{S} \frac{\rho(t-\tau,r')}{R(r,r')}\, ds' \tag{3}$$

$$\nabla' \cdot \underset{\sim}{J} + \frac{\partial \rho}{\partial t} = 0 \tag{4}$$

$$E_{tangential} = 0 \quad \text{on } S \tag{5}$$

Here, $\underset{\sim}{E}$ denotes the total electric field, $\underset{\sim}{E}^i$ the impressed field, $\underset{\sim}{A}$ the magnetic vector potential, Φ the electric scalar potential, $\underset{\sim}{J}$ the current density on the conducting body, ρ the surface charge density, and R the distance between source points and field point. The time delay, τ, given by

$$\tau = R(r,r')/v_p \tag{6}$$

is the propagation time between the source point r' and the field point r. v_p is the velocity of propagation of the surrounding medium in which the wire is imbedded. The medium will be assumed to be homogeneous and isotropic. The tangential boundary condition, Eq. (5), is replaced by a more general condition,

$$E_{tangential} = L_1(\underset{\sim}{J}) \tag{7}$$

in order that impedance type boundary conditions may be considered.

Some common forms of Eq. (7) are

$$E_{tangential} = K(t,r')J(t,r') \tag{8a}$$

$$E_{tangential} = K_1 \frac{dJ}{dt}(t,r') \tag{8b}$$

Equation (8a) is the general time dependent resistive boundary condition, and Eq. (8b) the general inductive boundary condition. For the remainder of the paper only boundary conditions of the type of Eq. (8a) will be considered. The perfectly conducting boundary condition (5) is a special case of Eq. (8a).

Equations (1) through (6) simplify considerably for the thin wire. Let ℓ denote the length variable along the axis of the wire. The electric field equation

$$E_\ell = - \frac{\partial A_\ell}{\partial t} - \frac{\partial \Phi}{\partial \ell} + E^i_\ell \tag{9}$$

is written on the wire surface in terms of the tangential components of the total electric field E_ℓ, the incident field E^i_ℓ, and the time derivative of the vector potential $\partial A_\ell/\partial t$. The scalar potential contribution $(\partial\Phi/\partial\ell)$, is the directional derivative of Φ along ℓ.

The vector and scalar potentials are given by single dimensional integrals over the axial sources $\underset{\sim}{I}$ and q

$$\underset{\sim}{A}(t,\ell) = \frac{\mu}{4\pi} \int_{\ell'} \frac{I(t-\tau,\ell')}{R(\ell,\ell')}\, d\ell' \tag{10}$$

$$\Phi(t,\ell) = \frac{1}{4\pi\epsilon} \int_{\ell'} \frac{q(t-\tau,\ell')}{R(\ell,\ell')}\, d\ell' \tag{11}$$

The resistive boundary condition, Eq. (8a), becomes

$$E_\ell = \Omega I \tag{12}$$

where Ω, the axial resistivity (ohms/meter) will be taken as time independent for simplicity. The continuity relationship is given in terms of the axial and time derivatives.

$$\frac{\partial I}{\partial \ell'} + \frac{\partial q}{\partial t} = 0 \tag{13}$$

Accurate treatment of time effects on the order of the transit time of the wire diameter are excluded in Eqs. (9) through (13). This is

equivalent in the frequency domain to the exclusion of effects for which the diameter is an appreciable fraction of a wavelength.

1.3. Operator Approximations

The electric field equation, Eq. (9), is approximated by difference operators in time and space. The approximation is:

$$E_\ell(t,\ell) \approx -\frac{1}{\Delta T}\left[A_\ell\left(t+\frac{\Delta T}{2},\ell\right) - A_\ell\left(t-\frac{\Delta T}{\ell},\ell\right)\right]$$

$$-\frac{1}{\Delta \ell}\left[\Phi\left(t,\ell+\frac{\Delta \ell}{2}\right) - \Phi\left(t,\ell-\frac{\Delta \ell}{2}\right)\right] + E^i_\ell(t,\ell) \qquad (14)$$

The continuity equation is similarly expressed by difference operators

$$\frac{1}{\Delta \ell}\left[I\left(t,\ell'+\frac{\Delta \ell}{2}\right) - I\left(t,\ell'-\frac{\Delta \ell}{2}\right)\right] + \frac{1}{\Delta T}\left[q\left(t+\frac{\Delta T}{2},\ell'\right) - q\left(t-\frac{\Delta T}{2},\ell'\right)\right] \approx 0 \qquad (15)$$

For simplicity,

$$\Delta \ell = v_p\, \Delta T$$

where v_p, the velocity of propagation in the surrounding medium.

1.4. The Method of Moments, Point Testing and Pulse Testing

These terms which are used extensively in this paper will be defined and illustrated in this section. The method of moments is a means of solving operator equations such as Eqs. (9) and (10) by a set of matrix operations. Let a function ψ be given by the equality

$$\psi(t,r) = L(t|t',\, r|r')\ \phi(t',r') \qquad (16)$$

where ϕ is a function in the domain of the operator L. Furthermore, let ϕ be approximated by a series expansion

$$\phi(t',r') \approx \sum_m \sum_k \Gamma(m,k)\, f_{m,k}(t',r') \tag{17}$$

where the Γ's are the expansion coefficients of ϕ and $f_{i,j}$ is a member of the set of expansion functions of the series. Assume L is a linear operator. The substitution of Eq. (17) into Eq. (16) results in the approximate expression

$$\psi(t,r) \approx \sum_m \sum_k \Gamma(m,k) L(t|t',r|r') f_{m,k}(t',r') \tag{18}$$

for ψ. Let the set of testing functions $S_{j,\ell}(t,r)$ be defined on the (t,r) space for each of the integers j and ℓ. The inner product of (18) with $S_{j,\ell}$ is denoted $\langle\psi(t,r),\ S_{m,\ell}(t,r)\rangle$ and defined by

$$\langle\psi(t,r), S_{j,\ell}(t,r)\rangle \equiv \int_0^\infty \int_{D(r)} \psi(t,r) S_{j,\ell}(-t,r)\,dr\,dt \tag{19}$$

This integral is commonly called a functional.[16] The testing procedure may be considered as the projective value of ψ onto the $S_{m,\ell}$ component of the space of testing functions.[16] More complete mathematical expositions are found in references 17 and 18. By virtue of (18)

$$\langle\psi(t,r), S_{j,\ell}(t,r)\rangle = G(\Gamma, j, \ell)\, \langle L f_{m,k}, S_{j,\ell}\rangle \tag{20}$$

where G is a function of the expansion coefficients and the indices j and ℓ. Generally the choice of expansion and testing functions, and the boundary and initial conditions determine whether G is readily solvable for the Γ's. The method of moments is thus described by the operations (16) through (20). When L is self-adjoint and the expansion and testing functions are the same, the method of moments is also known as Galerkin's method.[18]

Two useful projective operations are point* and pulse testing. If the testing function is a two-dimensional impulse $\delta(t+t_0)\ \delta(r-r_0)$, the operation (19) is called point testing and the resulting functional is $\psi(t_0,r_0)$. Point testing is recognized as an application of the sampling property of impulse functions. If the testing function in (19) is taken as a unit volume two-dimensional pulse, the operation is called pulse testing and the resulting functional is the average value of $\psi(t,r)$ over the domain of the pulse function. Point and pulse testing will be considered in more detail in Chapters 2 and 3, respectively.

1.5. Format

This dissertation is divided into three main subject areas: (1) point and pulse tested solutions for the straight wire, (2) the calculation of the radiation field for the straight wire, and (3) the extension of pulse testing to arbitrarily bent wires, and its application to radiation and scattering by the circular wire loop.

The first subject area is covered in Chapters 2 and 3. In Chapter 2 point matched solutions for the current and charge on a straight wire are developed. The difference approximations of Section (1.3) are used to evaluate the field point derivatives. Several examples of the straight wire as a scatterer excited by a plane wave electric field with a propagating unit step time dependence will be presented. Further results for the straight wire antenna excited at an arbitrary driving point by a localized voltage with unit step time dependence are also given. In Chapter 3, the pulse tested solution is developed for the straight wire and applied to

*Point testing is also referred to as point matching.

the same class of problems considered in Chapter 2, along with comparisons of the two methods.

The presentation of the second subject area is found for the most part in Chapter 4 and Appendix A. In Chapter 4, the pulse tested method of moments and the time reciprocity theorem of Appendix A is applied to the calculation of the radiation field of the straight wire antenna or scatterer. The same type analysis is applied to the calculation of the radiation field of the circular loop in Chapter 6.

The extension of the pulse tested moments solution to arbitrarily bent wires is found in Chapter 5, and its application to the circular wire loop is the subject matter of Chapter 6. Also in this chapter are found the results for the current, charge and radiation field for the loop as an antenna and scatterer. The excitations are the same as those for the straight wire. Conclusions and recommendations are found in Chapter 7.

A time domain reciprocity theorem for thin wire objects is proved in Appendix A. The equivalency between reciprocity and the definition of the adjoint operator is demonstrated. This theorem is of general use in the moments solutions for current and charge, and of particular use in the calculation of radiation fields. Potential integral integrations for point and pulse testing are discussed in Appendix B. Program instructions and listing are found in Appendix C.

Chapter 2

POINT TESTED SOLUTIONS FOR THE STRAIGHT WIRE

The straight conducting wire object is the basis for the simplest example of the application of the time domain electromagnetic formulation to radiation and scattering. Figure 2.1 illustrates the straight wire geometry.

The specialization of the thin wire equations (9) through (13) is straightforward. The field points are denoted by z, and the source points by z'. The electric field equation is written

$$E_z = - \frac{\partial A_z}{\partial t} - \frac{\partial \Phi}{\partial z} + E_z^i \tag{21}$$

where E_z is the total tangential electric field, E_z^i the tangential component of the incident electric field, A_z the tangential component of the vector potential and $\frac{\partial \Phi}{\partial z}$ the z-directed derivative of the scalar potential. The potentials are given by

$$A_z(t,z) = \frac{\mu}{4\pi} \int_{\ell'} \frac{I_z(t-\tau, z')}{R(z,z')} \, dz' \tag{22}$$

and

$$\Phi(t,z) = \frac{1}{4\pi\epsilon} \int_{\ell'} \frac{q(t-\tau, z')}{R(z,z')} \, dz' \tag{23}$$

where

$$\tau = |z-z'|/v_p \tag{24}$$

$$R = \sqrt{(z-z')^2 + a^2} \tag{25}$$

a = wire radius

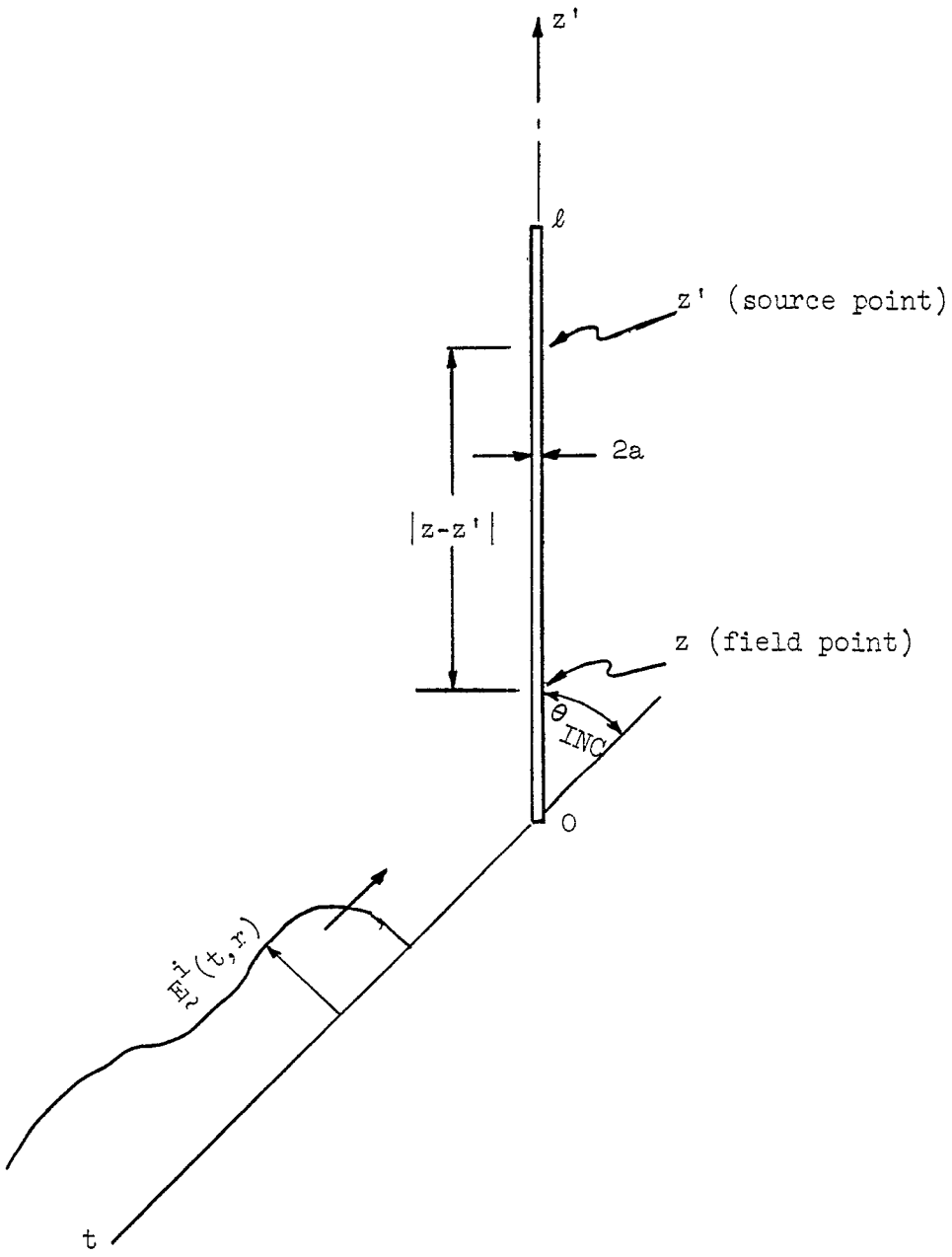

Straight Wire Coordinate Geometry

Figure 2.1

The integrations are performed over the axial sources I_z and q. The equation of continuity is

$$\frac{\partial I_z}{\partial z'} + \frac{\partial q}{\partial t} = 0 \tag{26}$$

The resistive boundary condition becomes

$$E_z = \Omega(z) I_z \qquad \text{on } \ell \tag{27}$$

with Ω the axial resistivity (ohms/meter).

2.1. The Point Matched Method of Moments Solution

The solution for current and charge along the wire will be effected by the point tested method of moments outlined in Section 1.4.

The inner product between two vector functions is defined in Appendix A. The specialization to the straight wire is given by (28).

$$\langle \underset{\sim}{K}, \underset{\sim}{B} \rangle = \int_0^\infty \left[\int_0^\ell \underset{\sim}{K}(t,z) \cdot \hat{u}_z B(-t,z) dz \right] dt \tag{28}$$

where $\underset{\sim}{K}$ is an arbitrary vector function defined over z and $0 \leq t < \infty$, B is a function defined over z and the adjoint time domain $-\infty < t \leq 0$, and $\hat{u}_z$ is a unit vector in the z direction. The function B will be replaced by the testing functions in the moments evaluation.

The current and charge will be expanded in terms of two-dimensional pulse functions. The basis functions of these expansions is denoted P(t,x), and defined by the relations:

$$P(t,x) = P_1(x) P_2(t) \tag{29a}$$

where

$$P_1(z) = 1 \qquad 0 \leq z < \Delta z$$
$$= 0 \qquad \text{otherwise} \tag{29b}$$

$$P_2(t) = 1 \qquad 0 \leq t < \Delta T$$
$$= 0 \qquad \text{otherwise} \tag{29c}$$

$P(t,x)$ is shown in Figure 2.2. The current I_z will be expanded in the two-dimensional series,

$$I_z(t,z') = \sum_{m=1}^{\infty} \sum_{k=1}^{N-1} \beta(m,k) P_1(z'-(k-.5)\Delta z) P_2(t-(m-1)\Delta T) \tag{30}$$

where the $\beta(m,k)$'s are the unknown current coefficients and $\Delta T = \Delta z/v_p$ (v_p - the velocity of propagation of the surrounding medium). This choice of expansion functions satisfies the boundary conditions at $z = 0$ and ℓ, as well as the initial condition on $I_z(0^+,z')$.[20] The charge is expanded in a similar representation

$$q(t,z') = \sum_{m=1}^{\infty} \sum_{k=1}^{N} \gamma(m,k) P_1(z'-(k-1)\Delta z) P_2(t-(m-.5)\Delta T) \tag{31}$$

It is apparent this expansion satisfies the initial and boundary conditions on the charge.

The temporal and spatial dependences of the current and charge expansions are shown in Figures 2.3(a,b) and 2.4(a,b), respectively.

The set of two-dimensional impulse functions $\{S_{j,\ell}\}$

$$S_{j,\ell} = \delta(t + (j-1)\Delta t)\delta(z' - \ell\Delta z) \tag{32}$$

are used as point testing functions. The time index j varies over the

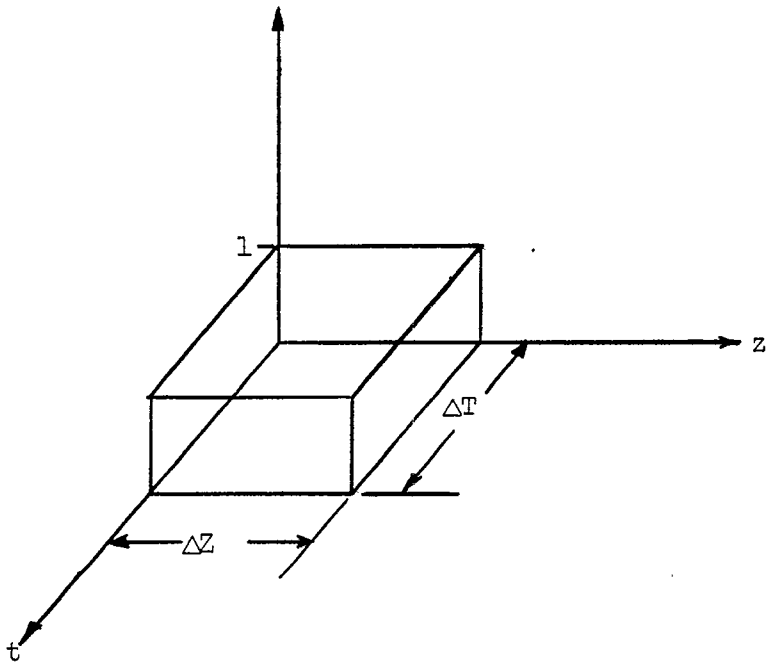

The Elementary Basis Function

$P_1(z)P_2(t)$

Figure 2.2

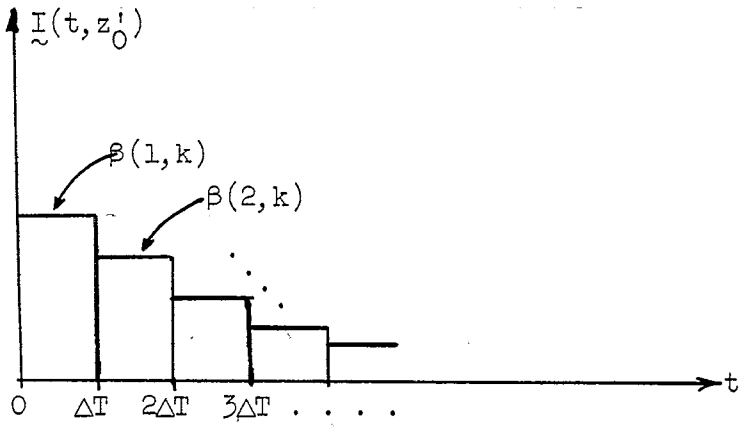

Time Representation of $\underset{\sim}{I}(t, z_k')$

Figure 2.3a

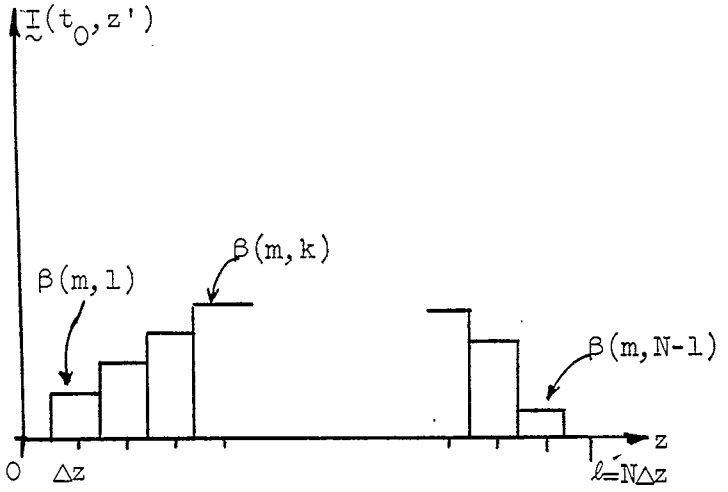

Spatial Representation of $\underset{\sim}{I}(t_m, z')$

Figure 2.3b

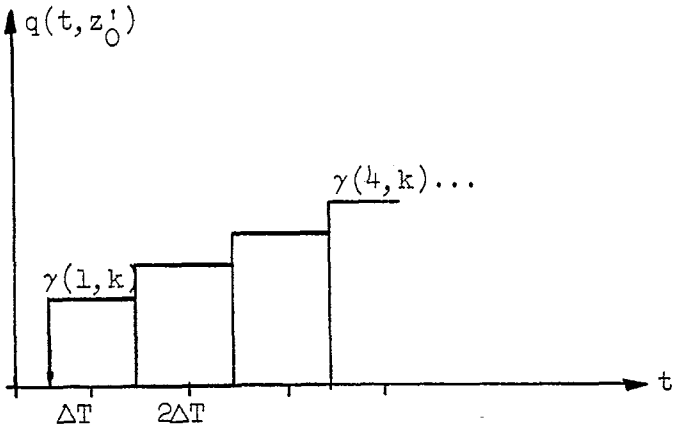

Time Representation of $q(t,z'_k)$

Figure 2.4a

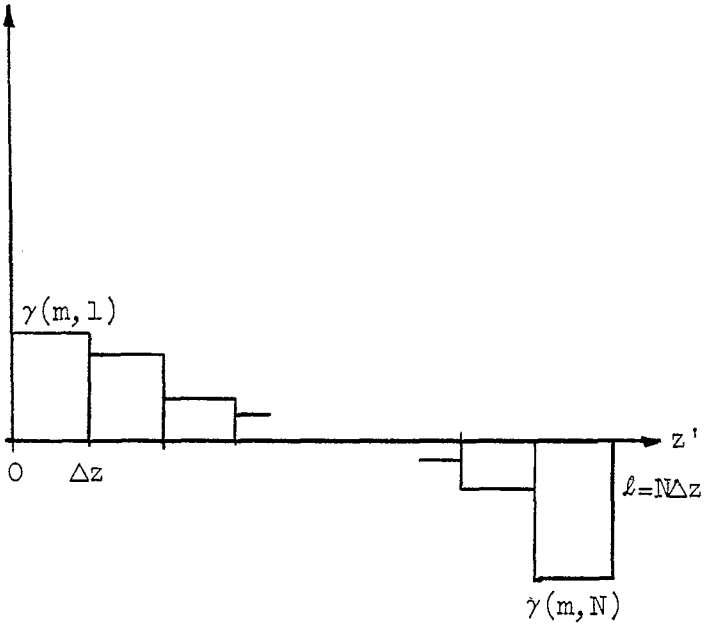

Spatial Representation of $q(t_m,z')$

Figure 2.4b

integer set 1,2,..., and the spatial index ℓ over the integers 1,2,...,N-1. The point tested method of moments solution proceeds by forming the inner product between the point testing functions and the electric field equation (21).

$$\langle E_z, S_{j,\ell} \rangle = -\left\langle \left(\frac{\partial A_z}{\partial t} + \frac{\partial \Phi}{\partial z}\right), S_{j,\ell} \right\rangle + \langle E_z^i, S_{j,\ell} \rangle \tag{33}$$

The definition of the inner product is given by (19). The resultant of the inner product operation is the tangential electric field equation sampled at $t_j = (j-1)\Delta T$, $z_\ell = \ell \Delta z$. This equation will be approximated by the difference equation (14) evaluated at the sample points. Thus

$$E_z^i(t_j, z_\ell) = \Omega(z_\ell) I_z(t_j, z_\ell) + \frac{1}{\Delta T}\left[A_z(t_j + \frac{\Delta T}{2}, z_\ell) - A_z(t_j - \frac{\Delta T}{2}, z_\ell)\right]$$

$$+ \frac{1}{\Delta z}\left[\Phi(t_j, z_\ell + \frac{\Delta z}{2}) - \Phi(t_j, z_\ell - \frac{\Delta z}{2})\right] \tag{34}$$

The resistive boundary condition (27) has been conveniently included.

The continuity equation (26) is approximated by the difference approximation (15) at the points $t_m = (m-.5)\Delta T$, $z_i' = (i-.5)\Delta z$, $m = 1,2,\ldots$, $i = 1,2,\ldots,N$.

$$\frac{1}{\Delta z}\left[I_z(t_m, z_i' + \frac{\Delta z}{2}) - I_z(t_m, z_i' - \frac{\Delta z}{2})\right] =$$

$$- \frac{1}{\Delta T}\left[q(t_m + \frac{\Delta T}{2}, z_i') - q(t_m - \frac{\Delta T}{2}, z_i')\right] \tag{35}$$

With the substitution of the current and charge expansions, (30) and (31) respectively into (35), the following relationships between the current and charge coefficients result.

Initial Conditions

$$\left.\begin{aligned} &\gamma(1,1) + \frac{\beta(1,1)}{v_p} = 0 \\ &\gamma(1,N) + \frac{\beta(1,N-1)}{v_p} = 0 \end{aligned}\right\} \text{End Conditions} \qquad (36a), (36b)$$

$$\gamma(1,k) + \frac{\beta(1,k) - \beta(1,k-1)}{v_p} = 0 \quad k=2,3,\ldots,N-1 \qquad (36c)$$

$$\left.\begin{aligned} &\gamma(m,1) - \gamma(m-1,1) + \frac{\beta(m,1)}{v_p} = 0 \\ &\gamma(m,N) - \gamma(m-1,N) - \frac{\beta(m,N-1)}{v_p} = 0 \end{aligned}\right\} \text{End conditions} \qquad (36d), (36e)$$

$$\gamma(m,k) - \gamma(m-1,k) + \frac{\beta(m,k) - \beta(m,k-1)}{v_p} = 0 \qquad (36f)$$

$$m=2,3,\ldots$$
$$k=2,3,\ldots,N-1$$

2.2. Evaluation of the Point Tested Potential Integrals

Before the iteration procedure is developed, the evaluation of the potential integrals will be undertaken. Equations (37) and (38) which follow show the explicit dependences of the vector and scalar potentials on the temporal and spatial domains. Thus,

$$A_z(t_j \pm \frac{\Delta T}{2}, z_\ell) = \frac{\mu}{4\pi} \int_\ell \frac{I_z(t_j \pm (\Delta T/2) - \tau, z')}{R(z_\ell, z')}\, dz' \qquad (37a)$$

where

$$\tau = \frac{|\ell\Delta z - z'|}{v_p} \qquad (37b)$$

$$R(z_\ell, z') = \sqrt{(\ell\Delta z - z')^2 + a^2} \qquad (37c)$$

and

$$\Phi(t_j, z_\ell \pm \frac{\Delta z}{2}) = \frac{1}{4\pi\epsilon} \int_\ell \frac{q(t_j - \tau, z')}{R(z_\ell \pm (\Delta z/2), z')} \, dz' \tag{38a}$$

where

$$\tau = \frac{|(\ell \pm .5)\Delta z - z'|}{v_p} \tag{38b}$$

$$R(z_\ell \pm \frac{\Delta z}{2}, z') = \sqrt{((\ell \pm .5)\Delta z - z')^2 + a^2} \tag{38c}$$

The functional forms of the scalar and vector potential integrals are similar. For this reason only the integration of the vector potential will be considered in detail. The evaluation of the scalar potential follows directly.

The retarded current in (37) can be written

$$I_z(t_j + \frac{\Delta T}{2} - \tau, z') =$$

$$\sum_{k=1}^{N-1} \beta(j+.5- \frac{\tau}{\Delta T}, k) \; P_1(z'-(k-.5)\Delta z) \; P_2(t-(j+.5- \frac{\tau}{\Delta T})\Delta T) \tag{39}$$

Causality imposes the restriction that any current coefficient whose retarded time index is less than unity vanish identically; that is

$$\beta(j + .5 - \frac{\tau}{\Delta T}, k) \equiv 0 \qquad \text{if } (j + .5 - \frac{\tau}{\Delta T}) < 1$$

and, over the interval $0^+ \leq t \leq \frac{\Delta T}{2}$, integration of (37a) may proceed only over those points z' such that

$$t - \frac{|\ell \Delta z - z'|}{v_p} \geq 0^+$$

With the substitution of (39) into (37), the vector potential is expressed explicitly in terms of the current expansion. Because the retarded

potential operator is a linear operator on the current, summation and integration may be interchanged.

$$A_z(t_j + \frac{\Delta T}{2}, z_\ell) = \frac{\mu}{4\pi} \sum_{k=1}^{N-1} \int_{(k-.5)\Delta z}^{(k+.5)\Delta z} \frac{\beta(j+.5-|\ell-z'/\Delta z|,k)}{\sqrt{(\ell\Delta z-z')^2 + a^2}}\, dz' \tag{40}$$

Examination of the retarded time coefficient over $(k-.5)\Delta z \leq z' \leq (k+.5)\Delta z$ reveals that the retarded coefficient is a constant with respect to z'. For $k \leq \ell$, the retarded coefficient is $\beta(j-(\ell-k),k)$, and for $\ell < k$, the coefficient is $\beta(j-(k-\ell),k)$. Hence (40) is written,

$$A_z(t_j + \frac{\Delta T}{2}, z_\ell) = \frac{\mu}{4\pi} \sum_{k=1}^{N-1} \beta(j-|\ell-k|,k) \left\{ \int_{(k-.5)\Delta z}^{(k+.5)\Delta z} \frac{dz'}{\sqrt{(\ell\Delta z-z')^2 + a^2}} \right\} \tag{41}$$

Summation proceeds only over those k's, such that

$$j - |\ell - k| \geq 1 \quad ; \quad j = 1,2,\ldots \qquad \ell = 1,2,\ldots,N-1$$

It is shown in Appendix B that integrals of the form

$$\int_{(k-.5)\Delta z}^{(k+.5)\Delta z} \frac{dz'}{\sqrt{(\ell\Delta z-z')^2 + a^2}}$$

are functions of the wire radius, subsection length, and the absolute value of the difference of the source and field subsection indices. These functions will be termed point tested geometry functions and denoted by $F(|\ell-k|)$. The vector potential can be written in terms of these functions

loaded subsections, the current is given by

$$\beta(j,\ell) = \frac{-[v_p \Delta A + \Delta\Phi]}{R_L(\ell) + \eta(F(0)/4\pi)} \tag{56}$$

where the $R_L(\ell)$ terms include the load resistances and the conductive resistance of the ℓ-th subsection. The charge coefficients are calculated from (36) and the iteration proceeds as previously described.

2.4. Summary of the Point Tested Solutions

The steps of the point tested solutions can be summarized:

I) Calculate the point tested geometry function F(n), n = 0,...,N-1.

II) Calculate the initial currents, charges and vector potentials from (45) or (55) and (56), (36a,b,c) and (42), respectively.

III) Calculate the first set of scalar potential terms from (43) and (44).

IV) Calculate the next set of currents, charges and vector potentials from (49) or (55) and (56), (36d,e,f) and (42) respectively.

V) Advance the time index by unity and go back to step III.

A computer program has been written to implement these steps and is contained in Appendix C, along with programming notes and instructions. The program is written in FORTRAN IV and results have been computed on an IBM 360/50 computer located at Syracuse University.

2.5. Point Tested Computed Results

A number of computations will be presented in this section which are indicative of what can be achieved with the point tested moment solutions.

Results for a center fed dipole, $(\frac{\ell}{2a}) = 74.2)$, excited by a unit step voltage are shown in Figures 2.6 through 2.10. Figures 2.6 and 2.7 show the driving point current for Rg = 0.0 and Rg = 50.0 ohms respectively. The generally periodic behavior of the current is evident, with the period corresponding closely to the fundamental mode of the center fed dipole. Also evident is the rapid loss of high frequency content in the waveform. This is indicative that high frequencies radiate more efficiently than low frequencies. As $t \longrightarrow \infty$, the antenna approaches asymptotically the static case of a charged dipole, with the corresponding vanishing of the current due to radiation. The effect of the generator resistance is to decrease the current magnitude and speed the damping process through heat loss I^2R_g. Figure 2.8 shows the input admittance calculated from the current shown in Figure 2.6. The values agree closely with Harrington's results found in Reference 1, page 72. The peak at $k\ell \approx 3.0$ is the fundamental antenna mode and corresponds closely in the time domain to twice the transit time from the feedpoint to the end of the antenna. Transform techniques were used to provide a check on the computed results due to the lack of reference material. An interesting rule of thumb was used to decide how far in time to consider results. The effects of truncation errors in the frequency domain are described by the convolution of the untruncated data with the function

$$Te^{-j(\omega T/2)} \quad \frac{\sin\ (\omega T/2)}{\omega T/2}$$

where T is the period of observation. The resonance peak width is inversely proportional to the Quality factor Q of the antenna, and for

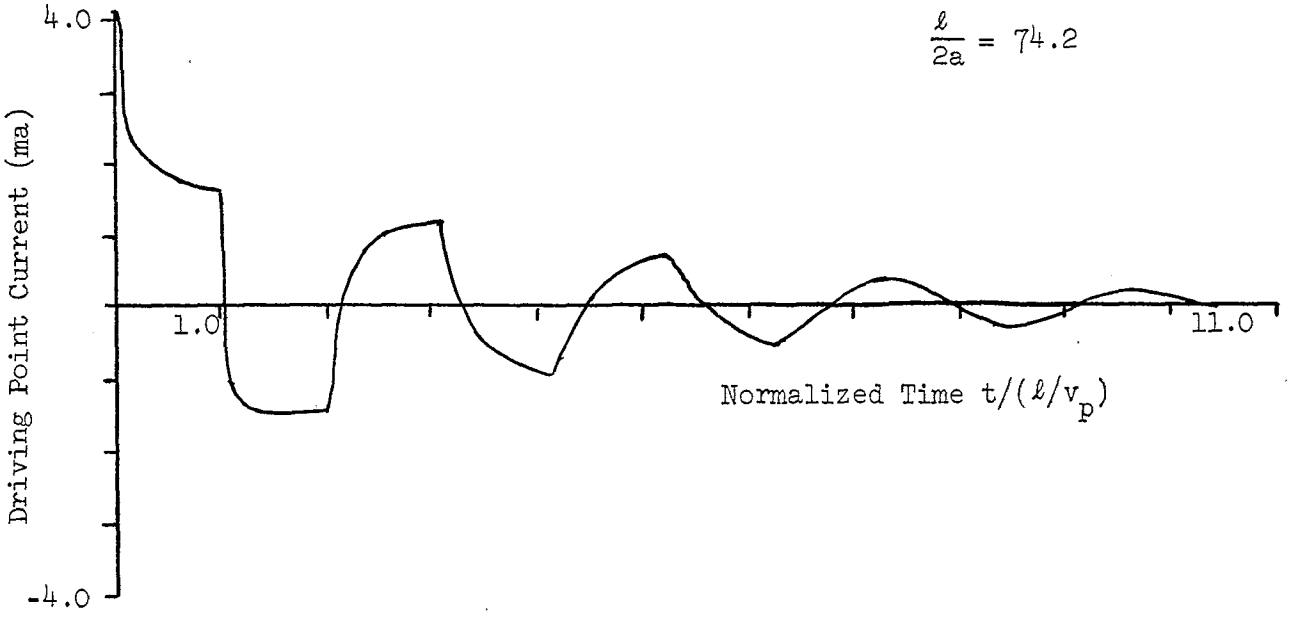

Point Tested Center Fed Antenna
Driving Point Current $R_g = 0.0$

Figure 2.6

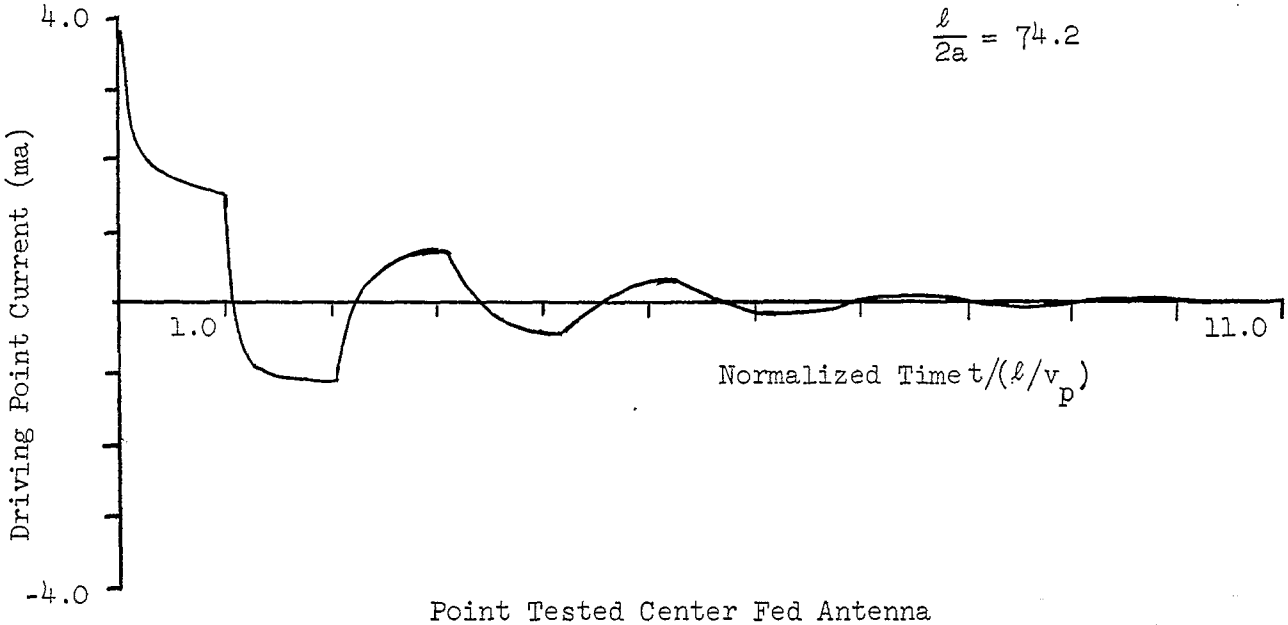

Point Tested Center Fed Antenna
Driving Point Current $R_g = 50.0$

Figure 2.7

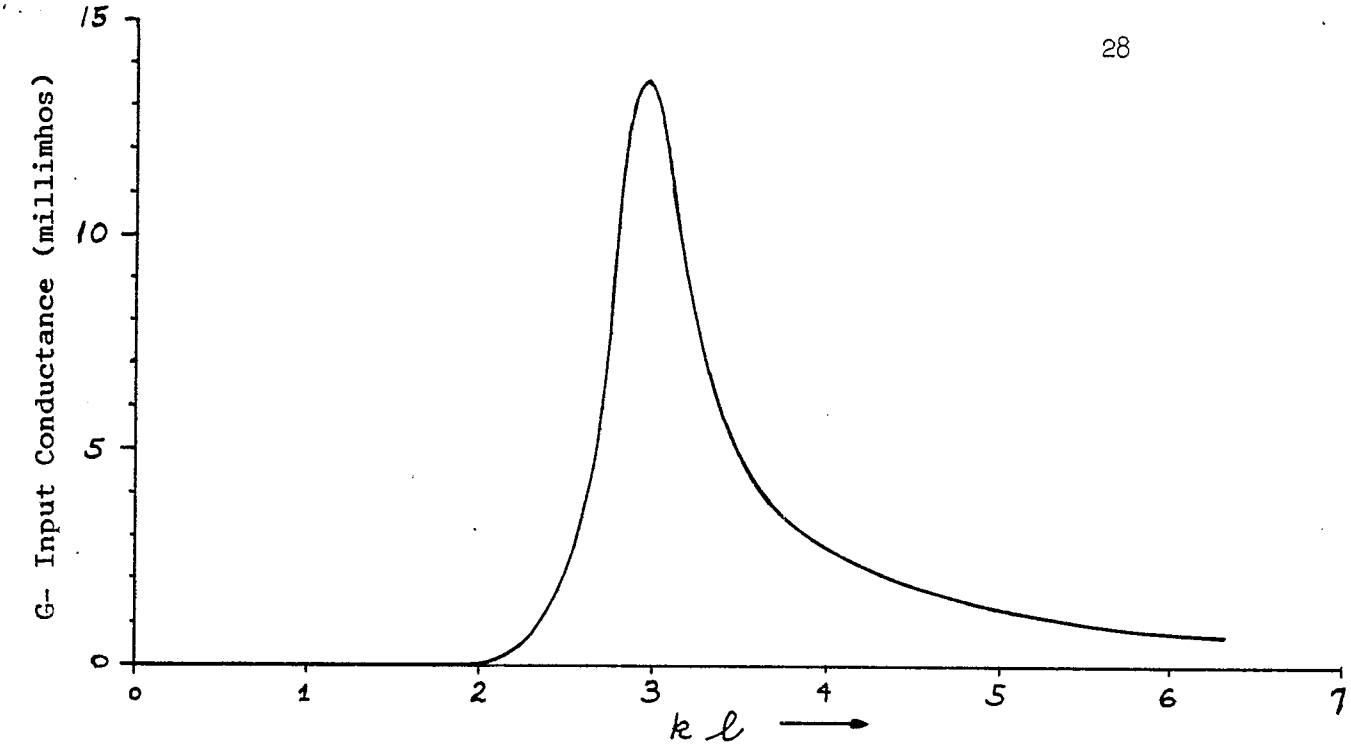

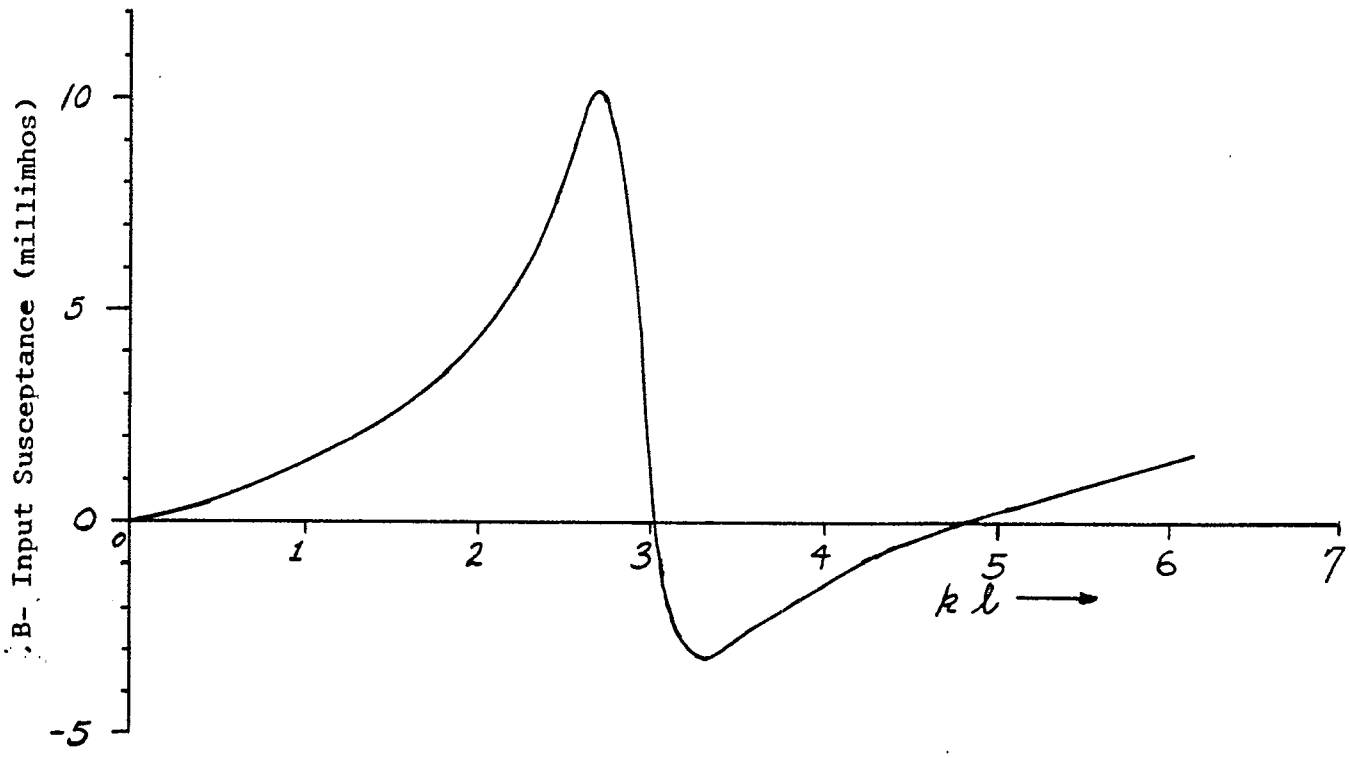

Driving Point Admittance
Calculated From Point Tested Current

Figure 2.8

moderate Q's, truncation errors would distort the resonance most severely. If T = 2Q, the truncator errors were found to be negligible. In addition, if the time waveform is approximated by $e^{-\alpha t}\cos 2\pi f_0 t$, then the antenna Q can be estimated using,

$$Q = \frac{\pi f_0}{\alpha}$$

The approximate Q estimated from Figure 2.6 is 4.5 which is well within a factor of two of the value found by frequency domain methods. The spatial distribution of current and charge on the center fed antenna, ($\frac{\ell}{2a} = 74.2$, $R_g = 50\ \Omega$), as a function of normalized time ($t/(\ell/v_p)$), is shown in Figure 2.9. The transient behavior along the antenna for $t < \tau_L^*/2$ is evidenced by the zero currents in the regions $|z-\ell/2| > v_p t$. The effect of reflection from the wire ends is shown for $t/\tau_L > 0.52$. The reflection is frequency sensitive with the high frequencies contributing to the radiation field and the low frequencies being almost completely reflected. In the time domain, this evidenced by the loss of the sharp rise time of the current wave. As $t \longrightarrow \infty$, computations show that the scalar potential approaches +0.5 on the upper half of the dipole and -0.5 on its lower half. This is the predicted D.C. steady state.

Figure 2.10 shows the point tested tangential component of a unit step propagating electric field incident on the wire scatterer from $\theta_{INC} = 30^\circ$ as a function of normalized time t/τ_L. Figure 2.11 shows the point tested current and charge induced on the wire by this excitation at selected instants of time.

---

*$\tau_L = \ell/v_p$

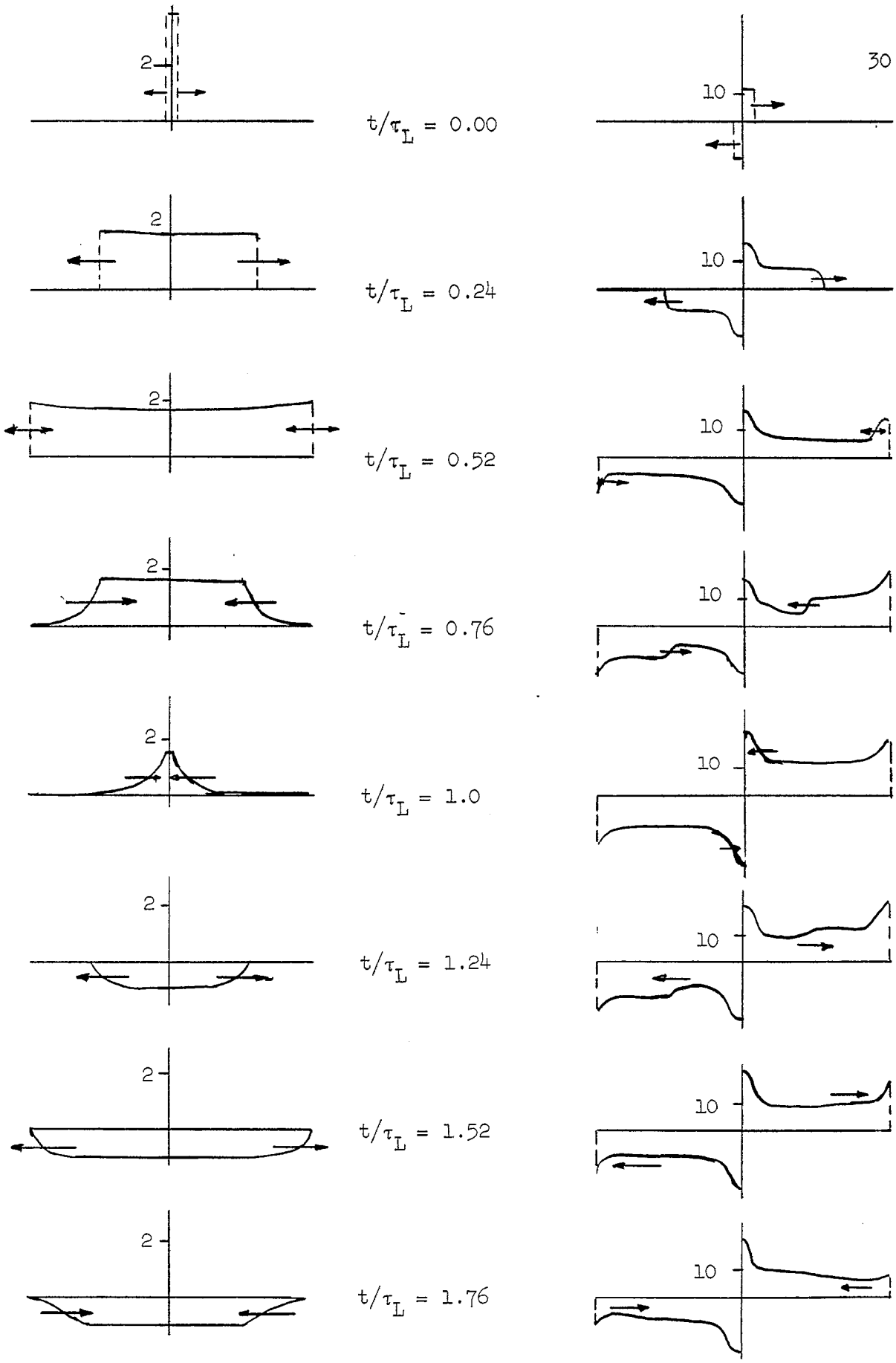

Point Tested Current and Charge on Center Fed Dipole $R_g = 0.0\Omega$

Figure 2.9

INCIDENT TANGENTIAL ELECTRIC FIELD

TIME =	0.0	0.04	0.08	0.12	0.16	0.20	0.24	0.28	0.32	0.36
1	0.500E 00	0.500E 00	0.500E 00	0.500E 00	0.500E 00	0.500E 00	0.500E 00	0.500E 00	0.500E 00	0.500E 00
2	0.0	0.500E 00	0.500E 00	0.500E 00	0.500E 00	0.500E 00	0.500E 00	0.500E 00	0.500E 00	0.500E 00
3	0.0	0.0	0.500E 00	0.500E 00	0.500E 00	0.500E 00	0.500E 00	0.500E 00	0.500E 00	0.500E 00
4	0.0	0.0	0.0	0.500E 00	0.500E 00	0.500E 00	0.500E 00	0.500E 00	0.500E 00	0.500E 00
5	0.0	0.0	0.0	0.0	0.500E 00	0.500E 00	0.500E 00	0.500E 00	0.500E 00	0.500E 00
6	0.0	0.0	0.0	0.0	0.0	0.500E 00	0.500E 00	0.500E 00	0.500E 00	0.500E 00
7	0.0	0.0	0.0	0.0	0.0	0.0	0.500E 00	0.500E 00	0.500E 00	0.500E 00
8	0.0	0.0	0.0	0.0	0.0	0.0	0.500E 00	0.500E 00	0.500E 00	0.500E 00
9	0.0	0.0	0.0	0.0	0.0	0.0	0.0	0.500E 00	0.500E 00	0.500E 00
10	0.0	0.0	0.0	0.0	0.0	0.0	0.0	0.0	0.500E 00	0.500E 00
11	0.0	0.0	0.0	0.0	0.0	0.0	0.0	0.0	0.0	0.500E 00
12	0.0	0.0	0.0	0.0	0.0	0.0	0.0	0.0	0.0	0.0
13	0.0	0.0	0.0	0.0	0.0	0.0	0.0	0.0	0.0	0.0
14	0.0	0.0	0.0	0.0	0.0	0.0	0.0	0.0	0.0	0.0
15	0.0	0.0	0.0	0.0	0.0	0.0	0.0	0.0	0.0	0.0
16	0.0	0.0	0.0	0.0	0.0	0.0	0.0	0.0	0.0	0.0
17	0.0	0.0	0.0	0.0	0.0	0.0	0.0	0.0	0.0	0.0
18	0.0	0.0	0.0	0.0	0.0	0.0	0.0	0.0	0.0	0.0
19	0.0	0.0	0.0	0.0	0.0	0.0	0.0	0.0	0.0	0.0
20	0.0	0.0	0.0	0.0	0.0	0.0	0.0	0.0	0.0	0.0
21	0.0	0.0	0.0	0.0	0.0	0.0	0.0	0.0	0.0	0.0
22	0.0	0.0	0.0	0.0	0.0	0.0	0.0	0.0	0.0	0.0
23	0.0	0.0	0.0	0.0	0.0	0.0	0.0	0.0	0.0	0.0
24	0.0	0.0	0.0	0.0	0.0	0.0	0.0	0.0	0.0	0.0
25	0.0	0.0	0.0	0.0	0.0	0.0	0.0	0.0	0.0	0.0

TIME =	0.40	0.44	0.48	0.52	0.56	0.60	0.64	0.68	0.72	0.76
1	0.500E 00	0.500E 00	0.500E 00	0.500E 00	0.500E 00	0.500E 00	0.500E 00	0.500E 00	0.500E 00	0.500E 00
2	0.500E 00	0.500E 00	0.500E 00	0.500E 00	0.500E 00	0.500E 00	0.500E 00	0.500E 00	0.500E 00	0.500E 00
3	0.500E 00	0.500E 00	0.500E 00	0.500E 00	0.500E 00	0.500E 00	0.500E 00	0.500E 00	0.500E 00	0.500E 00
4	0.500E 00	0.500E 00	0.500E 00	0.500E 00	0.500E 00	0.500E 00	0.500E 00	0.500E 00	0.500E 00	0.500E 00
5	0.500E 00	0.500E 00	0.500E 00	0.500E 00	0.500E 00	0.500E 00	0.500E 00	0.500E 00	0.500E 00	0.500E 00
6	0.500E 00	0.500E 00	0.500E 00	0.500E 00	0.500E 00	0.500E 00	0.500E 00	0.500E 00	0.500E 00	0.500E 00
7	0.500E 00	0.500E 00	0.500E 00	0.500E 00	0.500E 00	0.500E 00	0.500E 00	0.500E 00	0.500E 00	0.500E 00
8	0.500E 00	0.500E 00	0.500E 00	0.500E 00	0.500E 00	0.500E 00	0.500E 00	0.500E 00	0.500E 00	0.500E 00
9	0.500E 00	0.500E 00	0.500E 00	0.500E 00	0.500E 00	0.500E 00	0.500E 00	0.500E 00	0.500E 00	0.500E 00
10	0.500E 00	0.500E 00	0.500E 00	0.500E 00	0.500E 00	0.500E 00	0.500E 00	0.500E 00	0.500E 00	0.500E 00
11	0.500E 00	0.500E 00	0.500E 00	0.500E 00	0.500E 00	0.500E 00	0.500E 00	0.500E 00	0.500E 00	0.500E 00
12	0.500E 00	0.500E 00	0.500E 00	0.500E 00	0.500E 00	0.500E 00	0.500E 00	0.500E 00	0.500E 00	0.500E 00
13	0.0	0.500E 00	0.500E 00	0.500E 00	0.500E 00	0.500E 00	0.500E 00	0.500E 00	0.500E 00	0.500E 00
14	0.0	0.0	0.500E 00	0.500E 00	0.500E 00	0.500E 00	0.500E 00	0.500E 00	0.500E 00	0.500E 00
15	0.0	0.0	0.500E 00	0.500E 00	0.500E 00	0.500E 00	0.500E 00	0.500E 00	0.500E 00	0.500E 00
16	0.0	0.0	0.0	0.500E 00	0.500E 00	0.500E 00	0.500E 00	0.500E 00	0.500E 00	0.500E 00
17	0.0	0.0	0.0	0.0	0.500E 00	0.500E 00	0.500E 00	0.500E 00	0.500E 00	0.500E 00
18	0.0	0.0	0.0	0.0	0.0	0.500E 00	0.500E 00	0.500E 00	0.500E 00	0.500E 00
19	0.0	0.0	0.0	0.0	0.0	0.0	0.500E 00	0.500E 00	0.500E 00	0.500E 00
20	0.0	0.0	0.0	0.0	0.0	0.0	0.0	0.500E 00	0.500E 00	0.500E 00
21	0.0	0.0	0.0	0.0	0.0	0.0	0.0	0.0	0.500E 00	0.500E 00
22	0.0	0.0	0.0	0.0	0.0	0.0	0.0	0.0	0.0	0.500E 00
23	0.0	0.0	0.0	0.0	0.0	0.0	0.0	0.0	0.0	0.500E 00
24	0.0	0.0	0.0	0.0	0.0	0.0	0.0	0.0	0.0	0.0
25	0.0	0.0	0.0	0.0	0.0	0.0	0.0	0.0	0.0	0.0

Point Tested Incident Tangential Electric Field for $\theta_{INC} = 30^{\circ}$

Figure 2.10

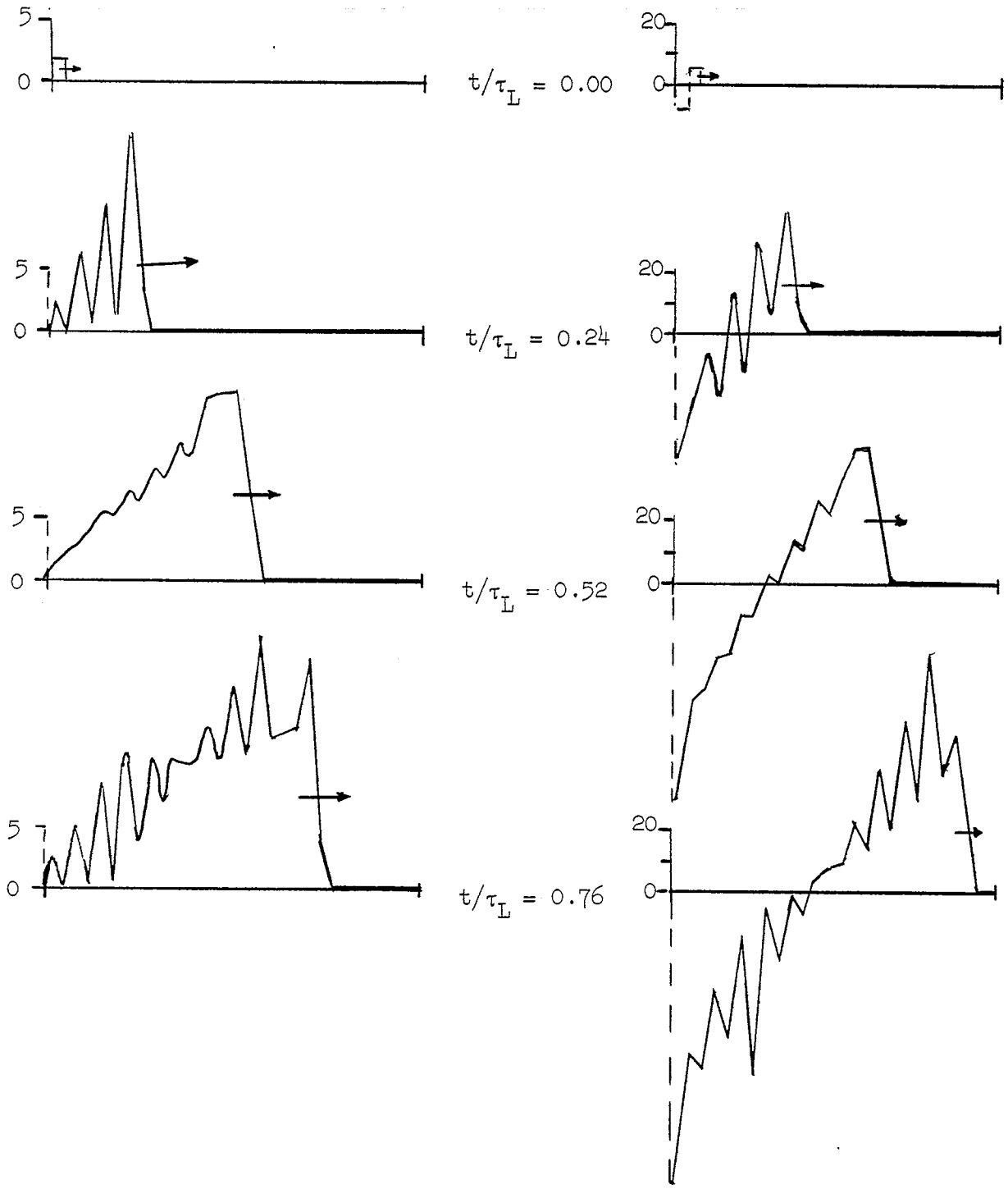

Point Tested Current and Charge on a Wire Scatterer $\theta_{INC} = 30^{\circ}$

Figure 2.11

Although the point tested method of moments demonstrates the qualitative features of the transient process, the numerical errors inherent in the method (especially in the case of scattering) cast doubt on the usefulness of the solution method. A marked improvement will be noted in the pulse tested solutions developed in the next chapter. The far field result for the point tested antenna and scatterers will be presented in Chapter 4.

where $P_2(t)$ was defined by (29c). The time index j ranges over 0,1,2,..., and the spatial index ℓ ranges over 1,2,...,N-1. Sample pulse testing functions are shown in Figure 3.1.

3.2. The Pulse Tested Method of Moments

The pulse tested electric field equation

$$\left\langle E_z^i, S_{j,\ell} \right\rangle = \left\langle \Omega I_z(t,z), S_{j,\ell} \right\rangle + \left\langle \frac{\partial A_z}{\partial t}, S_{j,\ell} \right\rangle + \left\langle \frac{\partial \Phi}{\partial z}, S_{j,\ell} \right\rangle \qquad (59)$$

is similar to (33), but differs markedly in the evaluation of the individual terms. The resistive boundary condition has been conveniently included. Substitution of the pulse testing functions for B(t,z) in (28) gives the pulse testing integral

$$\left\langle K_z, S_{j,\ell} \right\rangle = \left(\frac{1}{\Delta z \Delta T}\right) \int_{(j-.5)\Delta T}^{(j+.5)\Delta T} dt \int_{(\ell-.5)\Delta z}^{(\ell+.5)\Delta z} K_z(t,z)dz \qquad (60)$$

For j = 0, the lower limit of the time integration is changed to zero.

The pulse tested incident field will be denoted $\overline{E}_z^i(t_j, z_\ell)$ and is given by

$$\overline{E}_z^i(t_j, z_\ell) = \left\langle E_z^i, S_{j,\ell} \right\rangle = \frac{\sin\theta_{INC}}{\Delta z \Delta T} \int_{(j-.5)\Delta T}^{(j+.5)\Delta T} dt \int_{(\ell-.5)\Delta z}^{(\ell+.5)\Delta z} dz \left| \underset{\sim}{E}^i\left(t - \frac{z}{c}\cos\theta_{INC}\right) \right| \qquad (61)$$

As noted above for j = 0, the lower limit of the time integration is changed to zero in (61). Only the case where the incident electric field $\underset{\sim}{E}^i(t)$ is in the plane of incidence will be considered. Where $\underset{\sim}{E}^i(t)$ is orthogonal to this plane, there is no field scattered by the wire. $\underset{\sim}{E}^i(t)$ is in general causal. The geometry is as shown in Figure 2.1.

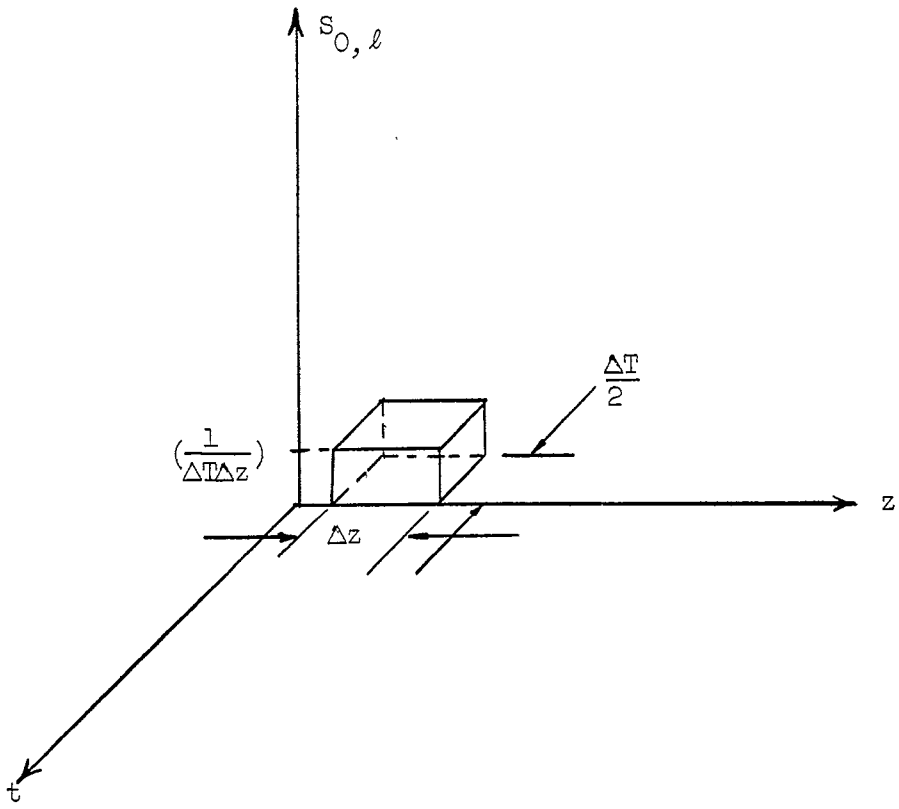

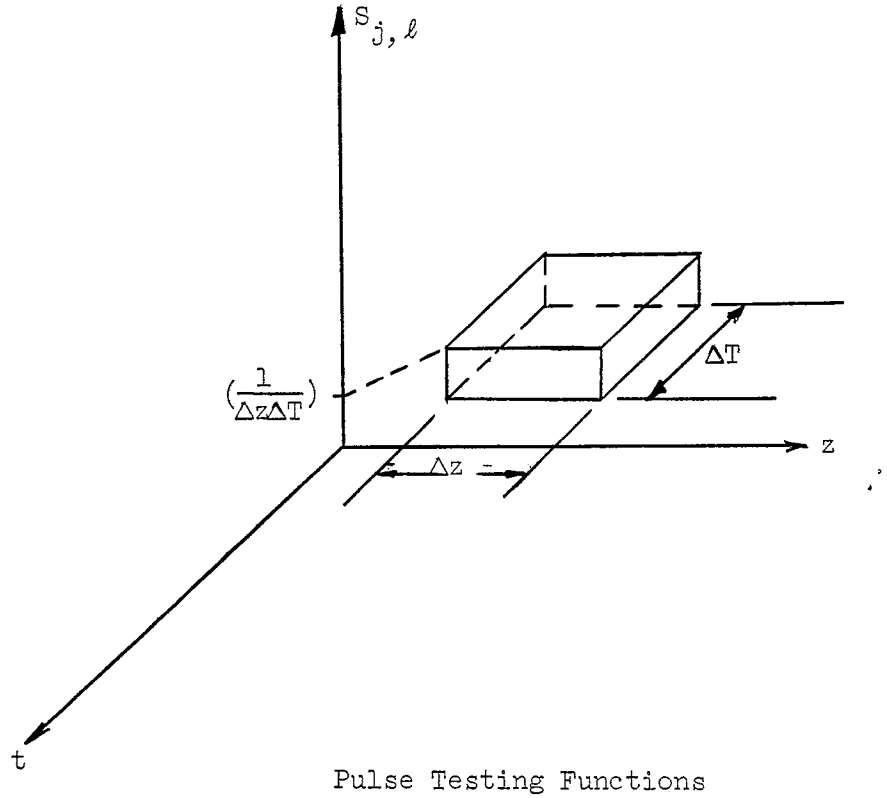

Pulse Testing Functions

Figure 3.1

A term-by-term consideration of the right-hand side of (59) will be pursued for the sake of clarity. It will be shown that an iteration procedure is evolved which is similar to that for the point tested solutions previously considered.

The same current and charge expansions used in the point tested solutions will be retained, and are noted again for convenience.

$$I_z(t,z') = \sum_{m=1}^{\infty} \sum_{k=1}^{N-1} \beta(m,k) P_1(z'-(k-.5)\Delta z) P_2(t-(m-1)\Delta T) \tag{62}$$

$$q(t,z') = \sum_{m=1}^{\infty} \sum_{k=1}^{N} \gamma(m,k) P_1(z'-(k-1)\Delta z) P_2(t-(m-.5)\Delta T) \tag{63}$$

The ohmic contribution $\langle \Omega I_z(t,z), S_{j,\ell} \rangle$ is the simplest term to evaluate. Substitution of (62) into the pulse tested integral (60) results in the following terms after integration.

$$\langle \Omega I_z, S_{0,\ell} \rangle = \frac{\Omega(\ell)}{2} \beta(1,\ell) \tag{64}$$

$$\langle \Omega I_z, S_{j,\ell} \rangle = \frac{\Omega(\ell)}{2} [\beta(j,\ell)+\beta(j+1,\ell)] \qquad j > 0 \tag{65}$$

$\Omega(\ell)$ is seen to be the average resistivity of the ℓ-th subsection.

The term $\left\langle \frac{\partial A_z}{\partial t}, S_{j,\ell} \right\rangle$ is the contribution to the electric field due to the time rate of change of the magnetic flux linking the ℓ-th subsection. The magnetic vector potential A_z is found from the retarded potential (22). Substitution of the current expansion (62) into this integral results in the following:

$$A_z = \frac{\mu}{4\pi} \sum_{m=1}^{\infty} \sum_{k=1}^{N-1} \int_{(k-.5)\Delta z}^{(k+.5)\Delta z} \frac{\beta(m-(\tau/\Delta T),k) P_2(t-(m-1-(\tau/\Delta T))\Delta T}{\sqrt{(z-z')^2 + a^2}} \, dz' \quad (66)$$

Evaluation of (66) is simplified with the following time delay approximation. The time delay τ is a continuous function of $|z-z'|$ which varies over the range

$$\{|k-\ell|-1\}\Delta T \leq \frac{|z-z'|}{v_p} \leq \{|k-\ell|+1\}\Delta T \quad (67)$$

for $\Delta z = v_p \Delta T$, and $|z-z'| \leq \Delta z$. For $k = \ell$, τ varies over

$$\frac{|z-z'|}{v_p} \leq \Delta T \quad (68)$$

The evaluation of (66) is considerably simplified if τ is allowed to take on the average values of (67) and (68). This approximation will incur only a small error if the wire is subdivided into sufficiently small subsections. The average values of τ for $\ell \neq k$ and $\ell = k$ are

$$\bar{\tau} = |\ell-k|\Delta T \qquad \ell \neq k \quad (69)$$

$$\bar{\tau} = \frac{\Delta T}{2} \qquad \ell = k \quad (70)$$

With the substitution of (69) and (70), Equation (66) may be written

$$A_z \approx \frac{\mu}{4\pi} \sum_{m=1}^{\infty} \sum_{k=1}^{N-1} \beta(m-|\ell-k|,k) P_2(t-(m-1-|\ell-k|)\Delta T) \int_{(k-.5)\Delta z}^{(k+.5)\Delta z} \frac{dz'}{\sqrt{(z-z')^2+a^2}} \quad (71)$$

The derivative of the vector potential given by (71) will be taken on a formal basis, since the resultant is an infinite series of impulses corresponding to the leading and trailing edges of the time pulse functions.

However, the functional $\left\langle \frac{\partial \underset{\sim}{A}}{\partial t}, \underset{\sim}{S}_{j,\ell} \right\rangle$ will be shown to be equivalent to the difference approximation to the time derivative applied to the locally averaged vector potential.

$$\frac{\partial A_z}{\partial t} \approx \frac{\mu}{4\pi} \sum_{m=1}^{\infty} \sum_{k=1}^{N-1} \beta(m-|\ell-k|,k) \{\delta(t-(m-1-|\ell-k|)\Delta T) - \delta(t-(m-|\ell-k|)\Delta T)\} \int_{(k-.5)\Delta z}^{(k+.5)\Delta z} \frac{dz'}{\sqrt{(z-z')^2 + a^2}} \tag{72}$$

The time integration of $\left\langle \frac{\partial A_z}{\partial t}, S_{j,\ell} \right\rangle$ is readily performed since over the interval $(j-.5)\Delta T \leq t \leq (j+.5)\Delta T$, only the impulses corresponding to $m = j$ and $m = j+1$ give a non-zero result. Thus

$$\left\langle \frac{\partial A_z}{\partial t}, S_{j,\ell} \right\rangle \approx \left(\frac{\mu}{4\pi}\right) \sum_{k=1}^{N-1} \left(\frac{\beta(j+1-|\ell-k|,k) - \beta(j-|\ell-k|,k)}{\Delta T} \right) \left(\frac{1}{\Delta z} \int_{(\ell-.5)\Delta z}^{(\ell+.5)\Delta z} dz \left[\int_{(k-.5)\Delta z}^{(k+.5)\Delta z} \frac{dz'}{\sqrt{(z-z')^2 + a^2}} \right] \right) \tag{73}$$

The summation proceeds over the index k such that $j-|k-\ell| \geq 1$, $j = 1,2,\ldots$ and $\ell = 1,2,\ldots,N-1$. For $j = 0$, only the single term

$$\left\langle \frac{\partial A_z}{\partial t}, S_{0,\ell} \right\rangle = \frac{\mu}{4\pi} \left(\frac{\beta(1,\ell)}{\Delta T}\right) \left[\frac{1}{\Delta z} \int_{(\ell-.5)\Delta z}^{(\ell+.5)\Delta z} \int_{(\ell-.5)\Delta z}^{(\ell+.5)\Delta z} \frac{dz\, dz'}{\sqrt{(z-z')^2 + a^2}} \right]$$

$$\ell = 1,2,\ldots,N-1 \tag{74}$$

is present. It is shown in Appendix B that the double integrals are functions only of the absolute value of the difference of the source and

field indices and are defined as $G(|\ell-k|)$. Equations (73) and (74) may be rewritten in terms of these functions as

$$\left\langle \frac{\partial A_z}{\partial t}, S_{j,\ell} \right\rangle \approx \frac{\mu}{4\pi} \sum_{k=1}^{N-1} \left(\frac{\beta(j+1-|\ell-k|,k) - \beta(j-|\ell-k|,k)}{\Delta T} \right) G(|\ell-k|) \qquad (75)$$

$$\text{for } j > 0$$

and

$$\left\langle \frac{\partial A_z}{\partial t}, S_{0,\ell} \right\rangle \approx \frac{\mu}{4\pi} \left(\frac{\beta(1,\ell)}{\Delta T} \right) G(0) \qquad \text{for } j = 0 \qquad (76)$$

The form of (75) and (76) is similar to the difference equation approximation developed in the previous chapter. The essential difference is in the interpretation given the testing operation in terms of a local average. Figure B.3-1 of Appendix B compares the geometry functions. In general when $|\ell-k|$ is a small integer value the pulse tested geometry functions G are somewhat less than the point tested geometry functions F. This is a result of the averaging operation inherent in using the pulse tested formulation. Equation (75) may be written in an equivalent form using the average vector potentials defined below. Thus

$$\left\langle \frac{\partial A_z}{\partial t}, S_{j,\ell} \right\rangle = \frac{\bar{A}_z(t_{j+1}, z_\ell) - \bar{A}_z(t_j, z_\ell)}{\Delta T} \qquad (77)$$

where

$$\bar{A}_z(t_{j+1}, z_\ell) = \frac{\mu}{4\pi} \sum_{k=1}^{N-1} \beta(j+1-|\ell-k|,k) G(|\ell-k|) \quad , \; j+1-|\ell-k| \geq 1 \qquad (78)$$

and

$$\bar{A}_z(t_j, z_\ell) = \frac{\mu}{4\pi} \sum_{k=1}^{N-1} \beta(j-|\ell-k|,k) G(|\ell-k|) \qquad j-|\ell-k| \geq 1 \qquad (79)$$

The pulse tested vector potential contribution is seen to be equivalent to the time domain difference approximation of the derivative of the average vector potential $\bar{A}_z$.

The final term of (59) to be evaluated is the scalar potential contribution to the electric field:

$$\left\langle \frac{\partial \Phi}{\partial z}, S_{j,\ell} \right\rangle = \left(\frac{1}{\Delta T \Delta z}\right) \left(\int_{(j-.5)\Delta T}^{(j+.5)\Delta T} dt \int_{(\ell-.5)\Delta z}^{(\ell+.5)\Delta z} \frac{\partial \Phi}{\partial z} \, dz \right) \tag{80}$$

It is convenient to replace the derivative $\frac{\partial \Phi}{\partial z}$ with the difference approximation

$$\frac{\partial \Phi}{\partial z} \approx \frac{\Phi(t, z+(\Delta z/2)) - \Phi(t, z-(\Delta z/2))}{\Delta z} \tag{81}$$

The substitution of (81) into (80) results in the following approximate expression for $\left\langle \frac{\partial \Phi}{\partial z}, S_{j,\ell} \right\rangle$:

$$\left\langle \frac{\partial \Phi}{\partial z}, S_{j,\ell} \right\rangle = \left(\frac{1}{\Delta T \Delta z}\right) \left[\int_{(j-.5)\Delta T}^{(j+.5)\Delta T} dt \left(\int_{(\ell-.5)\Delta z}^{(\ell+.5)\Delta z} \left[\frac{\Phi(t, z+(\Delta z/2)) - \Phi(t, z-(\Delta z/2))}{\Delta z} \right] \right) \right] \tag{82}$$

Each scalar potential in (82) will be examined individually. The substitution of the charge density expansion (63) into (23) gives the scalar potentials $\Phi(t, z \pm \frac{\Delta z}{2})$ as

$$\Phi(t, z \pm \frac{\Delta z}{2}) = \frac{1}{4\pi\epsilon} \sum_{m=1}^{\infty} \sum_{k=1}^{N} \int_{(k-1)\Delta z}^{k\Delta z} \left(\frac{\gamma(m-(\tau/\Delta T), k) dz'}{\sqrt{(z \pm (\Delta z/2) - z')^2 + a^2}} \right) P_2(t-(m-.5-\tau/\Delta T)\Delta T) \tag{83}$$

with

$$\tau = \frac{|z \pm (\Delta z/2) - z'|}{v_p}$$

Following substitution of (83) into (82), the time integration may be performed immediately, leaving the z integration,

$$\left\langle \frac{\partial \Phi}{\partial z}, S_{j,\ell} \right\rangle \approx \left(\frac{1}{\Delta z}\right) \int_{(\ell-.5)\Delta z}^{(\ell+.5)\Delta z} \left[\frac{\Phi(t_j, z+(\Delta z/2)) - \Phi(t_j, z-(\Delta z/2))}{\Delta z} \right] dz \tag{84}$$

to be performed. The potentials $\Phi(t_j, z \pm \Delta z/2)$ are given by

$$\Phi(t_j, z \pm \frac{\Delta z}{2}) = \frac{1}{4\pi\epsilon} \sum_{k=1}^{N} \int_{(k-1)\Delta z}^{k\Delta z} \frac{\gamma(j - (\tau/\Delta T), k)dz'}{\sqrt{(z \pm (\Delta z/2) - z')^2 + a^2}} \qquad j \neq 0$$

$$= 0 \qquad j = 0 \tag{85}$$

Integration of (84) is accomplished with the following changes in the variable of integration. In the first term of (84), let $\eta = z + \frac{\Delta z}{2}$, and in the second, let $\xi = z - \frac{\Delta z}{2}$. Equation (84) can then be written:

$$\left\langle \frac{\partial \Phi}{\partial z}, S_{j,\ell} \right\rangle = \frac{1}{\Delta z}[\bar{\Phi}(t_j, z_{\ell+1}) - \bar{\Phi}(t_j, z_\ell)] \tag{86}$$

where

$$\bar{\Phi}(t_j, z_{\ell+1}) = \frac{1}{4\pi \epsilon \Delta z} \left[\int_{\ell\Delta z}^{(\ell+1)\Delta z} d\eta \left(\sum_{k=1}^{N} \int_{(k-1)\Delta z}^{k\Delta z} \frac{\gamma(j - (|\eta - z'|/\Delta z), k)dz'}{\sqrt{(\eta - z')^2 + a^2}} \right) \right] \tag{87}$$

and

$$\bar{\Phi}(t_j, z_\ell) = \frac{1}{4\pi \epsilon \Delta z} \left[\int_{(\ell-1)\Delta z}^{\ell\Delta z} d\xi \left(\sum_{k=1}^{N} \int_{(k-1)\Delta z}^{k\Delta z} \frac{\gamma(j - (|\xi - z'|/\Delta z), k)dz'}{\sqrt{(\xi - z')^2 + a^2}} \right) \right] \tag{88}$$

The mean time delay approximations (69) and (70) will be used in evaluating (87) and (88). Over the domain of integration, the time delay is now a constant; hence the charge coefficients can be moved outside of the integrals.

Thus (87) and (88) can be written as

$$\overline{\Phi}(t_j, z_{\ell+1}) = \left(\frac{1}{4\pi\ \epsilon\ \Delta z}\right) \sum_{k=1}^{N} \gamma(j-|\ell+1-k|, k) \left[\int_{\ell\Delta z}^{(\ell+1)\Delta z} d\eta \int_{(k-1)\Delta z}^{k\Delta z} \frac{dz'}{\sqrt{(\eta-z')^2 + a^2}} \right] \tag{89}$$

and

$$\overline{\Phi}(t_j, z_{\ell}) = \left(\frac{1}{4\pi\ \epsilon\ \Delta z}\right) \sum_{k=1}^{N} \gamma(j-|\ell-k|, k) \left[\int_{(\ell-1)\Delta z}^{\ell\Delta z} d\xi \int_{(k-1)\Delta z}^{k\Delta z} \frac{dz'}{\sqrt{(\xi-z')^2 + a^2}} \right] \tag{90}$$

The double integral terms are recognized as the pulse tested geometry functions $G(|\ell+1-k|)$ and $G(|\ell-k|)$. Equations (89) and (90) are rewritten in terms of these functions as

$$\overline{\Phi}(t_j, z_{\ell+1}) = \left(\frac{1}{4\pi\epsilon}\right) \sum_{k=1}^{N} \gamma(j-|\ell+1-k|, k)\ G(|\ell+1-k|) \tag{91}$$

$$\overline{\Phi}(t_j, z_{\ell}) = \left(\frac{1}{4\pi\epsilon}\right) \sum_{k=1}^{N} \gamma(j-|\ell-k|, k)\ G(|\ell-k|) \tag{92}$$

$$\begin{aligned} j &= 1, 2, \ldots \\ \ell &= 1, 2, \ldots, N-1 \end{aligned}$$

The summations proceed over the index k such that neither $j-|\ell+1-k|$ nor $j-|\ell-k|$ is less than unity. The substitution of (91) and (92) into (86) shows that the scalar potential contribution is the same as if the difference approximation to the z derivative had been applied to the average potential over a subsection.

The contribution the right-hand side of (59) will be combined to construct an iterative algorithm of the same type developed in Chapter 2.

Advantage will be taken of the same basic program structure already developed.

3.3. The Development of Pulse Tested Algorithms for the Wire as a Scatterer and an Antenna

3.3-1. The Wire as a Scatterer

For $j = 0$, Equations (61), (64), and (76) are applicable. The pulse tested electric field is written,

$$\bar{E}_z^i(0,z_\ell) = \frac{\Omega(\ell)}{2}\beta(1,\ell) + \left(\frac{\mu}{4\pi}\right)\frac{\beta(1,\ell)}{\Delta T}G(0) \tag{93}$$

and solved for the $\beta(1,\ell)$'s,

$$\beta(1,\ell) = \frac{\bar{E}_z^i(0,z_\ell)}{(\Omega(\ell)/2) + (\mu G(0)/4\pi\Delta T)} \qquad \ell = 1,2,\ldots,N-1 \tag{94}$$

The first set of charge coefficients is given by (36a,b,c). The scalar potentials $\bar{\Phi}(t_1,z_{\ell+1})$ and $\bar{\Phi}(t_1,z_\ell)$ are calculated by substitution of the first set of charge coefficients into (91) and considering the sum to run over a single index $k = \ell$, for $\ell = 1,2,\ldots,N$.

For $j > 0$, the electric field is given by substitution of (61), (65), (77), and (86) into (59).

$$\bar{E}_z^i(t_j,z_\ell) = \frac{\Omega(\ell)}{2}[\beta(j,\ell)+\beta(j+1,\ell)] + \left[\frac{\bar{A}_z(t_{j+1},z_\ell) - \bar{A}_z(t_j,z_\ell)}{\Delta T}\right] + \left[\frac{\bar{\Phi}(t_j,z_{\ell+1}) - \bar{\Phi}(t_j,z_\ell)}{\Delta z}\right] \tag{95}$$

The unknown current coefficients $\beta(j+1,\ell)$ only enter into the ohmic contribution $\Omega(\ell)\,\beta(j+1,\ell)/2$, and the vector potential $\bar{A}_z(t_{j+1},z_\ell)$. Equation (95) can be readily solved for the unknown coefficients. Thus,

$$\beta(j+1,\ell) = \frac{\bar{E}_z^i(t_j,z_\ell)-(\Omega(\ell)/2)\beta(j,\ell)-(1/\Delta T)[\Delta\bar{A}]-(1/\Delta z)[\Delta\bar{\Phi}]}{[\Omega(\ell)/2 + (\mu G(0)/4\pi\Delta T)]} \tag{96}$$

Here,

$$\Delta\bar{A} = \bar{a}_z(t_{j+1},z_\ell) - \bar{A}_z(t_j,z_\ell). \tag{97}$$

and

$$\Delta\bar{\Phi} = \bar{\Phi}(t_j,z_{\ell+1}) - \bar{\Phi}(t_j,z_\ell) \tag{98}$$

$\bar{A}_z(t_j,z_\ell)$ is given by (79) and $\bar{a}_z(t_{j+1},z_\ell)$ is given by

$$\bar{a}_z(t_{j+1},z_\ell) = \frac{\mu}{4\pi}\sum_{\substack{k=1\\k\neq\ell}}^{N-1} \beta(j+1-|\ell-k|,k)\ G(|\ell-k|) \tag{99}$$

The summation in (99) proceeds over the index k such that $j-|\ell-k| \geq 0$. The scalar potentials are given by (91) and (92).

In Chapter 2 it was shown that the expression for the point tested current could be interpreted as the ratio of a voltage to a resistance term. Equation (96) may be rewritten to reflect a similar interpretation:

$$\beta(j+1,\ell) = \frac{\bar{V}_z^i(t_j,z_\ell) - R(\ell)\beta(j,\ell)/2 - v_p\Delta\bar{A} - \Delta\bar{\Phi}}{[R(\ell)/2 + \eta G(0)/4\pi)]} \tag{100}$$

Here, η is the wave impedance of the surrounding medium, v_p the velocity of propagation in the surrounding medium, and $R(\ell)$ the resistance of the ℓ-th subsection, $\Delta z\Omega(\ell)$. The exciting voltage $\bar{V}_z^i(t_j,z_\ell)$ may be either an impressed voltage or the equivalent voltage

$$\bar{V}^i(t_j,z_\ell) = \bar{E}_z^i(t_j,z_\ell)\Delta z \tag{101}$$

The remaining terms in the numerator of (100) are the voltage due to the time rate of change of the magnetic flux linking the ℓ-th subsection and the scalar potential difference across the ℓ-th subsection. The denominator is the sum of the self impedance $\eta G(0)/4\pi$ and the conduction resistance $\frac{R(\ell)}{2}$. The factor $\eta G(0)/4\pi$ is a measure of the interaction of the subsection with the excitation.

When the straight wire is excited as an antenna, (100) is somewhat modified to reflect the localized excitation. In the excited subsection, the driving point current is given by

$$\beta(j+1,p) = \frac{\bar{V}^i(t_j,z_p) - R_g(p)\beta(j,p)/2. - v_p\Delta\bar{A} - \Delta\bar{\Phi}}{[R_g(p)/2. + \eta G(0)/4\pi]} \tag{102}$$

and, at the loaded ports

$$\beta(j+1,\ell) = -\frac{R_L(\ell)\beta(j,\ell)/2. + v_p\Delta\bar{A} - \Delta\bar{\Phi}}{[R_L(\ell)/2. + \eta G(0)/4\pi]} \qquad \ell \neq P \tag{103}$$

Conduction losses are assumed to be included in the source resistance $R_g(p)$ or the load resistances $R_L(\ell)$. The exciting voltage applied to the p-th subsection is given for $j = 0$ by

$$\bar{V}^i(t_0,z_p) = \frac{1}{\Delta T\Delta z}\int_0^{.5\Delta T} dt \int_{(p-.5)\Delta z}^{(p+.5)\Delta z} v^i(t,z)dz \tag{104}$$

and for $j > 0$ by

$$\bar{V}^i(t_j,z_p) = \frac{1}{\Delta T\Delta z}\int_{(j-.5)\Delta T}^{(j+.5)\Delta T} dt \int_{(p-.5)\Delta z}^{(p+.5)\Delta z} v^i(t,z)dz \tag{105}$$

For $j = 0$, (102) is further specialized to

$$\beta(1,p) = \frac{\overline{V}^i(0,z_p)}{[R_g(p)/2.+nG(0)/4\pi]} \quad , \qquad \ell = p \tag{106}$$

and

$$\beta(1,\ell) = 0 \qquad\qquad \ell \neq p$$

The same procedure as discussed earlier is used to find the charge coefficients and the vector and scalar potentials.

3.4. Summary of the Pulse Tested Algorithm

1) Calculate the pulse tested geometry functions from equations B.2-4 and B.2-5.

2) Calculate the initial current coefficients from (94) or (106), the initial vector potentials from (76), the initial sets of charge coefficients from (36a,b,c).

3) Advance the time index by unity.

4) Calculate the first set of scalar potentials from (91) and (92).

5) Calculate the next set of current coefficients from (100) or (102) and (103). Calculate the next set of vector potentials from (75), and charge coefficients from (36d,e,f).

6) Go back to 3).

A computer program has been written to implement these steps. The program instructions appear in Appendix C. The program is written in Fortran IV and results were computed on an IBM 360/50 computer located at Syracuse University.

3.5. Pulse Tested Computed Results

Similar pulse tested computations will be presented for the straight wire as an antenna and scatterer as were presented in Chapter 2. The pulse tested results for the straight wire antenna do not differ substantially from the point tested results. Figures 3.2 and 3.3 show the driving point current for the center fed dipole antenna ($\ell/2a = 74.2$) for $R_g = 50\ \Omega$ and 100 Ω respectively. The importance of the latter case is that it is approximately the matched condition, i.e., $R_g \approx \eta G(0)/4\pi$, and is useful in a discussion of the transmission line model of the dipole considered by a number of authors.[9,10,11]

A detailed discussion of this point will be delayed until the last chapter of the paper. The current and charge distributions for $R_g = 50\ \Omega$ are essentially the same as those found in Figure 2.9. It is to be noted that increasing the generator resistance does not change the general shape of the time response but does cause it to decay faster. Frequency domain considerations would interpret this as increasing the real part of the poles of the current response while leaving the imaginary parts unchanged. This observation is an aid in determining the reflection coefficient of the end of a wire.

The pulse tested tangential incident electric field is shown in Figure 3.4. The effect of the pulse testing operation can be seen if this figure is compared to Figure 2.10. The pulse testing operation gives the average tangential field in the neighborhood of a point of time t over a given subsection, whereas point testing gives the value of the tangential electric field in the center of a subsection at the point of

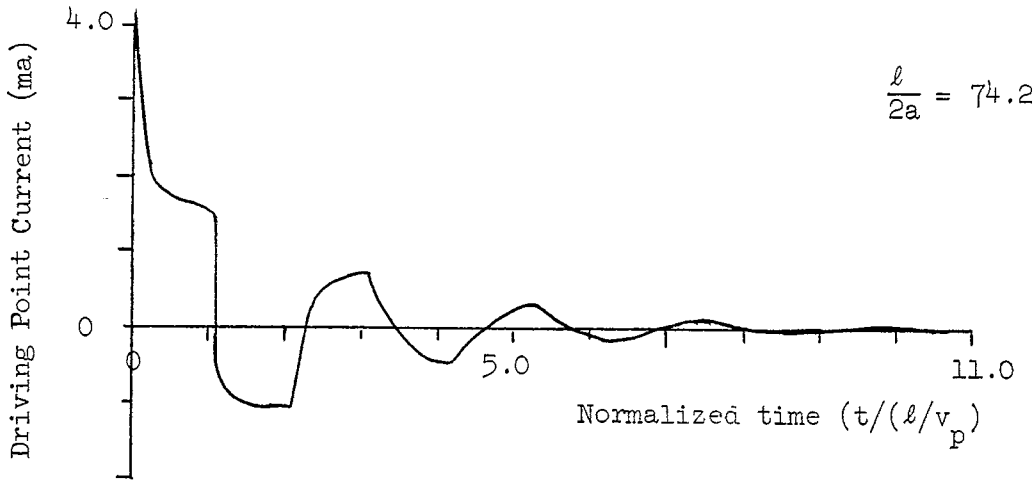

Pulse Tested Center Fed Antenna
Driving Point Current $R_g = 50.0$

Figure 3.2

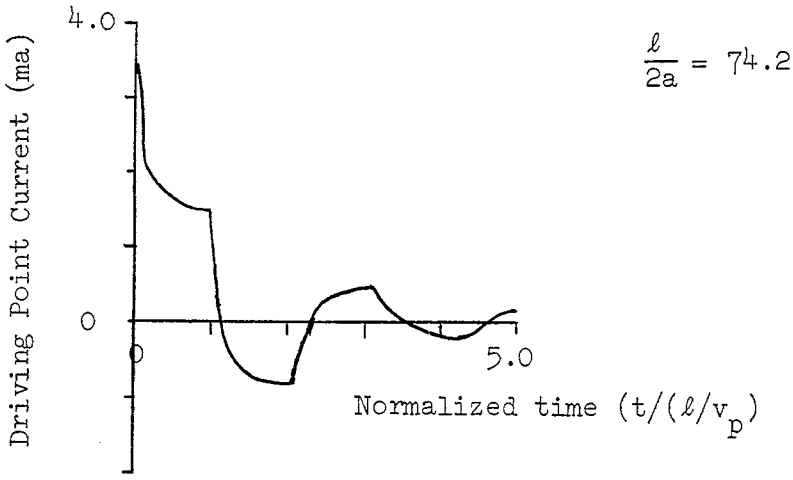

Pulse Tested Center Fed Antenna
Driving Point Current $R_g = 100.0$

Figure 3.3

INCIDENT TANGENTIAL ELECTRIC FIELD

TIME =	0.0	0.05	0.10	0.15	0.20	0.25	0.30	0.35	0.40	0.45
1	0.164E 00	0.500E 00	0.500E 00	0.500E 00	0.500E 00	0.500E 00	0.500E 00	0.500E 00	0.500E 00	0.500E 00
2	0.0	0.202E 00	0.500E 00	0.500E 00	0.500E 00	0.500E 00	0.500E 00	0.500E 00	0.500E 00	0.500E 00
3	0.0	0.0	0.241E 00	0.500E 00	0.500E 00	0.500E 00	0.500E 00	0.500E 00	0.500E 00	0.500E 00
4	0.0	0.0	0.0	0.500E 00	0.500E 00	0.500E 00	0.500E 00	0.500E 00	0.500E 00	0.500E 00
5	0.0	0.0	0.0	0.297E-01	0.500E 00	0.500E 00	0.500E 00	0.500E 00	0.500E 00	0.500E 00
6	0.0	0.0	0.0	0.0	0.684E-01	0.500E 00	0.500E 00	0.500E 00	0.500E 00	0.500E 00
7	0.0	0.0	0.0	0.0	0.0	0.107E 00	0.500E 00	0.500E 00	0.500E 00	0.500E 00
8	0.0	0.0	0.0	0.0	0.0	0.0	0.146E 00	0.500E 00	0.500E 00	0.500E 00
9	0.0	0.0	0.0	0.0	0.0	0.0	0.0	0.184E 00	0.500E 00	0.500E 00
10	0.0	0.0	0.0	0.0	0.0	0.0	0.0	0.0	0.223E 00	0.500E 00
11	0.0	0.0	0.0	0.0	0.0	0.0	0.0	0.0	0.0	0.250E 00
12	0.0	0.0	0.0	0.0	0.0	0.0	0.0	0.0	0.0	0.118E-01
13	0.0	0.0	0.0	0.0	0.0	0.0	0.0	0.0	0.0	0.0
14	0.0	0.0	0.0	0.0	0.0	0.0	0.0	0.0	0.0	0.0
15	0.0	0.0	0.0	0.0	0.0	0.0	0.0	0.0	0.0	0.0
16	0.0	0.0	0.0	0.0	0.0	0.0	0.0	0.0	0.0	0.0
17	0.0	0.0	0.0	0.0	0.0	0.0	0.0	0.0	0.0	0.0
18	0.0	0.0	0.0	0.0	0.0	0.0	0.0	0.0	0.0	0.0
19	0.0	0.0	0.0	0.0	0.0	0.0	0.0	0.0	0.0	0.0
20	0.0	0.0	0.0	0.0	0.0	0.0	0.0	0.0	0.0	0.0

TIME =	0.50	0.55	0.60	0.65	0.70	0.75	0.80	0.85	0.90	0.95
1	0.500E 00	0.500E 00	0.500E 00	0.500E 00	0.500E 00	0.500E 00	0.500E 00	0.500E 00	0.500E 00	0.500E 00
2	0.500E 00	0.500E 00	0.500E 00	0.500E 00	0.500E 00	0.500E 00	0.500E 00	0.500E 00	0.500E 00	0.500E 00
3	0.500E 00	0.500E 00	0.500E 00	0.500E 00	0.500E 00	0.500E 00	0.500E 00	0.500E 00	0.500E 00	0.500E 00
4	0.500E 00	0.500E 00	0.500E 00	0.500E 00	0.500E 00	0.500E 00	0.500E 00	0.500E 00	0.500E 00	0.500E 00
5	0.500E 00	0.500E 00	0.500E 00	0.500E 00	0.500E 00	0.500E 00	0.500E 00	0.500E 00	0.500E 00	0.500E 00
6	0.500E 00	0.500E 00	0.500E 00	0.500E 00	0.500E 00	0.500E 00	0.500E 00	0.500E 00	0.500E 00	0.500E 00
7	0.500E 00	0.500E 00	0.500E 00	0.500E 00	0.500E 00	0.500E 00	0.500E 00	0.500E 00	0.500E 00	0.500E 00
8	0.500E 00	0.500E 00	0.500E 00	0.500E 00	0.500E 00	0.500E 00	0.500E 00	0.500E 00	0.500E 00	0.500E 00
9	0.500E 00	0.500E 00	0.500E 00	0.500E 00	0.500E 00	0.500E 00	0.500E 00	0.500E 00	0.500E 00	0.500E 00
10	0.500E 00	0.500E 00	0.500E 00	0.500E 00	0.500E 00	0.500E 00	0.500E 00	0.500E 00	0.500E 00	0.500E 00
11	0.500E 00	0.500E 00	0.500E 00	0.500E 00	0.500E 00	0.500E 00	0.500E 00	0.500E 00	0.500E 00	0.500E 00
12	0.500E 00	0.500E 00	0.500E 00	0.500E 00	0.500E 00	0.500E 00	0.500E 00	0.500E 00	0.500E 00	0.500E 00
13	0.504E-01	0.500E 00	0.500E 00	0.500E 00	0.500E 00	0.500E 00	0.500E 00	0.500E 00	0.500E 00	0.500E 00
14	0.0	0.891E-01	0.500E 00	0.500E 00	0.500E 00	0.500E 00	0.500E 00	0.500E 00	0.500E 00	0.500E 00
15	0.0	0.0	0.128E 00	0.500E 00	0.500E 00	0.500E 00	0.500E 00	0.500E 00	0.500E 00	0.500E 00
16	0.0	0.0	0.0	0.166E 00	0.500E 00	0.500E 00	0.500E 00	0.500E 00	0.500E 00	0.500E 00
17	0.0	0.0	0.0	0.0	0.205E 00	0.500E 00	0.500E 00	0.500E 00	0.500E 00	0.500E 00
18	0.0	0.0	0.0	0.0	0.0	0.244E 00	0.500E 00	0.500E 00	0.500E 00	0.500E 00
19	0.0	0.0	0.0	0.0	0.0	0.0	0.500E 00	0.500E 00	0.500E 00	0.500E 00
20	0.0	0.0	0.0	0.0	0.0	0.0	0.325E-01	0.500E 00	0.500E 00	0.500E 00

Pulse Tested Incident Tangential Electric Field for $\theta_{INC} = 30^{\circ}$

Figure 3.4

time t. If the incident field has not yet reached the midpoint of a subsection at t, the point tested algorithm gives a zero result. This has been found to introduce large errors in the scatterer formulation, and hence the improvement due to the pulse testing algorithm. The current and charge induced by this excitation is shown in Figure 3.5. The improvement is apparent when this figure is compared to Figure 2.11. The sawtooth nature of the results is due to the errors introduced in the average time delay approximation. It is felt that an improved approximation to time delay would improve the solution. Because of the averaging operation inherent in the pulse tested solutions, averaging of adjacent points would also improve the smoothness of the solution.

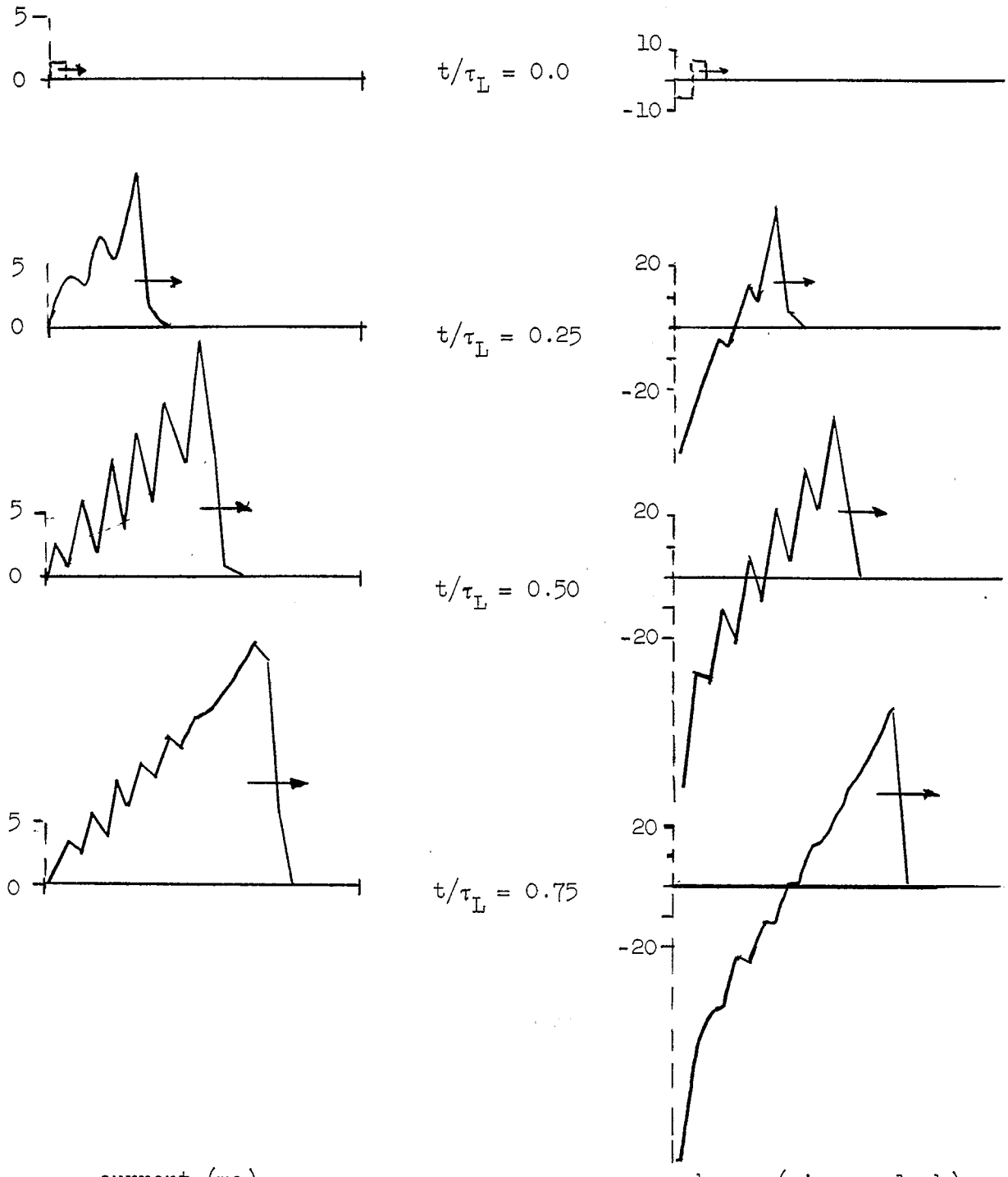

Pulse Tested Current and Charge on a Wire Scatterer $\theta_{INC} = 30^{\circ}$

Figure 3.5

Chapter 4

EVALUATION OF THE STRAIGHT WIRE RADIATION FIELD BY RECIPROCITY METHODS

The time dependent radiation field will be calculated for the straight wire by pulse testing the Reciprocity Theorem developed in Appendix A.

4.1. The Far Field Algorithm

The reciprocity theorem is conveniently written

$$\left\langle \underset{\sim}{E}_1(t,\xi),\ \underset{\sim}{I}_2(t,\xi) \right\rangle = \left\langle \underset{\sim}{I}_1(t,z'),\ \underset{\sim}{E}_2(t,z') \right\rangle \tag{107}$$

Here, $\underset{\sim}{I}_1$ is assumed to be the current on the straight wire, and $\underset{\sim}{I}_2$ is the testing current at the far field point. The fields $\underset{\sim}{E}_1$ and $\underset{\sim}{E}_2$ are the fields excited by $\underset{\sim}{I}_1$ and $\underset{\sim}{I}_2$, respectively. $\underset{\sim}{E}_1$ is calculated from the retarded potential integral solution operating on the causal current $\underset{\sim}{I}_1$. $\underset{\sim}{E}_2$ is an anti-causal function, that is, it vanishes for $t > 0$, and is calculated from the advanced potential integral solution operating on the current $\underset{\sim}{I}_2$ which is itself anti-causal. The advanced potential operator is shown in Appendix A to be the adjoint operator to the retarded potential operator. The domain $-\infty < t < 0$ is referred to as the adjoint time domain. Interpretation of the field $\underset{\sim}{E}_2$ and its relationship to the source $\underset{\sim}{I}_2$ is found in Welsh.[13] Summarizing his discussion, $\underset{\sim}{E}_2$ can be thought of as either an outward propagating field excited by $\underset{\sim}{I}_2$ with time running backwards from $t = 0$, or $\underset{\sim}{E}_2$ is an inward propagating wave which excites $\underset{\sim}{I}_2$ with time starting from $t = +\infty$.

The far field testing current is assumed to flow in the $\hat{u}_\theta$ direction, where $\hat{u}_\theta$ is a unit vector directed in the θ direction of the standard

spherical coordinate system as defined in Harrington.[24] Since the radiation field of the straight wire is azimuthally symmetric, the testing current can be considered to always lie in the plane of incidence. The testing current is written

$$\underset{\sim}{I}_2(t,\xi) = \left(\frac{1}{\Delta\xi\Delta T}\right) P_1(\xi-\xi_0)\, P_2(t-\tau-t_0)\hat{u}_\theta \tag{108}$$

The transit time between the time reference and the field point is τ, t_0 is an arbitrary time delay and $\Delta\xi = v_p\Delta T$. The latter assures a uniform quantization of the time domain throughout the problem. Equation (28) will be used to define the inner product relationships. The left-hand side of (107) will be termed $\bar{E}_\theta$ (the subscript indicating the far field direction). Thus,

$$\bar{E}_\theta = \left\langle \underset{\sim}{E}_1(t,\xi),\ \underset{\sim}{I}_2(t,\xi) \right\rangle = \frac{1}{\Delta\xi\Delta T} \int_{\xi_0}^{\xi_0+\Delta\xi} d\xi \left[\int_{t_0}^{t_0+\Delta T} |\underset{\sim}{E}_1(t'+\tau)|\, dt' \right] \tag{109}$$

The barred notation is indicative of the averaging operation in the vicinity of $\left(t_0 + \frac{\Delta T}{2}, \xi_0 + \frac{\Delta\xi}{2}\right)$. The time axis was shifted in (109) to remove the time delay between the source and field point. The far field excited by $\underset{\sim}{I}_2$ can be written

$$\underset{\sim}{E}_2(t,R) = -\frac{\mu}{4\pi}\left(\frac{1}{R}\right)\frac{\partial}{\partial t} \int_{\xi} \underset{\sim}{I}_2(t+\tau,\xi)\, d\xi \tag{110}$$

where R is the distance from a reference point on the wire to the field point. The substitution of $\underset{\sim}{I}_2$ given by (108) into (110) results in the expression for the electric field $\underset{\sim}{E}_2$ in the vicinity of the wire object:

$$\underset{\sim}{E}_2(t,R) = -\frac{\mu}{4\pi}\left(\frac{1}{R}\right)\frac{\delta(-t+t_0)\quad \delta(-t+t_0+\Delta T)}{\Delta T}\ \hat{U}_\theta \tag{111}$$

The right-hand side of (107) is evaluated after the substitution of (111) and the current expansion (62). The dot product between $\underset{\sim}{E}_2$ and $\underset{\sim}{I}_1$ is taken and the time dependence of (111) must be modified to reflect that time is now measured with respect to the tangential coordinates of the current. The result of this operation is shown in (112).

$$\underset{\sim}{I}_1(t,z'),\underset{\sim}{E}_2(t,z') =$$

$$-\left(\frac{\mu}{4\pi}\right)\left(\frac{\sin\theta_R}{\Delta T}\right)\int_0^\infty dt\int_0^\ell\left[\frac{\delta(t-t_0+(z'/v_p)\cos\theta_R)-\delta(t-t_0-\Delta T+(z/v_p)\cos\theta_R)}{R_0}\right]$$

$$\sum_{m=1}^{\infty}\sum_{k=1}^{N-1}\beta(m,k)P_1(z'-(k-.5)\Delta z)P_2(t-(m-1)\Delta T)dz' \tag{112}$$

where R_0 is the distance between the field point to the time reference of $\underset{\sim}{I}_1$. The geometry is shown in Figure 4.1.

The time and space integrations are interchanged in (112) and the time integration performed. The sampling property of the impulses picks out the proper current coefficients which contribute to the radiation field at the time t'. The resultant of the time and spatial integrations can be shown to be

$$\underset{\sim}{I}_1(t,z'),\underset{\sim}{E}_2(t,z') =$$

$$-\frac{\mu}{4\pi}\frac{\sin\theta_R}{R_0}\sum_{k=1}^{N-1}\int_{(k-.5)\Delta z}^{(k+.5)\Delta z}\left[\frac{\beta(\xi,k)-\beta(\xi-1,k)}{\Delta T}\right]dz \tag{113}$$

where $\xi = \overset{*}{\text{Fix}}[t_0/\Delta T + z'/\Delta z\ \cos\theta_R]$.

*The function Fix(x) gives the largest integer less than or equal to x.

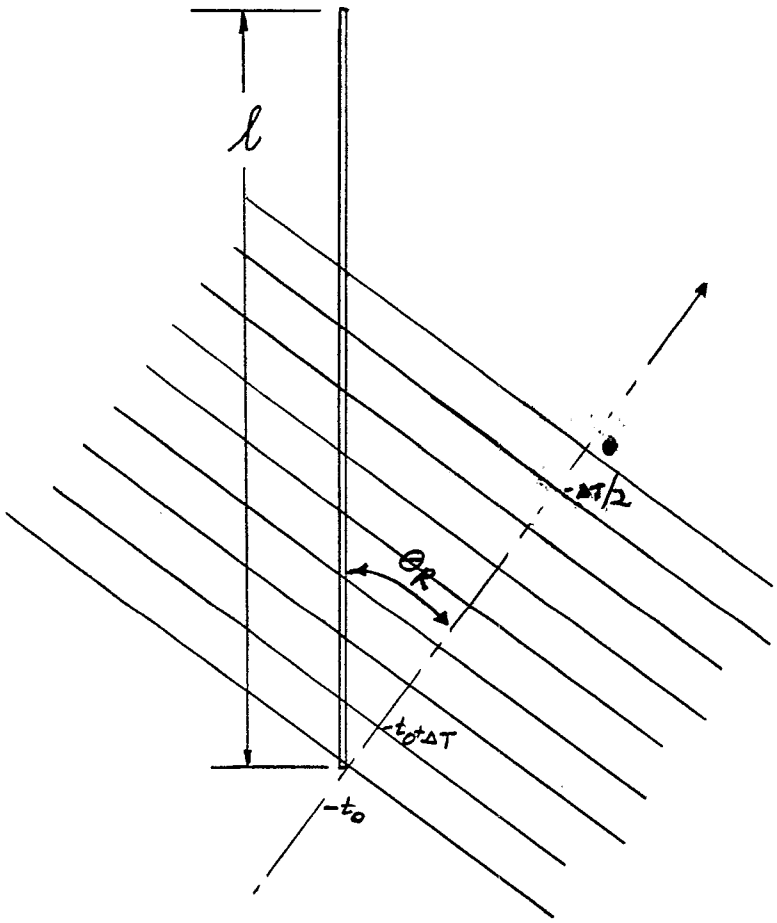

Propagation of Testing Field $\underset{\sim}{E}_2$
Over the Straight Wire

Figure 4.1

Equation (113) may be viewed as a line integral in the t-z plane. The integration path is shown in Figure 4.2 for $t_0 = (j-.5)\Delta T$, $j = 1,2,\ldots$ Note that for broadside incidence the time delay is zero.

A subroutine has been written to compute the normalized far field $R_0 \left\langle \underset{\sim}{I}_1(t,z'), \underset{\sim}{E}_2(t,z') \right\rangle$. The subroutine is listed in Appendix C.

4.2. Results

The normalized field scattered by a linear wire has been evaluated for both the point tested and pulse tested results of the preceding chapters. Figure 4.3 shows the wire excited by a unit step plane wave electric field from the direction $\theta_{INC} = 30^\circ$. The current was found using the point tested algorithm of Chapter 2. The time axis major divisions are normalized with respect to the transit time of the wire $\tau_L = L/v_p$. Major divisions of the ordinate correspond to 1 volt/meter. The normalized scattered field for identical excitation but using the pulse tested algorithm is shown in Figure 4.4. Comparison of the far fields demonstrates the improvement which results from the pulse tested algorithm. The time reference $t = 0$ is the point first struck by the incident wavefront.

The far field algorithm has also been used to evaluate the radiation field of a dipole antenna. Again, both point and pulse tested solutions have been compared. Figure 4.5 shows the normalized far field radiated by a center fed dipole excited by a unit step voltage source with 50 ohm internal resistance. The effect of the load is evident in the broadside field (90°) where the field strength takes a sudden drop at $t/\tau_L = 1$. This is a discontinuity introduced by the source resistance.

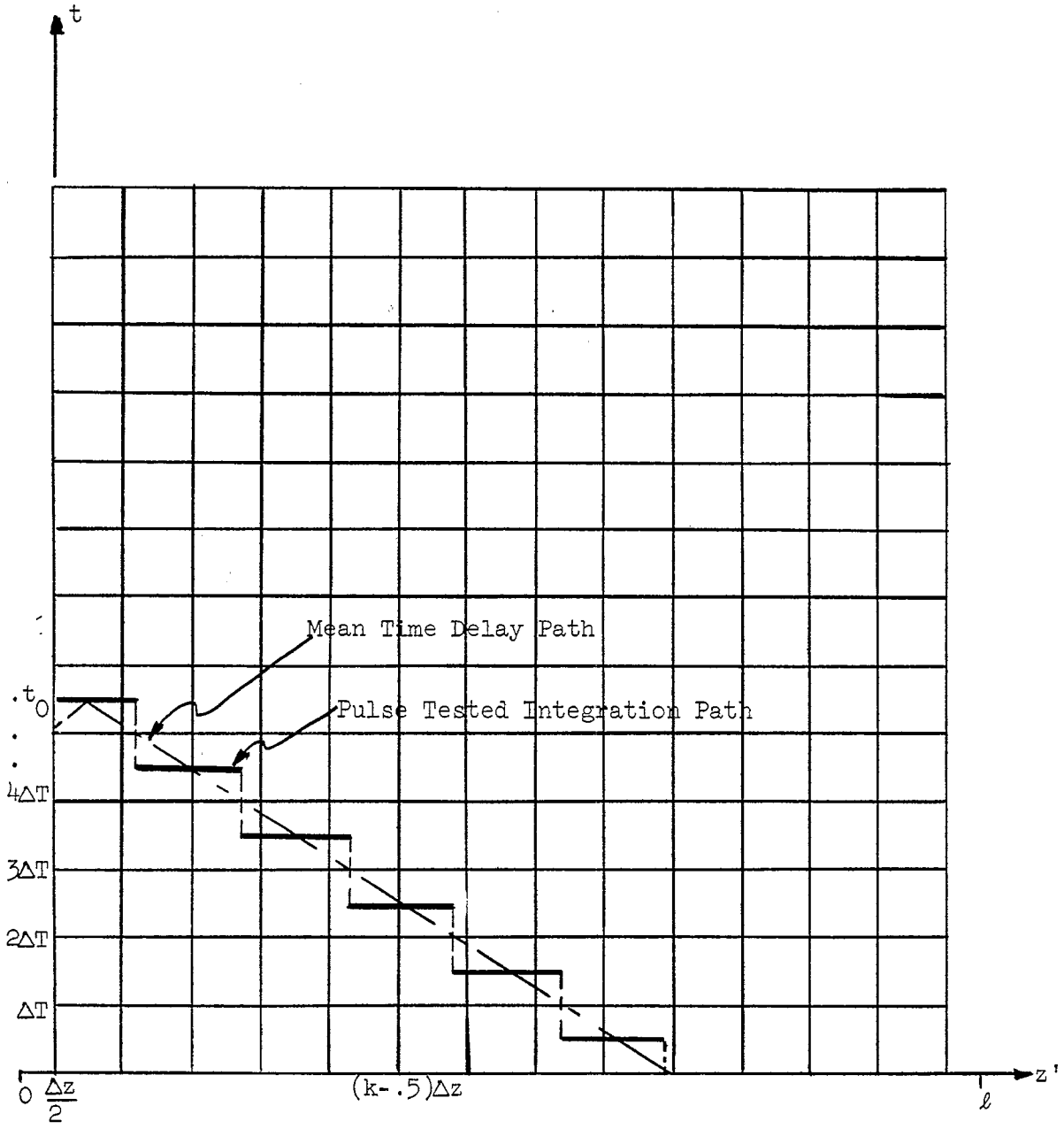

Far Field Pulse Tested Integration Paths
in the Time-Space Plane

Figure 4.2

A major ordinate division is .1 volt/meter. The time axis is referenced to the driven terminal.

Figure 4.6 shows a normalized radiated far field for the same excitation shown in Figure 4.5. The current was computed using the pulse tested solution presented in Chapter 3. There is some small improvement in the results. All scaling is as described for Figure 4.5.

A detailed discussion of these results will be delayed until the last chapter.

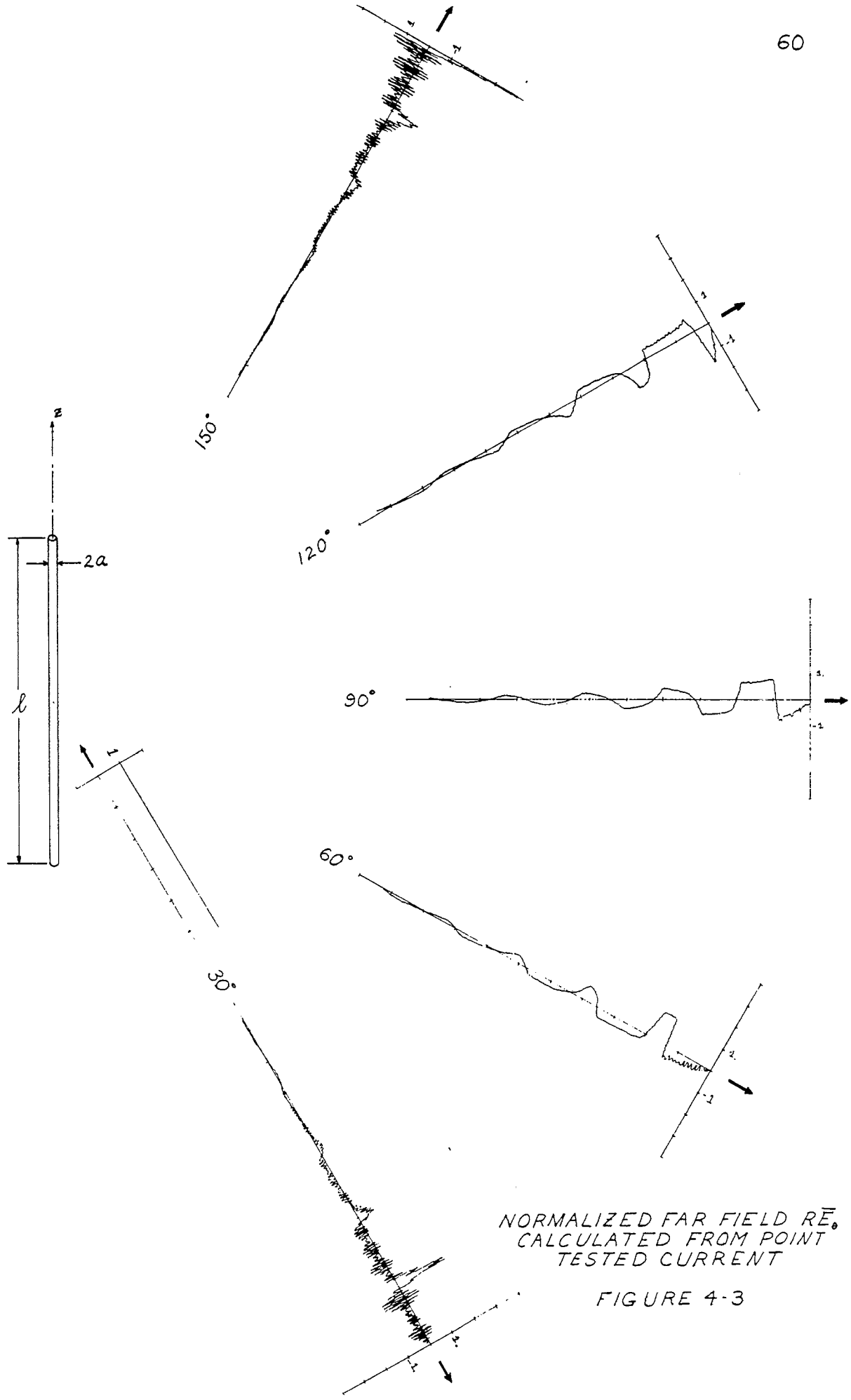

NORMALIZED FAR FIELD $R\bar{E}_\theta$ CALCULATED FROM POINT TESTED CURRENT

FIGURE 4-3

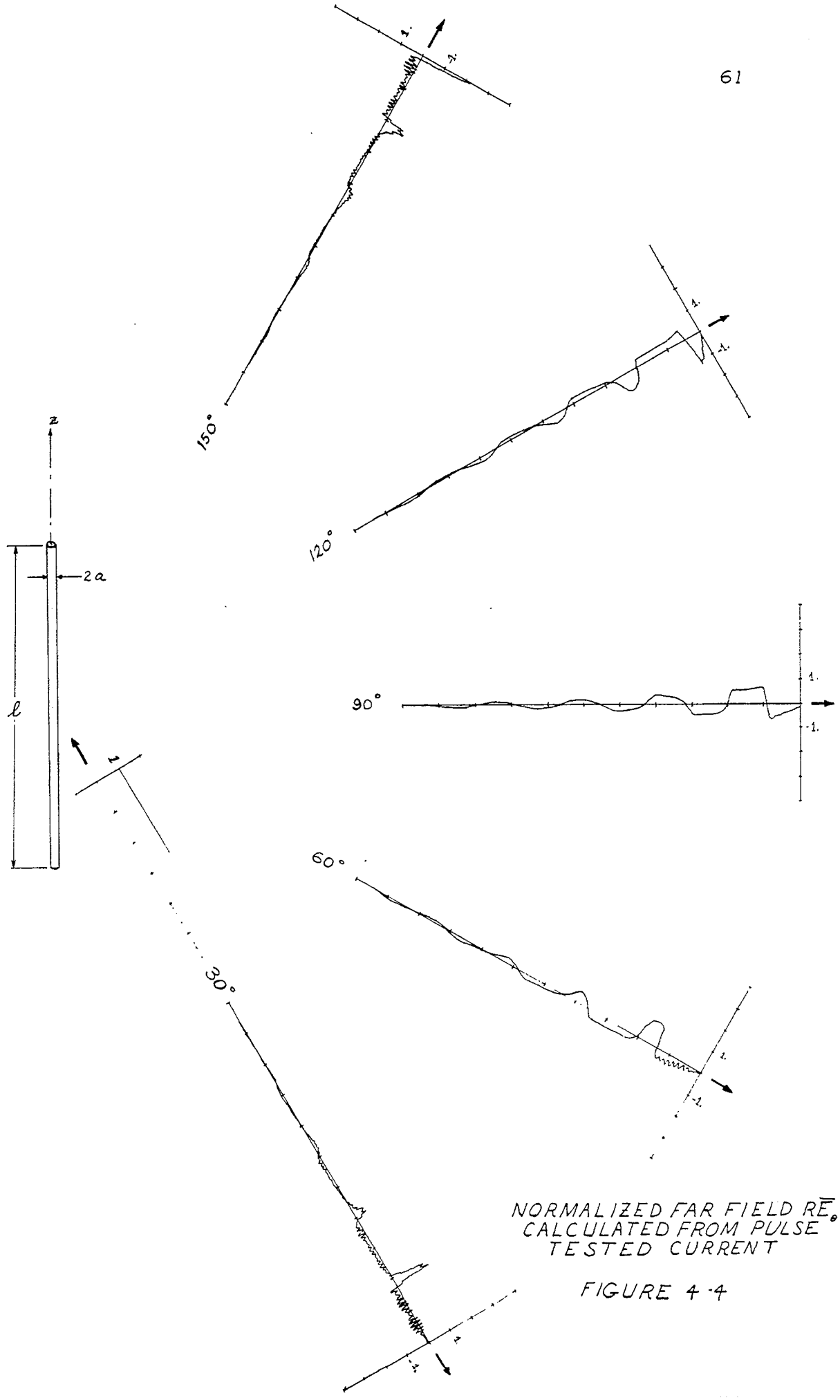

NORMALIZED FAR FIELD RE_θ CALCULATED FROM PULSE TESTED CURRENT

FIGURE 4-4

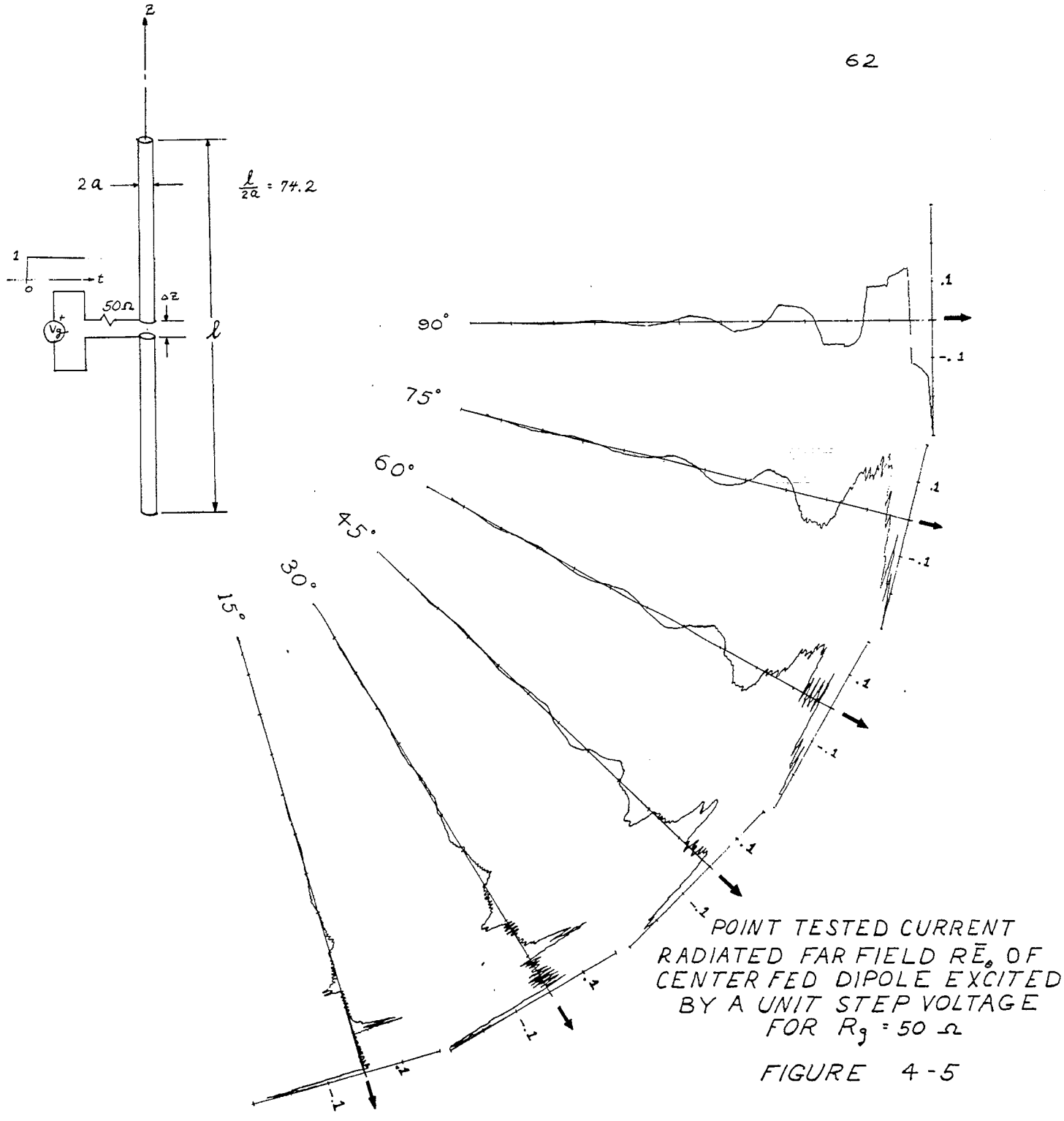

POINT TESTED CURRENT RADIATED FAR FIELD $R\bar{E}_\phi$ OF CENTER FED DIPOLE EXCITED BY A UNIT STEP VOLTAGE FOR $R_g = 50\ \Omega$

FIGURE 4-5

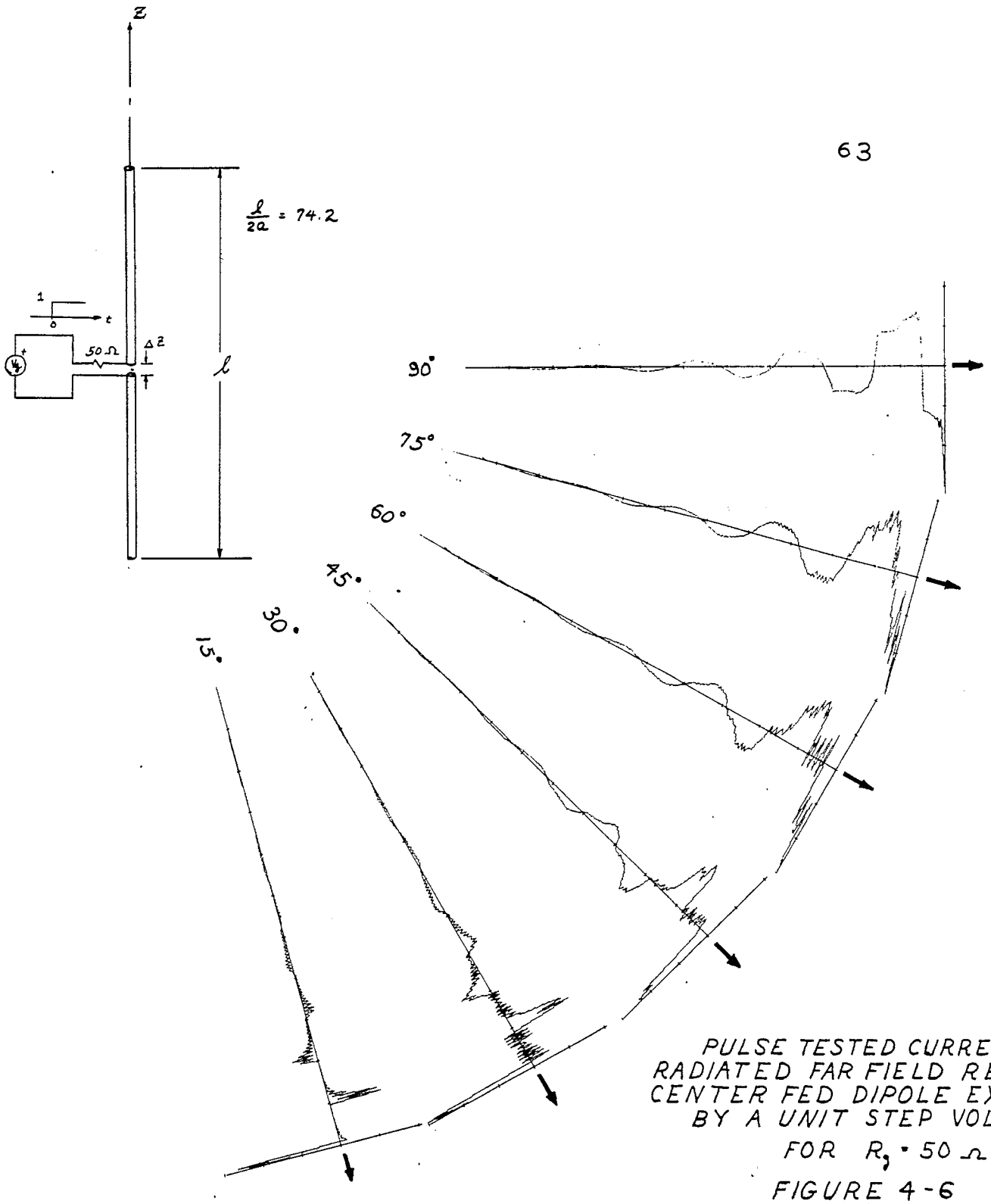

PULSE TESTED CURRENT RADIATED FAR FIELD RE. OF CENTER FED DIPOLE EXCITED BY A UNIT STEP VOLTAGE FOR $R_g = 50\ \Omega$

FIGURE 4-6

Chapter 5

SCATTERING BY AND RADIATION FROM ARBITRARILY BENT WIRE OBJECTS

A pulse tested method of moments solution is developed which can be applied to radiation and scattering by arbitrarily bent wires. For simplicity, the analysis will be restricted to wires lying in a plane. The method, however, is not limited by this simplification. Both open and closed wires will be discussed with the major emphasis on the analysis of closed wire objects. The closed circular wire loop will be analyzed in the following chapter as an application of the method to be developed herein.

Equations (9) and (12) express the relationships between the total electric field, the excitation and the source dependent potentials. These equations are repeated here for convenience:

$$E_\ell = - \frac{\partial A_\ell}{\partial t} - \frac{\partial \Phi}{\partial \ell} + E_\ell^i \tag{114}$$

$$E_\ell = \Omega I \tag{115}$$

Here, E_ℓ is the total tangential electric field on the wire surface, A_ℓ is the tangential component of the magnetic vector potential, $\frac{\partial \Phi}{\partial \ell}$ is the tangential derivative of the scalar potential, E_ℓ^i is the tangential component of the incident time dependent field, Ω is the axial resistivity, and I is the axial current. The terms $\frac{\partial A_\ell}{\partial t}$ and $\frac{\partial \Phi}{\partial \ell}$ are given explicitly by

$$\frac{\partial A_\ell}{\partial t} = \hat{\ell} \cdot \frac{\partial \tilde{A}}{\partial t} = \hat{\ell} \cdot \frac{\partial}{\partial t} \left(\frac{\mu}{4\pi} \int_{\ell'} \frac{\tilde{I}(t-\tau, \ell')}{R(\ell, \ell')} \, d\ell' \right) \tag{116}$$

$$\frac{\partial \Phi}{\partial \ell} = \hat{\ell} \cdot \nabla \Phi = \frac{\partial}{\partial \ell} \left(\frac{1}{4\pi\epsilon} \int_{\ell'} \frac{q(t-\tau, \ell')}{R(\ell, \ell')} \, d\ell' \right) \tag{117}$$

where $\hat{\ell}$ is a unit vector tangent to the field point ℓ, and q is the axial charge density. The distance between source point ℓ' and field point ℓ, is given by

$$R = \sqrt{(\ell - \ell')^2 + a^2} \qquad a = \text{wire radius} \tag{118}$$

The time delay, τ, will be approximated by

$$\frac{|\ell - \ell'|}{v_p} \quad . \tag{119}$$

5.1-1. Current and Charge Expansions for the Arbitrarily Bent Wire

The current and charge will be expanded in pulse type expansions similar to (30) and (31) for the straight wire. There are two distinct types of arbitrarily bent wires: those which are closed and those which are open. The circular wire loop and the straight wire are examples, respectively, of each type. The proper boundary conditions satisfied by $\underset{\sim}{I}$ and q depend on whether the wire is open or closed. This in turn affects the functional form of these expansions for the current and charge. As we have seen for the straight wire, open wire geometries require that the current vanish at the ends of the wire. Provision for charge buildup at the wire ends is necessary as well. Closed wire geometries, however, require that both I and q satisfy periodic boundary conditions. That is, for a closed wire of length L, the current and charge satisfy

$$\underset{\sim}{I}(t,0) = \underset{\sim}{I}(t,L)$$

and

$$q(t,0) = q(t,L)$$

The initial conditions satisfied by the current and charge remain the same.

The wire will be subdivided into N subsections of length $\Delta\ell = L/N$. The unit vector $\hat{U}_k$ will be taken as tangent to the midpoint of the k-th subsection. In terms of these quantities the current and charge on the open wire are given by

$$\underset{\sim}{I}(t,\ell') = \sum_{m=1}^{\infty}\sum_{k=1}^{N-1} \beta(m,k)P_1(\ell'-(k-.5)\Delta\ell)P_2(t-(m-1)\Delta T)\hat{U}_k \tag{120}$$

$$q(t,\ell') = \sum_{m=1}^{\infty}\sum_{k=1}^{N} \gamma(m,k)P_1(\ell'-(k-1)\Delta\ell)P_2(t-(m-.5)\Delta T) \tag{121}$$

and for the closed wire

$$\underset{\sim}{I}(t,\ell') = \sum_{m=1}^{\infty}\sum_{k=1}^{N} \beta(m,k)P_1(\ell'-(k-.5)\Delta\ell)P_2(t-(m-1)\Delta T)\hat{U}_k \tag{122}$$

and

$$\beta(m,N+j) = \beta(m,j) \tag{123}$$

$$q(t,\ell') = \sum_{m=1}^{\infty}\sum_{k=1}^{N} \gamma(m,k)P_1(\ell'-(k-1)\Delta\ell)P_2(t-(m-.5)\Delta T) \tag{124}$$

and

$$\gamma(m,N+j) = \gamma(m,j) \tag{125}$$

Equations (123) and (125) are a direct consequence of the periodic boundary conditions. The pulse functions P_1 and P_2 are as previously defined by (29b) and (29c). The spatial summation in (122) is extended to an upper

limit of N to insure, along with (123), that the current is piecewise continuous over the entire wire. On the open wire, the vanishing of the current at the wire ends is guaranteed by the upper summation limit of N-1. As before, the charges are offset by a half interval in space and time and vanish in the neighborhood of t = 0.

5.1-2. Continuity Relationships

The continuity equation will be satisfied by the difference operator given by (15). The substitution of (120) and (121) into (15) results in the same set of relationships between the current and charge coefficients as found for the straight wire (Chapter 2, (36a,b,c,d,e,f) if $\Delta\ell = v_p\Delta T$. Substitution of (122) through (125) into (15) results in a somewhat different set of relationships between the current and charge coefficients for the closed wire, namely

$$\gamma(1,k) = -\left(\frac{\beta(1,k)-\beta(1,k-1)}{v_p}\right) \qquad k = 2,3,\ldots,N \tag{126a}$$

Initial Conditions [m = 1]

$$\gamma(1,1) = -\left(\frac{\beta(1,1)-\beta(1,N)}{v_p}\right) \tag{126b}$$

$$\gamma(m,k) = -\left(\frac{\beta(m,k)-\beta(m,k-1)}{v_p}\right) + \gamma(m-1,k) \tag{126c}$$

$m = 2,3,\ldots$ $\qquad k = 2,3,\ldots,N$

$$\gamma(m,1) = -\left(\frac{\beta(1,1)-\beta(1,N)}{v_p}\right) + \gamma(m-1,1) \tag{126d}$$

5.2. Pulse Testing Functions

The proper testing functions for the arbitrarily bent wire problem are vector functions. It was pointed out by Welsh[13] that the testing

functions can be interpreted as currents which enter into the reciprocity integral relationship. This was used in Chapter 4 to compute the pulse tested radiation field. The vector pulse testing functions are defined by (127) and (128) which follow:

$$\underset{\sim}{S}_{0,i}(t,\ell) = \frac{\hat{\ell}_i}{\Delta\ell\Delta T} P_1(\ell-(i-.5)\Delta\ell), -\frac{\Delta T}{2} \leq t < 0$$
$$= 0 \quad \text{otherwise} \tag{127}$$

$$\underset{\sim}{S}_{j,i}(t,\ell) = \frac{\hat{\ell}_i}{\Delta\ell\Delta T} P_1(\ell-(i-.5)\Delta\ell) P_2(t-(j-.5)\Delta T) \tag{128}$$

Here $\hat{\ell}_i$ is a unit vector tangent to the i-th field subsection, and P_2^a the adjoint time pulse function defined by (58). The index j runs over $j = 1,2,\ldots$ and i runs over $1,2,\ldots,(N-1)$ for the open wire and $1,2,\ldots,N$ for the closed wire.

5.3-1. The Pulse Tested Algorithm

The pulse tested electric field equation can be written in vector form as

$$\left\langle \underset{\sim}{E}^i, \underset{\sim}{S}_{j,i} \right\rangle = \left\langle \Omega \underset{\sim}{I}(t,\ell), \underset{\sim}{S}_{j,i} \right\rangle + \left\langle \frac{\partial \underset{\sim}{A}}{\partial t}, \underset{\sim}{S}_{j,i} \right\rangle + \left\langle \nabla\Phi, \underset{\sim}{S}_{j,i} \right\rangle \tag{129}$$

The definition of the inner product between vector functions, (28), includes the dot product. This was not important in the analysis of the straight wire since all the components on the right-hand side of (59) were colinear.

Further analysis of (129) will be specialized to the development of pulse tested solutions suitable for closed wire objects. All spatial

indices will thus be assumed to vary over $1 \leq i \leq N$. The incident propagating plane electric field may be written

$$\underset{\sim}{E}^i(r,t) = A\left(t - \frac{\underset{\sim}{r} \cdot \hat{U}_n}{v_p}\right) \hat{U}_E \tag{130}$$

The unit vector $\hat{U}_n$ is assumed normal to the plane wave and pointed in the direction of propagation, $\underset{\sim}{r}$ is a radial vector in a spherical coordinate system, the center of which is the time reference $t = 0$. A is assumed to be causal, and as such vanishes for $(t - \underset{\sim}{r} \cdot \hat{U}_n/v_p) < 0$ · $\hat{U}_E$ is the direction of polarization of the incident field.

The pulse tested incident electric field $\langle \underset{\sim}{E}^i, \underset{\sim}{S}_{j,i} \rangle$ is obtained by the substitution of (130) and the testing functions (127) and (128) into the definition of the inner product given by (28); thus,

$$\left\langle \underset{\sim}{E}^i(t,r), \underset{\sim}{S}_{j,i} \right\rangle = \frac{\hat{\ell}_i \cdot \hat{U}_E}{\Delta T \Delta z} \int_{(j-.5)\Delta T}^{(j+.5)\Delta T} dt \int_{(i-.5)\Delta \ell}^{(i+.5)\Delta \ell} A\left(t - \frac{\underset{\sim}{r}(\ell) \cdot \hat{U}_n}{v_p}\right) d\ell$$

$$j = 1,2,3,\ldots$$
$$i = 1,2,\ldots,N \tag{131}$$

For $j = 0$, the lower limit of the time integration is zero, since $\underset{\sim}{S}_{0,i}$ vanishes for $t > 0$. The dot product between the unit vectors $\hat{\ell}_i$ and $\hat{U}_E$ gives the tangential component of $\underset{\sim}{E}^i$ over the i-th subsection. $\underset{\sim}{r}(\ell)$ is the shape of the wire and is a function of the field coordinates ℓ. In practice $\underset{\sim}{r}(\ell)$ is given in terms of the axial coordinate ℓ' since the thin wire approximation excludes time effects on the order of the transit time of the wire radius. The point $\underset{\sim}{r}(\ell) = 0$ will be taken as the point on the wire first struck by the incident wave; and the time axis of the wire will be referenced to this point.

The ohmic contribution, $\langle \Omega \underset{\sim}{I}(t,\ell), S_{j,i} \rangle$, to the total electric field is identical to the same term as considered in Chapter 3 and is given by (64) and (65). These equations are included again for reference:

$$\langle \Omega \underset{\sim}{I}(t,\ell), \underset{\sim}{S}_{0,i} \rangle = \frac{\Omega(i)}{2} \beta(1,i) \tag{132}$$

$$\langle \Omega \underset{\sim}{I}(t,\ell), \underset{\sim}{S}_{j,i} \rangle = \frac{\Omega(i)}{2} [\beta(j+1,i)+\beta(j,i)] \quad j > 0 \tag{133}$$

The component of the total electric field, $\langle \frac{\partial \underset{\sim}{A}}{\partial t}, S_{j,i} \rangle$, can be written

$$\langle \frac{\partial \underset{\sim}{A}}{\partial t}, \underset{\sim}{S}_{j,i} \rangle = \frac{\mu}{4\pi}\left(\frac{1}{\Delta T \Delta \ell}\right) \int_{(j-.5)\Delta T}^{(j+.5)\Delta T} dt \int_{(i-.5)\Delta \ell}^{(i+.5)\Delta \ell} d\ell_i \left[\sum_{m=1}^{\infty} \sum_{k=1}^{N} \hat{\ell}_i \cdot \hat{U}_k \right.$$

$$\left. \int_{(k-.5)\Delta \ell}^{(k+.5)\Delta \ell} d\ell_k \left(\beta\left(m - \frac{\tau}{\Delta T}, k\right) \left[\frac{\delta(t+\tau-(m-1)\Delta T) - \delta(t+\tau-\Delta T)}{R(\ell_i, \ell_k)} \right] \right) \right] \tag{134}$$

The sampling property of the impulses permits direct time integration of (134). Thus

$$\langle \frac{\partial \underset{\sim}{A}}{\partial t}, \underset{\sim}{S}_{j,i} \rangle = \frac{\mu}{4\pi}\left(\frac{1}{\Delta T \Delta \ell}\right) \sum_{k=1}^{N} \hat{\ell}_i \cdot \hat{U}_k \int_{(i-.5)\Delta \ell}^{(i+.5)\Delta \ell} d\ell_i \int_{(k-.5)\Delta \ell}^{(k+.5)\Delta \ell} d\ell_k \left[\frac{\beta(j+1-\tau/\Delta T, k) - \beta(j-\tau/\Delta T, k)}{R(\ell_i, \ell_k)} \right.$$

(135)

The distance $R(\ell_i, \ell_k)$ is found from simple vector considerations and may be written

$$R(\ell_i, \ell_k) = [(\underset{\sim}{r}_{i,k} + \underset{\sim}{\ell}_k - \underset{\sim}{\ell}_i) \cdot (\underset{\sim}{r}_{i,k} + \underset{\sim}{\ell}_k - \underset{\sim}{\ell}_i)]^{\frac{1}{2}} \tag{136}$$

where $\underset{\sim}{r}_{i,k}$ is the vector between the beginning of the i-th subsection

($\underset{\sim}{\ell}_i = 0$) and the beginning of the k-th subsection ($\underset{\sim}{\ell}_k = 0$). Figure 5.1 illustrates the geometry involved. After completing the square, $R(\ell_i, \ell_k)$ can be written in the form,

$$R(\ell_i, \ell_k) = [(\ell_i - A(i,k))^2 + B(i,k)]^{\frac{1}{2}} \tag{137}$$

where

$$A(i,k) = r_{i,k} \cos(\psi_i - \theta_{i,k}) + \ell_k \cos(\psi_i - \psi_k) \tag{138}$$

$$B(i,k) = r_{i,k}^2 + \ell_k^2 + 2r_{ik}\ell_k \cos(\psi_k - \theta_{i,k}) - A^2(i,k) \tag{139}$$

(Note: the magnitudes of $\underset{\sim}{r}_{i,k}$, $\underset{\sim}{\ell}_k$, etc. are written $r_{i,k}$, ℓ_k.) Integration of (135) with respect to ℓ_i can be carried out analytically with the substitution of (137). The current coefficients are constant over the domain of the ℓ_i integration. With the integration with respect to ℓ_i completed, $\left\langle \frac{\partial \underset{\sim}{A}}{\partial t}, \underset{\sim}{S}_{j,i} \right\rangle$ can be written,

$$\left\langle \frac{\partial \underset{\sim}{A}}{\partial t}, \underset{\sim}{S}_{j,i} \right\rangle = \frac{\mu}{4\pi}\left(\frac{1}{\Delta T \Delta \ell}\right) \sum_{k=1}^{N} \hat{\ell}_i' \cdot \hat{U}_k \int_{(k-.5)\Delta\ell}^{(k+.5)\Delta\ell} \{\beta(j+1-\alpha_k, k) - \beta(j-\alpha_k, k)\} F(i\Delta\ell, \ell_k) d\ell \tag{140}$$

where

$$\alpha_k = \text{Fix}\left(\frac{R(i\Delta\ell, \ell_k)}{\Delta\ell}\right) \tag{141}$$

and

$$F(i\Delta\ell, \ell_k) = \log_e \left[\frac{(i+.5)\Delta\ell - A(i,k) + \sqrt{((i+.5)\Delta\ell - A(i,k))^2 + B(i,k)}}{(i-.5)\Delta\ell - A(i,k) + \sqrt{((i-.5)\Delta\ell - A(i,k))^2 + B(i,k)}} \right] \tag{142}$$

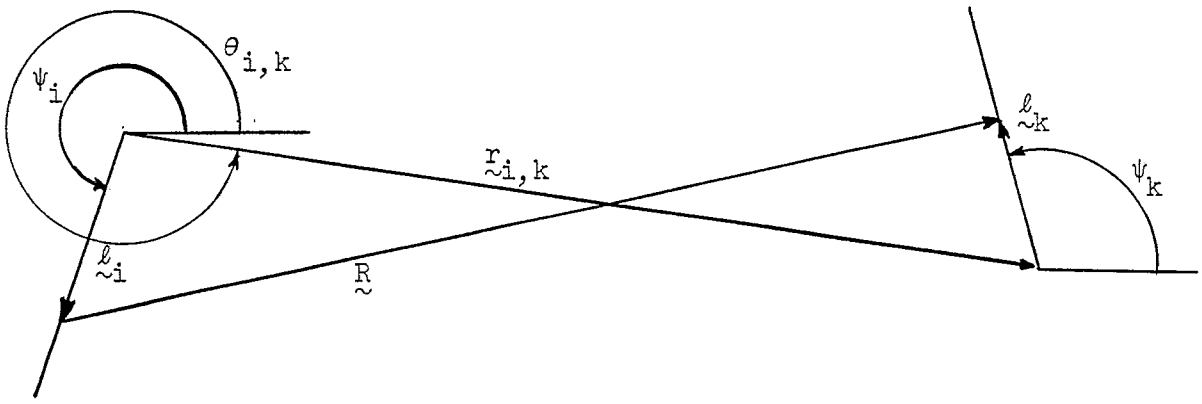

Geometry of Two Arbitrarily Oriented
Planar Wire Segments

Figure 5.1

The function $\text{Fix}\left(\frac{R(i\Delta\ell, \ell_k)}{\Delta\ell}\right)$ returns the largest integer less than or equal to the argument $\left\{\frac{R(i\Delta\ell, \ell_k)}{\Delta\ell}\right\}$.

Further integration of (140) can proceed over those regions of ℓ_k where the current coefficients are constant, or equivalently over the regions of ℓ_k where α_k is constant. An overlay of the regions of constant time delay over a closed wire object is shown in Figure 5.2. Examination of this figure shows that some subsections (2,4,8,9,10,14) are wholly contained in a constant time delay region, while others (1,3,5,6,7,11,12,13) lie in two time delay regions. Investigation of the integral

$$\int F(i\Delta\ell, \ell_k)d\ell_k \tag{143}$$

showed that this integration can be performed analytically whenever $\hat{\ell}_i \cdot \hat{\ell}_k = \pm 1$. The straight wire integrations satisfy the criterion. In general, integration of (143) must be done numerically. Let α_k be assumed constant over a portion of the k-th subsection $a_k \leq \ell_k < b_k$. Since any subsection is contained in at most two constant time delay regions, a_k is either the beginning of an interval and b_k is an intermediary point or b_k is the end of an interval and a_k an intermediary point. (In the case α_k is constant over an entire interval, a_k is the beginning of the k-th subsection, and b_k is the end point of the subsection. Over $a_k \leq \ell_k < b_k$, the time indices of the current coefficients $(j+1-\alpha_k)$ and $(j-\alpha_k)$ are constant with respect to the ℓ_k integration, and the coefficients may be moved outside the integral giving terms of the form

$$\{\beta(j+1-\alpha_k, k) - \beta(j-\alpha_k, k)\}\int_{a_k}^{b_k} F(i\Delta\ell, \ell_k)d\ell_k \tag{144}$$

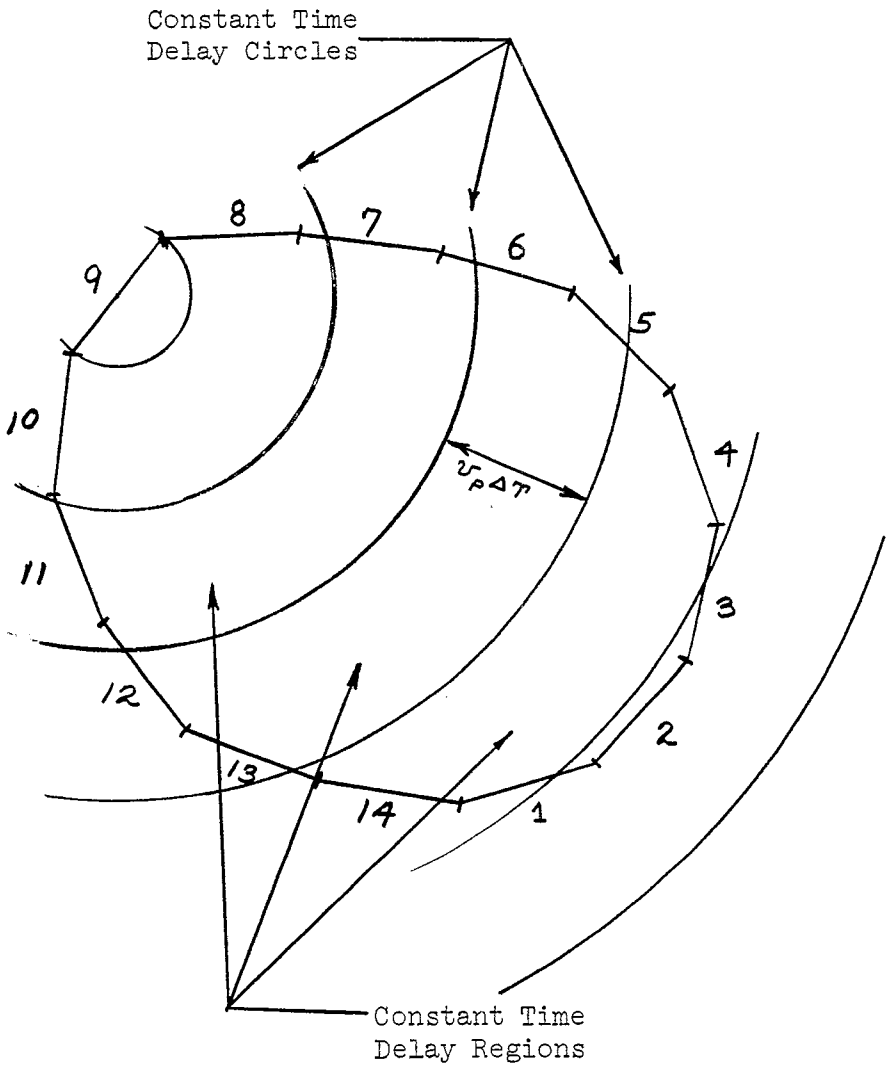

Overlay of the Constant Time Delay Regions
on the Subsectional Approximation to a
Closed Wire Object

Figure 5.2

A numerical integration of (144) of the form

$$\frac{\Delta\ell}{M}\sum_{s=0}^{P}\log_e\left[\frac{(i+.5)\Delta\ell)-A_s(i,k)+\sqrt{[(i+.5)\Delta\ell-A_s(i,k)]^2+B_s(i,k)}}{(i-.5)\Delta\ell)-A_s(i,k)+\sqrt{[(i-.5)\Delta\ell-A_s(i,k)]^2+B_s(i,k)}}\right] \tag{145}$$

where

$$P = \text{Fix}\quad\left(\frac{b_k-a_k}{\Delta\ell}\right) M \tag{146}$$

M = number of sample points
in entire subinterval

$$A_s(i,k) = r_{i,k}\cos(\psi_i-\theta_{i,k})+(a_k+\frac{s\Delta\ell}{M})\cos(\psi_i-\psi_k) \tag{147}$$

$$B_s(i,k) = r_{i,k}^2+(a_k+\frac{s\Delta\ell}{M})^2+2r_{i,k}(a_k+\frac{s\Delta\ell}{M})\cos(\psi_k-\theta_{i,k})-A_s^2(i,k) \tag{148}$$

has been successfully used for the case of the wire loop. The details will be delayed to the next chapter. The relationship of the time delay index α and the source and field points i and k, respectively, is not simple for the arbitrary wire. For computational simplicity it is convenient to define the function $G(\alpha,i,k)$ as

$$G(\alpha,i,k) \equiv \frac{1}{\Delta\ell}\int_{a_k}^{b_k} F(i\Delta\ell,\ell_k)d\ell_k \tag{149}$$

whenever the α constant time delay region, centered on the field point $i\Delta\ell$, includes a portion of the k-th source subsection, and

$$G(\alpha,i,k) \equiv 0.0 \quad \text{otherwise} \tag{150}$$

In the evaluation of the potential integrals, $G(\alpha,i,k)$ is analogous to

the previous geometry functions $F(|i-k|)$ and $G(|i-k|)$ of Chapters 2 and 3. It is more general in the sense that a subsection can fall into more than one time delay region, which does not occur in straight wire problems.

The calculation of $\left\langle \frac{\partial \underset{\sim}{A}}{\partial t}, \underset{\sim}{S}_{j,i} \right\rangle$ begins with finding the points on the wire where the time delay circles shown in Figure 5.2 intersect the wire. The regions between the points of intersection are the constant time delay regions. Over each region beginning with $\alpha = 0$, and proceeding to successive α's in turn, the $G(\alpha,i,k)$ are calculated from (137, 138, 139, 142, 149, 150). Unless symmetry considerations can be used to simplify the geometry, $G(\alpha,i,k)$ must be calculated over every k for each α and i. The storage requirements are α times as large as those required to store Green's function integration results required in method of moments investigations of the same wire object in the frequency domain. Now, $\left\langle \frac{\partial \underset{\sim}{A}}{\partial t}, \underset{\sim}{S}_{j,i} \right\rangle$ can be written in terms of $G(\alpha,i,k)$ by inspection as

$$\left\langle \frac{\partial \underset{\sim}{A}}{\partial t}, \underset{\sim}{S}_{j,i} \right\rangle = \frac{\mu}{4\pi} \sum_{k=1}^{N} \sum_{\alpha=0}^{\alpha_M(i)} \hat{\ell}_i \cdot \hat{U}_k \left[\frac{\beta(j+1-\alpha,k)-\beta(j-\alpha,k)}{\Delta T} \right] G(\alpha,i,k) \quad i=1,2,\ldots,N \tag{151}$$

where $\alpha_M(i)$ is the index of the largest time delay region centered on the midpoint of the i-th subsection which encloses the wire object. During the transient buildup period, summation is terminated if the time coefficient $(j-\alpha)$ is less than unity. During this period (151) is written for $j \neq 0$, as

$$\left\langle \frac{\partial \underset{\sim}{A}}{\partial t}, \underset{\sim}{S}_{j,i} \right\rangle = \frac{\mu}{4\pi} \sum_{k=1}^{N} \left(\sum_{\alpha=0}^{j-1} \left[\frac{\beta(j+1-\alpha,k)-\beta(j-\alpha,k)}{\Delta T} \right] G(\alpha,i,k) + \frac{\beta(1,k)}{\Delta T} G(j,i,k) \right) \hat{\ell}_i \cdot \hat{U}_k \tag{152}$$

and, for j = 0, as

$$\left\langle \frac{\partial \underset{\sim}{A}}{\partial t}, \underset{\sim}{S}_{0,i} \right\rangle = \frac{\bar{A}_\ell(t_1, \ell_i)}{\Delta T} = \frac{\mu}{4\pi} \beta(1,i) \frac{G(0,i,i)}{\Delta T} \tag{153}$$

G(0,i,i) is recognized as the self element term and is equal to G(0) defined in Chapter 3. This provides a useful check on the precision of the numerical integration of the geometry functions for the bent wire problem. The pulse testing integral (60) can be interpreted as a general averaging operator on the integrand, and in this light, (151) can be written,

$$\left\langle \frac{\partial \underset{\sim}{A}}{\partial t}, \underset{\sim}{S}_{j,i} \right\rangle = \frac{\bar{A}_\ell(t_{j+1}, \ell_i) - \bar{A}_\ell(t_j, \ell_i)}{\Delta T} \tag{154}$$

with the bar denoting the average taken over the i-th subsection of the tangential component of $\underset{\sim}{A}$.

The final term on the right-hand side of (129) to be analyzed is the scalar potential contribution $\left\langle \nabla\Phi, \underset{\sim}{S}_{j,i} \right\rangle$. That is

$$\left\langle \nabla\Phi, \underset{\sim}{S}_{j,i} \right\rangle = \frac{1}{4\pi\epsilon}\left(\frac{1}{\Delta T \Delta \ell}\right) \int_{(j-.5)\Delta T}^{(j+.5)\Delta T} dt \int_{(i-.5)\Delta \ell}^{(i+.5)\Delta \ell} d\ell_i \left\{ \frac{\partial}{\partial \ell_i} \sum_{m=1}^{\infty} \sum_{k=1}^{N} \int_{(k-1)\Delta \ell}^{k\Delta \ell} d\ell_k \left[\frac{\gamma(m-(\tau/\Delta T), k) P_2(t+\tau-(m-.5)\Delta T)}{R(\ell_i, \ell_k)} \right] \right\} \tag{155}$$

where $R(\ell_i, \ell_k)$ is given by (137), and the time delay τ between source and field points is $R(\ell_i, \ell_k)/v_p$. The partial derivative operator will be approximated by the difference operator of Section 1-3. The pulse tested scalar potential contribution will be shown to be proportional to the difference of the pulse tested scalar potentials $\bar{\Phi}(t_j, \ell_i + \Delta\ell/2)$ and $\bar{\Phi}(t_j, \ell_i - \Delta\ell/2)$.

If equation (155) is written in terms of the difference operator, it can be integrated with respect to the time variable. An immediate result is the $j = 0$ term vanishes.. This result follows directly from the shifted pulse expansion for the charge (124) which assumes that over the period $0 \leq t < 0.5\Delta T$, the charge is zero. Physically this approximation assumes that any charge buildup that occurs during this period has a negligible effect on the scalar potential, which in turn has a negligible effect on the tangential electric field. The remaining terms ($j > 0$) are given by

$$\left\langle \nabla\Phi, \underset{\sim}{S}_{j,i} \right\rangle = \frac{1}{4\pi\epsilon}\left(\frac{1}{\Delta\ell}\right)^2 \int_{(i-.5)\Delta\ell}^{(i+.5)\Delta\ell} d\ell_i \sum_{k=1}^{N} \left\{ \int_{(k-1)\Delta\ell}^{k\Delta\ell} \left(\frac{\gamma(j-\alpha^+,k)}{R(\ell_i+(\Delta\ell/2),\ell_k)} - \frac{\gamma(j-\alpha^-,k)}{R(\ell_i-(\Delta\ell/2),\ell_k)} \right) d\ell_k \right\} \tag{156}$$

where

$$\alpha^+ = \text{Fix}\ \frac{R(\ell_i+(\Delta\ell/2),\ell_k)}{\Delta\ell} \tag{157}$$

$$\alpha^- = \text{Fix}\ \frac{R(\ell_i-(\Delta\ell/2),\ell_k)}{\Delta\ell} \tag{158}$$

The local subsectional geometry is illustrated in Figure 5.3. Further analysis of (156) will be aided by defining an average potential

$$\bar{\Phi}(t_j,\ell_i+\frac{\Delta\ell}{2}) = \frac{1}{4\pi\epsilon}\left(\frac{1}{\Delta\ell}\right) \int_{(i-.5)\Delta\ell}^{(i+.5)\Delta\ell} d\ell_i \left(\sum_{k=1}^{N} \int_{(k-1)\Delta\ell}^{k\Delta\ell} \frac{\gamma(j-\alpha^+,k)}{R(\ell_i+(\Delta\ell/2),\ell_k)}\, d\ell_k \right) \tag{159}$$

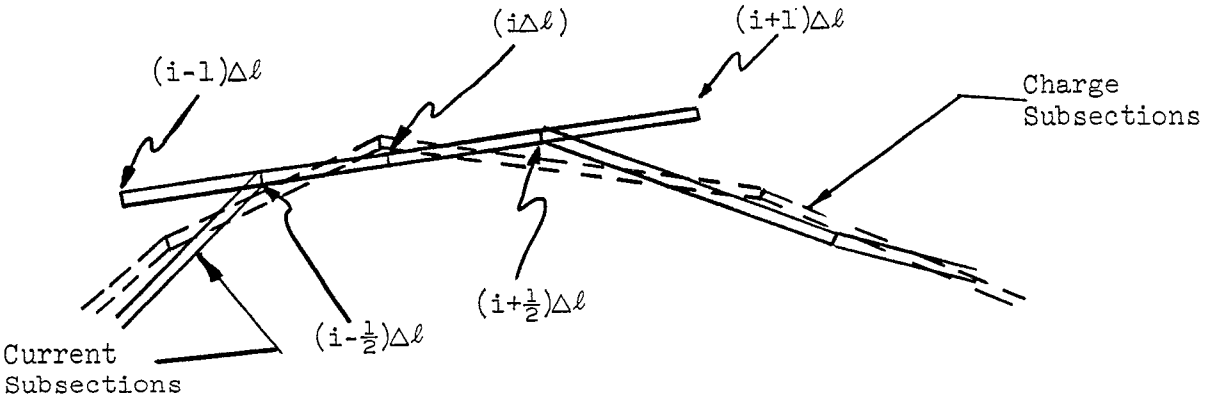

Local Subsection Geometry Useful in the
Evaluation of the Pulse Tested
Scalar Potential Contribution

Figure 5.3

Equation (159) is transformed into an integral which can be evaluated in terms of the geometry functions $G(\alpha,i,k)$ by the substitution $\eta_i = \ell_i + .5\Delta\ell$

$$\bar{\Phi}(t_j, \ell_i + \frac{\Delta\ell}{2}) = \frac{1}{4\pi\epsilon}\left(\frac{1}{\Delta\ell}\right) \int_{i\Delta\ell}^{(i+1)\Delta\ell} d\eta_i \left(\sum_{k=1}^{N} \int_{(k-1)\Delta\ell}^{k\Delta\ell} \frac{\gamma(j-\alpha^+,k)}{R(\eta_i,\ell_k)} \, d\ell_k \right) \tag{160}$$

$$\alpha^+ = \text{Fix} \quad \frac{R(\eta_i,\ell_k)}{c\Delta T}$$

Over the regions of constant time delay the charge coefficients are constant with respect to the variables of integration and may be moved outside the integrals. The double integral is the same type as (149) which defines $G(\alpha,i,k)$. Evaluation of (160) proceeds in the same manner as the evaluation of $\left\langle \frac{\partial \underset{\sim}{A}}{\partial t}, \underset{\sim}{S}_{j,\ell} \right\rangle$. $\bar{\Phi}(t_j, \ell_i + \frac{\Delta\ell}{2})$ can be shown to be given by

$$\bar{\Phi}(t_j, \ell_i + \frac{\Delta\ell}{2}) = \frac{1}{4\pi\epsilon} \sum_{k=1}^{N} \sum_{\alpha=0}^{\alpha_M(i)} \gamma(j-\alpha,k)\, G(\alpha,(i+1),k) \tag{161}$$

and similarly,

$$\bar{\Phi}(t_j, \ell_i - \frac{\Delta\ell}{2}) = \frac{1}{4\pi\epsilon} \sum_{k=1}^{N} \sum_{\alpha=0}^{\alpha_M(i)} \gamma(j-\alpha,k)\, G(\alpha,i-k) \tag{162}$$

where $\alpha_M(i)$ is defined following equation (151). Summation is terminated when $(j-\alpha) < 1$. The pulse tested scalar potential term $\left\langle \nabla\Phi, \underset{\sim}{S}_{j,i} \right\rangle$ is then

$$\left\langle \nabla\Phi, \underset{\sim}{S}_{j,i} \right\rangle = \frac{\bar{\Phi}(t_j, \ell_i + (\Delta\ell/2) - \bar{\Phi}(t_j, \ell_i - (\Delta\ell/2)}{\Delta\ell} \tag{163}$$

The relationships developed in Chapter 3 for the solution of the

current coefficients $\beta(j+1,i)$ hold formally for the arbitrarily closed bent wire. The quantities involved, however, are those which have been analyzed in this chapter. The relationships will be included for completeness. The first set of current coefficients $\beta(1,i)$ is given by

$$\beta(1,i) = \frac{E^i, S_{0,i}}{\Omega(i)/2 + (\mu G(0,i,i)/4\pi\Delta T} \tag{164}$$

where $i = 1,2,\ldots,N$. The first set of charge coefficients is found from equations (126a,b). The current coefficients $\beta(j,i)$ for $j > 0$ are given by:

$$\beta(j+1,i) = \frac{\langle \underset{\sim}{E}^i, \underset{\sim}{S}_{j,i} \rangle - (\Omega(\ell)/2)\,\beta(j,i) - (1/\Delta T)(\Delta\bar{A}) - (1/\Delta z(\Delta\bar{\Phi})}{[\Omega(\ell)/2 + (\mu G(0,i,i)/4\pi\Delta T)]} \tag{165}$$

Here,

$$\Delta\bar{A} = \bar{a}_\ell(t_{j+1}, \ell_i) - \bar{A}_\ell(t_j, \ell_i) \tag{166}$$

and

$$\Delta\bar{\Phi} = \bar{\Phi}(t_j, \ell_i + \Delta\ell/2) - \bar{\Phi}(t_j, \ell_i - \Delta\ell/2) \tag{167}$$

The vector potential terms $\bar{a}_\ell$ and $\bar{A}_\ell$ are given by

$$\bar{a}_\ell(t_{j+1}, z_i) = \frac{\mu}{4\pi} \sum_{\substack{k=1 \\ k\neq i}}^{N} \sum_{\alpha=0}^{\alpha_M(i)} \beta(i+1-\alpha, k)\, G(\alpha, i, k) \tag{168}$$

and

$$\bar{A}_\ell(t_{j+1}, z_i) = \frac{\mu}{4\pi}\,\beta(j+1,i)\, G(0,i,i) + \bar{a}_\ell(t_{j+1}, z_i) \tag{169}$$

and

$$\bar{A}_{\ell}(t_j, z_i) = \frac{\mu}{4\pi} \sum_{k=1}^{N} \sum_{\alpha=0}^{\alpha_M(i)} \beta(j-\alpha, k)\, G(\alpha, i, k) \tag{170}$$

where $\alpha_M(i)$ is defined following equation (151). The scalar potentials $\bar{\Phi}(t_j, \ell_i + \frac{\Delta\ell}{2})$ and $\Phi(t_j, \ell_i \frac{\Delta\ell}{2})$ are given by (161) and (162), respectively. The charge coefficients $\gamma(j,i)$ are found from (126c,d). The same impedance interpretation can be given to (165) as was developed in Chapters 2 and 3. Equation (165) can then be rewritten,

$$\beta(j+1, i) = \frac{\bar{V}^i(t_j, \ell_i) - R(i)/2\ \beta(j,i) - v_p \Delta\bar{A} - \Delta\bar{\Phi}}{[R(i)/2 + \eta G(0,i,i)/4\pi]} \tag{171}$$

The same comments following equation (100) in Chapter 3 pertain. The exciting voltage $\bar{V}^i(t_j, \ell_i)$ is defined by

$$\bar{V}^i(t_j, \ell_i) = \Delta\ell \left\langle \underset{\sim}{E}^i, \underset{\sim}{S}_{j,i} \right\rangle \tag{172}$$

If the wire is excited as an antenna at the p-th port, equations (102) and (103) hold formally, and are repeated for convenience. At the driven port, the driving point current is given by

$$\beta(j+1, p) = \frac{\bar{V}^i(t_j, z_p) - (R_g/2.)\, \beta(j,i) - v_p \Delta\bar{A} - \Delta\bar{\Phi}}{[R_g(p)/2 + \eta G(0,i,i)/4\pi]} \tag{173}$$

and

$$\beta(j+1, \ell) = -\frac{R_L(i)\ \beta(j,i)/2. + v_p \Delta\bar{A} + \Delta\bar{\Phi}}{[R_L(i)/2 + \eta G(0,i,i)/4\pi]} \tag{174}$$

For $j = 0$, the initial set of current coefficients is given by

$$\beta(1, p) = \frac{\bar{V}^i(t_0, \ell_p)}{[R_g(p)/2 + \eta G(0,i,i)/4\pi]} \qquad \ell = p \tag{175a}$$

and

$$\beta(1,\ell) = 0 \qquad \ell \neq p \tag{175b}$$

Conduction losses are assumed to be included in the source resistance $R_g(p)$ and the load resistances $R_L(i)$. The exciting voltage applied to the p-th subsection is given for $j = 0$ by

$$\bar{V}^i(t_0, \ell_p) = \frac{1}{\Delta\ell\Delta T} \int_0^{.5\Delta T} dt \left(\int_{(p-.5)\Delta\ell}^{(p+.5)\Delta\ell} V^i(t, \ell_i) d\ell_i \right) \tag{176}$$

and for $j > 0$ by

$$\bar{V}^i(t_j, \ell_i) = \frac{1}{\Delta\ell\Delta T} \int_{(j-.5)\Delta T}^{(j+.5)\Delta T} dt \left(\int_{(p-.5)\Delta\ell}^{(p+.5)\Delta\ell} V^i(t, \ell_i) d\ell_i \right) \tag{177}$$

5.4. Summary

The steps for the solution of the current and charge coefficients on an arbitrarily bent wire may be summarized.

1) Calculate the points of intersection between the wire and the circles of constant time delay. From these calculate the geometry functions $G(\alpha, i, k)$ from (137, 138, 139, 142, 149 and 150).

2) Calculate the first set of current coefficients from (164) if the wire is a scatterer or (175a,b) if an antenna. Calculate the charge coefficients from (136a,b). Calculate the vector potential from (153) and the scalar potentials from (161) and (162).

3) Calculate the current coefficients from (165) if wire is a scatterer or from (173) and (174) if an antenna.

4) Calculate the vector potentials from (169), the charge coefficients from (136c,d) and the scalar potentials from (161) and (162).

5) Advance the time index by one unit and go back to step 3).

These steps will be illustrated in the next chapter where the circular wire loop is analyzed.

Chapter 6

SCATTERING AND RADIATION BY THE CIRCULAR WIRE LOOP

Radiation and scattering by the circular wire loop are investigated by specializing the pulse tested solution for the arbitrarily bent wire to the circular loop geometry. The rotational symmetry of the loop is used to simplify the pulse tested geometry functions. Results are presented for the current and charge induced on the loop for a unit step propagating incident electric field, and for a unit step voltage applied across a subsection. The normalized radiated far field is presented for both cases of excitation.

6.1-1. The Current and Charge Expansions for the Loop

The form of the current and charge expansions for closed wire objects is given by (122) through (125), which are included here for convenience:

$$\underset{\sim}{I}(t,\ell') = \sum_{m=1}^{\infty}\sum_{k=1}^{N}\beta(m,k)P_1(\ell'-(k-.5)\Delta\ell)P_2(t-(m-1)\Delta T)\hat{U}_k \tag{178}$$

and

$$\beta(m,N+j) = \beta(m,j) \tag{179}$$

$$q(t,\ell') = \sum_{m=1}^{\infty}\sum_{k=1}^{N}\gamma(m,k)P_1(\ell'-(k-1)\Delta\ell)P_2(t-(m-.5)\Delta T) \tag{180}$$

and

$$\gamma(m,N+j) = \gamma(m,j) \tag{181}$$

where for the loop, $\Delta\ell = 2\pi r/N$, $\Delta T = \Delta\ell/v_p$, $\hat{U}_k$ is a unit vector tangent

to the direction of the k-th subsection, and r is the radius of the loop. The loop geometry is shown in Figure 6.1. The current subsectional geometry is shown in Figure 6.2.

The continuity relationships are given by (136a,b,c,d) which are repeated for convenience:

Initial Conditions [m=1]

$$\gamma(1,k) = -\left(\frac{\beta(1,k) - \beta(1,k-1)}{v_p}\right) \qquad k=2,3,\ldots,N \qquad (182a)$$

$$\gamma(1,1) = -\left(\frac{\beta(1,1) - \beta(1,N)}{v_p}\right) \qquad (182b)$$

$m = 2,3,\ldots$

$$\gamma(m,k) = \gamma(m-1,k) - \left(\frac{\beta(m,k)-\beta(m,k-1)}{v_p}\right) \qquad k=2,3,\ldots,N \qquad (182c)$$

$$\gamma(m,1) = \gamma(m-1,1) - \left(\frac{\beta(1,1)-\beta(1,N)}{v_p}\right) \qquad (182d)$$

6.1-2. The Pulse Testing Functions for the Loop

The pulse testing functions for the arbitrarily bent wire were given in the last chapter by equation (127) and equation (128) and are repeated for referral. Thus,

$$\underset{\sim}{S}_{0,i} = \frac{\hat{\ell}_i}{\Delta\ell\Delta T} P_1(\ell-(i-.5)\Delta\ell) \quad \text{for } -\frac{\Delta T}{2} \leq t < 0 \qquad (183)$$

$$\underset{\sim}{S}_{j,i} = \frac{\hat{\ell}_i}{\Delta\ell\Delta T} P_1(\ell-(i-.5)\Delta\ell)P_2(t-(j-.5)\Delta T) \qquad (184)$$

where $\hat{\ell}_i$ is a unit vector tangent to the i-th field subsection, P_2^a is the adjoint pulse function defined by (58b), and $\Delta\ell$ and ΔT are defined in Section (6.1-1).

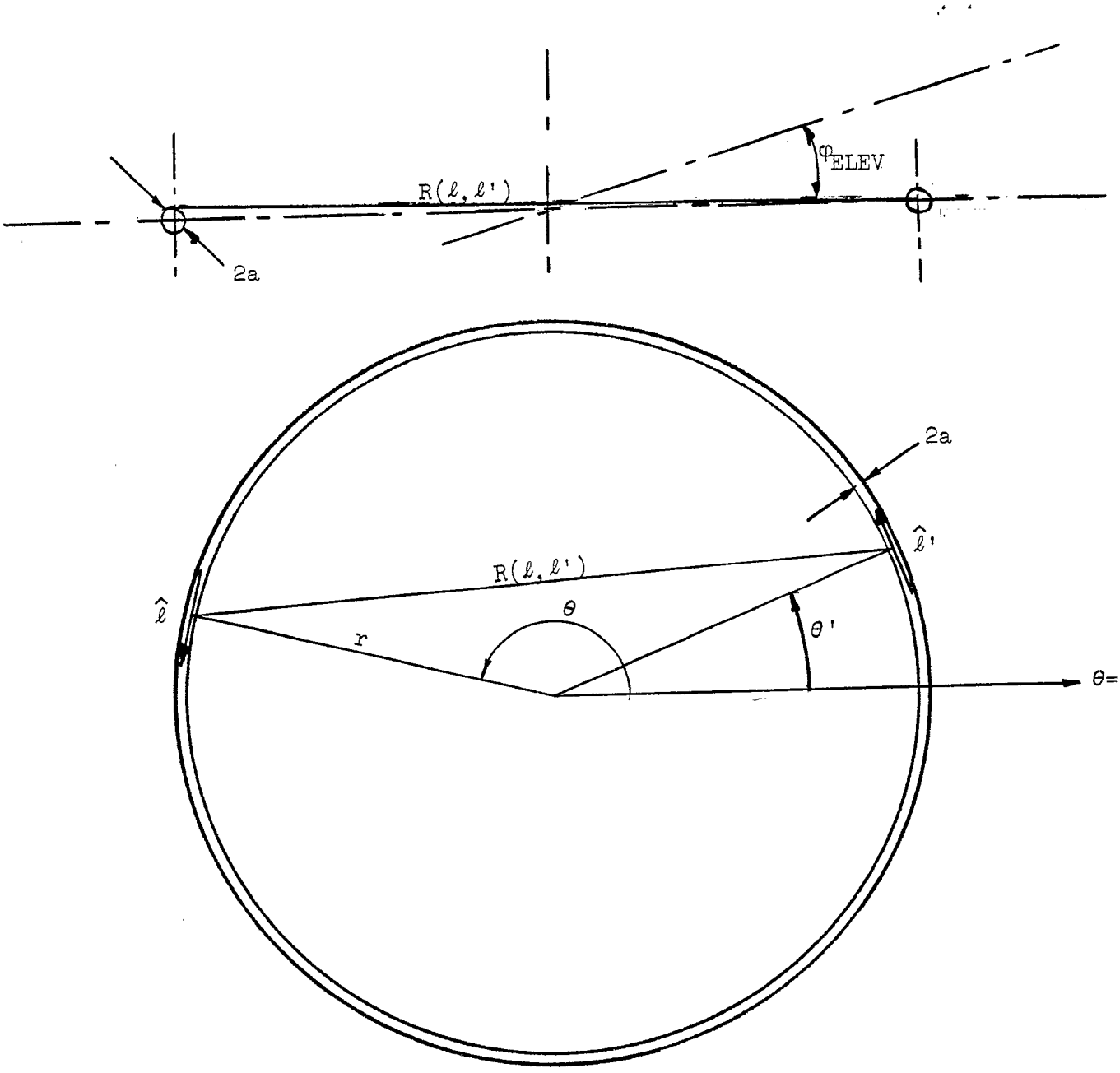

Geometry of the Loop

Figure 6.1

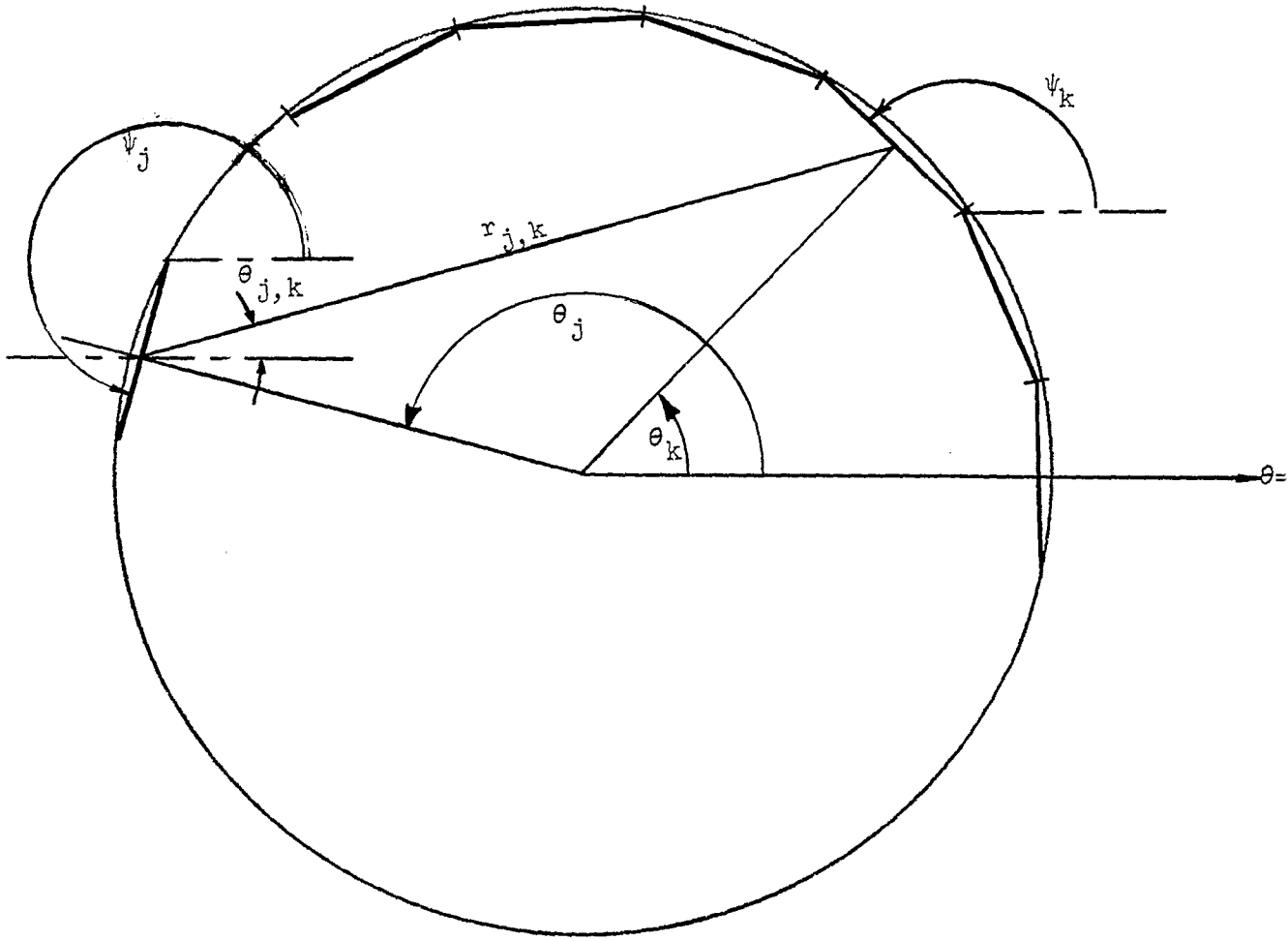

Current Subsectional Geometry

Figure 6.2

6.2. The Pulse Tested Solution for the Loop Current and Charge Coefficients

The solution steps outlined in Section 5.3 will be specialized to the loop in this section.

The circles of constant time delay intersect the loop at the points $\ell^+(\alpha,i)$ and $\ell^-(\alpha,i)$, where

$$\ell^+(\alpha,i) = i\Delta\ell + 2r \text{ arcsine } (\frac{2\pi(\alpha-.5)}{N}) \tag{185}$$

and

$$\ell^-(\alpha,i) = i\Delta\ell - 2r \text{ arcsine } (\frac{2\pi(\alpha-.5)}{N}) \tag{186}$$

The time delay index α takes the integer values $\alpha = 1,\ldots,S$, where $S = \text{Fix}(\frac{N}{\pi})$. The intersections ℓ^+ and ℓ^- are shown in Figure 6.3.

The loop pulse tested geometry functions are calculated from

$$G(\alpha,|i-k|) = \frac{1}{M}\sum_{m=0}^{MP} \log_e\left[\frac{(i+.5)\Delta\ell-A_m(i,k)+\sqrt{[(i+.5)\Delta\ell-A_m(i,k)]^2+B_m(i,k)}}{(i-.5)\Delta\ell-A_m(i,k)+\sqrt{[(i-.5)\Delta\ell-A_m(i,k)]^2+B_m(i,k)}}\right] \tag{187}$$

where α takes on the integer values $= 0,1,2,\ldots,S$

M is the number of sample points in an interval $\Delta\ell$

MP is the number of sample points in the interval $a_k \le z' \le b_k$

$$MP = \frac{b_k(\alpha) - a_k(\alpha)}{\Delta\ell}\ M \tag{188}$$

$$A_m(i,k) = [a_k(\alpha)+\frac{m\Delta\ell}{M}]\cos(\theta_i-\theta_k) - [r_{ik}+a]\sin(\theta_j-\theta_k) \tag{189}$$

$$B_m(i,k) = r_{ik}^2 + [a_k(\alpha)+\frac{m\Delta\ell}{M}]^2 + a^2 + 4r_{jk}a\sin^2(\frac{\theta_j-\theta_k}{2}) - 2r_{jk}[a_k(\alpha)+\frac{m\Delta\ell}{M}]\sin(\theta_j-\theta_k) - A_m^2(i,k) \tag{190}$$

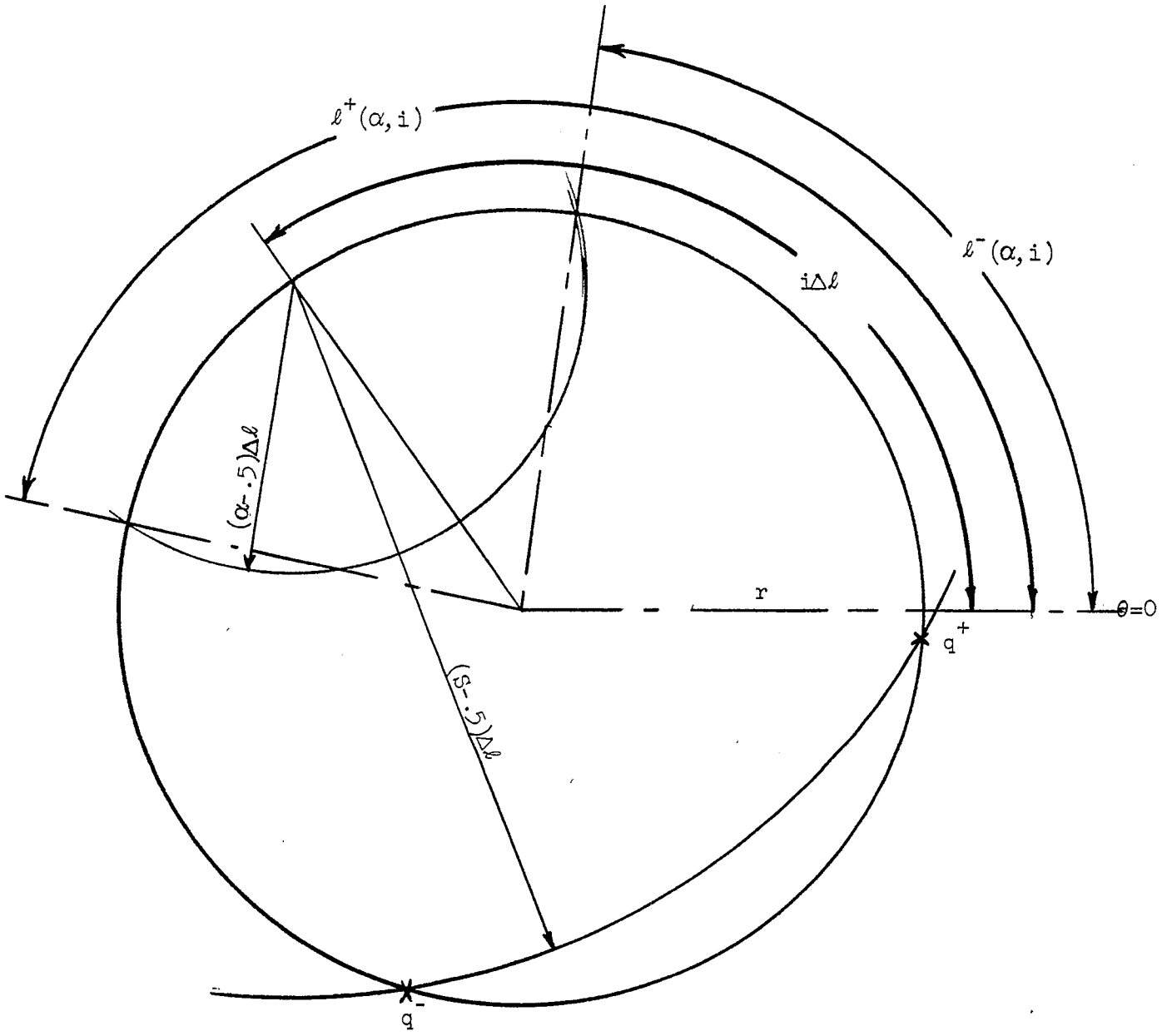

Intersections of a Constant Time Delay Circle and the Loop

Figure 6.3

and

$$r_{jk} = 2r \sin\{\frac{\theta_k - \theta_j}{2}\} \tag{191}$$

A simplification due to the rotational symmetry of the loop is that the geometry functions are functions of the absolute difference of the source and field subsection indices. This result permits a reduction of storage requirements for G by a factor of N. A further reduction in storage requirements is possible due to the mirror symmetry of the loop about any diameter. That is, for every source subsection k there is another source subsection ℓ which satisfies one of the following:

$$|i-k| = |\ell-i| \qquad 1 \leq k \leq i \leq \ell \leq N \tag{192}$$

or

$$|i-k| = |\ell-i+N| \qquad 1 \leq \ell \leq k \leq i \leq N \tag{193}$$

or

$$|i-k+N| = |\ell-i| \qquad 1 \leq i \leq \ell \leq k \leq N \tag{194}$$

It will be shown in the following sections that the quantities $\cos[\frac{2\pi}{N}(i-k)]$ and $G(\alpha, |i-k|)$ always occur together as a product. This product will be referred to as the modified pulse tested loop geometry functions. The modified pulse testing functions for a twenty subsection loop which has a radius of 5 meters and a loop radius to wire diameter ratio of 18.9 are given in Table 6.1. The symmetry demonstrated by equations (192) through (194) is readily evident for $\alpha = 1,2,3,\ldots,6$. If the difference of the subsectional indices is such that the source point is outside of the α time delay region, the geometry function is set to zero as required by (150).

$\alpha = 0$

1	3.2938	2	0.0	3	0.0	4	0.0	5	0.0
6	0.0	7	0.0	8	0.0	9	0.0	10	0.0
11	0.0	12	0.0	13	0.0	14	0.0	15	0.0
16	0.0	17	0.0	18	0.0	19	0.0	20	0.0

$\alpha = 1$

1	0.0	2	0.4664	3	0.003410	4	0.0	5	0.0
6	0.0	7	0.0	8	0.0	9	0.0	10	0.0
11	0.0	12	0.0	13	0.0	14	0.0	15	0.0
16	0.0	17	0.0	18	0.0	19	0.003410	20	0.4664

$\alpha = 2$

1	0.0	2	0.0	3	0.1856	4	0.007000	5	0.0
6	0.0	7	0.0	8	0.0	9	0.0	10	0.0
11	0.0	12	0.0	13	0.0	14	0.0	15	0.0
16	0.0	17	0.0	18	0.007000	19	0.1856	20	0.0

$\alpha = 3$

1	0.0	2	0.0	3	0.0	4	0.08170	5	0.007462
6	0.0	7	0.0	8	0.0	9	0.0	10	0.0
11	0.0	12	0.0	13	0.0	14	0.0	15	0.0
16	0.0	17	0.007462	18	0.08170	19	0.0	20	0.0

$\alpha = 4$

1	0.0	2	0.0	3	0.0	4	0.0	5	0.02722
6	0.60623×10^{-7}	7	0.0	8	0.0	9	0.0	10	0.0
11	0.0	12	0.0	13	0.0	14	0.0	15	0.0
16	0.60623×10^{-7}	17	0.02722	18	0.0	19	0.0	20	0.0

$\alpha = 5$

1	0.0	2	0.0	3	0.0	4	0.0	5	0.0
6	0.5903×10^{-7}	7	-0.02451	8	-0.006186	9	0.0	10	0.0
11	0.0	12	0.0	13	0.0	14	-0.006186	15	-0.02451
16	0.5903×10^{-7}	17	0.0	18	0.0	19	0.0	20	0.0

$\alpha = 6$

1	0.0	2	0.0	3	0.0	4	0.0	5	0.0
6	0.0	7	0.0	8	-0.03656	9	-0.05656	10	-0.06676
11	-0.07342	12	-0.06676	13	-0.05656	14	-0.03656	15	0.0
16		17	0.0	18	0.0	19	0.0	20	0.0

Modified Pulse Tested Geometry Functions for a 20 Subsection Loop

Table 6.1

Before the loop current coefficients can be evaluated the pulse tested incident electric field must be found. Unlike the straight wire, the loop interacts with both horizontally and vertically polarized plane wave incident electric fields.* Let us denote these two cases by $\underset{\sim}{E}^{i(H)}$ and $\underset{\sim}{E}^{i(V)}$, respectively. The incident plane wavefront will be assumed to be normal to the plane $\theta = 0$.

The tangential component of the vertically polarized incident field is given by:

$$\left\langle \underset{\sim}{E}^{i(V)}, \underset{\sim}{S}_{j,i} \right\rangle =$$

$$\frac{\sin \varphi_{elev}}{\Delta T \Delta \ell} \int_{(j-\frac{1}{2})\Delta T}^{(j+\frac{1}{2})\Delta T} dt \int_{(i-\frac{1}{2})\Delta \ell}^{(i+\frac{1}{2})\Delta \ell} \left| E^i\left(t - \frac{r}{v_p}\left(1-\cos\left(\frac{\ell}{r}\right)\right)\cos\varphi_{elev}\right)\right| \sin\left(\frac{\ell}{r}\right) d\ell \tag{195}$$

For sufficiently fine sampling, this equation can be approximated by

$$\left\langle \underset{\sim}{E}^{i(V)}, \underset{\sim}{S}_{j,i} \right\rangle \approx \sin\left(\frac{i\Delta\ell}{r}\right)\sin\varphi_{elev} \left| E^i\left(j\Delta T - \frac{r}{v_p}\left(1-\cos\left(\frac{i\Delta\ell}{r}\right)\cos\varphi_{elev}\right)\right)\right| \tag{196}$$

over those indices i such that

$$(j+.5)\Delta T - \frac{r}{v_p}\left(1-\cos\left(\frac{i\Delta\ell}{r}\right)\cos\varphi_{elev}\right) > 0 \tag{197}$$

for each $j = 0, 1, 2, \ldots$. The tangential component of the horizontally polarized incident field is found by an analogous procedure to be

$$\left\langle \underset{\sim}{E}^{i(H)}, \underset{\sim}{S}_{j,i} \right\rangle \approx \cos\left(\frac{i\Delta\ell}{r}\right) \left| E^i\left(j\Delta T - \frac{r}{v_p}\left(1-\cos\frac{i\Delta\ell}{r}\right)\cos\varphi_{elev}\right)\right| \tag{198}$$

for all j,i such that (197) is satisfied.

*A vertically polarized plane wave field has a vector component normal to the plane of the loop. A horizontally polarized plane wave field is defined as a field whose direction is parallel to the plane of the loop. An arbitrarily polarized plane wave field can always be decomposed into a linear combination of vertical and horizontal polarizations.

During the transient period in which the plane wave has not yet traversed the diameter of the loop, the pulse testing integral weights the partially excited subsections by the ratio of the excited portion of the subsection to the total subsection length. Equations (196) and (198) must be multiplied by a factor of $(\frac{1}{2})$ for j = 0 due to the half interval time testing function $\underset{\sim}{S}_{0,i}$. The first set of current coefficients is given by (164)

$$\beta(1,i) = \frac{\langle \underset{\sim}{E}^{i}, \underset{\sim}{S}_{0,i} \rangle}{(\Omega(i)/2) + (\mu G(0,0)/4\pi\Delta T)} \qquad i = 1,\ldots,N \tag{199}$$

$\underset{\sim}{E}^{i}$ is either $\underset{\sim}{E}^{i(H)}$ or $\underset{\sim}{E}^{i(V)}$. The first set of charge coefficients is found from (182a,b). The vector potential is given by

$$\bar{A}(t_1, \ell_i) = \frac{\mu}{4\pi} \beta(1,i)\ G(0,0) \tag{200}$$

and the first scalar potentials by

$$\bar{\Phi}(t_1, \ell_i + \frac{\Delta\ell}{2}) = \frac{1}{4\pi\epsilon} \gamma(1,i+1)\ G(0,0) \tag{201}$$

$$\bar{\Phi}(t, \ell_i - \frac{\Delta\ell}{2}) = \frac{1}{4\pi\epsilon} \gamma(1,i)\ G(0,0) \tag{202}$$

The algorithm proceeds in the manner described in the preceding chapters.

The vector potential contribution $\langle \frac{\partial \underset{\sim}{A}}{\partial t}, \underset{\sim}{S}_{j,i} \rangle$ as noted in the previous chapter can be expressed in terms of the difference of the averaged vector potentials $\bar{A}(t_{j+1}, \ell_i)$ and $\bar{A}(t_j, \ell_i)$.

$$\langle \frac{\partial \underset{\sim}{A}}{\partial t}, \underset{\sim}{S}_{j,i} \rangle = \frac{1}{\Delta T}[\bar{A}(t_{j+1}, \ell_i) - \bar{A}(t_j, \ell_i)] \tag{203}$$

The vector potentials are given by:

$$\bar{A}(t_{j+1}, \ell_i) = \frac{\mu}{4\pi}\left[\beta(j+1,i)\ G(0,0) + \sum_{\alpha=1}^{S-1}\left(\sum_{p=m^-}^{m^+} \beta(j+1-\alpha,p)\ G(\alpha,|i-p|) + \sum_{p=n^-}^{n^+} \beta(j+1-\alpha,p)\ G(\alpha,|i-p|)\right) + \sum_{p=q^-}^{q^+} \beta(j+1-S,p)\ G(S,|i-p|)\right] \tag{204}$$

where summation terminates in all cases when $j + 1 - \alpha < 1$. $\alpha = 1,2,\ldots,S$, and by

$$\bar{A}(t_j, \ell_i) = \frac{\mu}{4\pi}\left[\beta(j,i)\ G(0,0) + \sum_{\alpha=1}^{S-1}\left(\sum_{p=m^-}^{m^+} \beta(j-\alpha,p)\ G(\alpha,|i-p|) + \sum_{p=n^-}^{n^+} \beta(j-\alpha,p)\ G(\alpha,|i-p|)\right) + \sum_{p=q^-}^{q^+} \beta(j-S,p)\ G(S,|i-p|)\right] \tag{205}$$

where summation terminates in all cases when $j - \alpha < 1$, $\alpha = 1,2,\ldots,S$.

Note that

$$\begin{aligned} S &= \mathrm{Fix}(N/\pi) \\ m^+ &= \mathrm{Fix}(\ell^+(\alpha+1,i)/\Delta\ell \\ m^- &= \mathrm{Fix}(\ell^+(\alpha,i)/\Delta\ell \\ n^+ &= \mathrm{Fix}(\ell^-(\alpha,i)/\Delta\ell \\ n^- &= \mathrm{Fix}(\ell^-(\alpha+1,i)/\Delta\ell) \\ q^+ &= \mathrm{Fix}(\ell^+(S,i)/\Delta\ell) \\ q^- &= \mathrm{Fix}(\ell^-(S,i)/\Delta\ell) \\ j &= 1,2,\ldots \\ i &= 1,2,\ldots,N \end{aligned} \tag{206}$$

S is the number of time delay circles which intersect the loop. The next time delay circle (S+1) would completely enclose the loop. The summations over m^- to m^+ and n^- to n^+ are the summations over the source coordinates which lie in the α time delay region. If the time delay circles bounding the α time delay region intersect a subsection between its endpoints, then $m^-(\alpha+1) = m^+(\alpha)$ and $n^-(\alpha+1) = n^+(\alpha)$; however, if the time delay circle intersects the loop at the beginning of a subsection, then $m^-(\alpha+1) = m^+(\alpha) + 1$ and $n^-(\alpha+1) = n^+(\alpha) + 1$. If the intersections of the S' time delay circle occur within source subsections, then $q^- = m^+(S)$ and $q^+ = n^-(S)$, and if at the beginning or end of a subsection, $q^- = m^+(S) + 1$ and $q^+ = n^-(S) - 1$. Figure 6.4 illustrates these quantities.

The pulse tested scalar potential contribution has been shown to be expressible as the difference

$$\left\langle \nabla\Phi, \underset{\sim}{S}_{j,i} \right\rangle = \frac{1}{\Delta\ell}\left[\bar{\Phi}(t_j, \ell_i + \frac{\Delta\ell}{2}) - \bar{\Phi}(t_j, \ell_i - \frac{\Delta\ell}{2})\right] \tag{207}$$

The extension to $j > 1$ proceeds in a manner analogous to the calculation of $\left\langle \frac{\partial \underset{\sim}{A}}{\partial t}, \underset{\sim}{S}_{j,i} \right\rangle$. The potentials $\bar{\Phi}(t_j, \ell_i + \frac{\Delta\ell}{2})$ and $\bar{\Phi}(t_j, \ell_i - \frac{\Delta\ell}{2})$ can be shown to be given by

$$\bar{\Phi}(t_j, \ell_i + \frac{\Delta\ell}{2}) = \frac{1}{4\pi\epsilon}\Bigg[\gamma(j, i+1)G(0,0) + \sum_{\alpha=1}^{S-1}\Bigg(\sum_{p=m^-}^{m^+}\gamma(j-\alpha, p+1)G(\alpha, |p+1-i|) + \sum_{p=n^-}^{n^+}\gamma(j-\alpha, p+1)G(\alpha, |p+1-i|)\Bigg) + \sum_{p=q^-}^{q^+}(\gamma(j-S, p+1)G(S, |p+1-i|)\Bigg] \tag{208}$$

where summation terminates for $j-\alpha < 1$, $\alpha = 1, \ldots, S$, and by

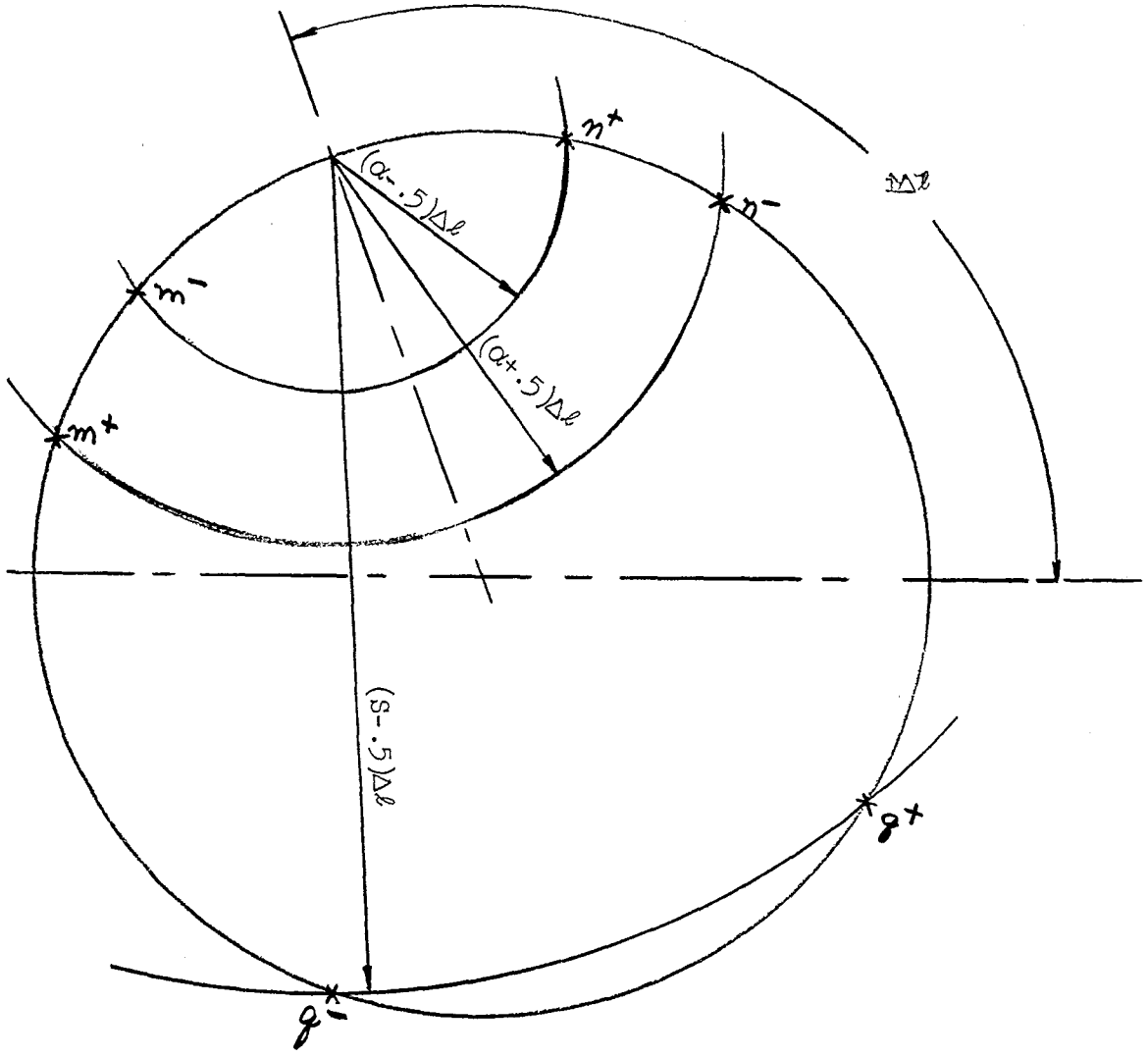

Intersections of the Loop and a Set of
Constant Time Delay Circles

Figure 6.4

$$\bar{\Phi}(t_j, \ell_i - \frac{\Delta\ell}{2}) = \frac{1}{4\pi\epsilon}\Bigg[\gamma(j,i)G(0,0) + \sum_{\alpha=1}^{S-1}\Bigg(\sum_{p=m^-}^{m^+}\gamma(j-\alpha,p)G(\alpha,|p-i|) + \sum_{p=n^-}^{n^+}\gamma(j-\alpha,p)G(\alpha,|p-i|)\Bigg) + \sum_{p=q^-}^{q^+}\gamma(j-S,p)G(s,|p-i|)\Bigg] \tag{209}$$

where summations terminate for $j-\alpha < 1$, $\alpha = 1,\ldots,S$. All quantities S, m^+, m^-, etc. are as defined in (206).

A general note on the summations involved in (204), (205), (208), and (209) is in order. When necessary, the periodic boundary conditions

$$\gamma(j,k+N) = \gamma(j,k) \tag{210a}$$

$$\beta(j,k+N) = \gamma(j,k) \tag{210b}$$

and

$$\gamma(j,k-p) = \gamma(j,N-(p-k)) \qquad p \geq k \tag{210c}$$

$$\beta(j,k-p) = \beta(j,N-(p-k)) \tag{210d}$$

must be applied. The current coefficients are found by the substitution of the vector and scalar potentials into (164) and (165). The charge coefficients are found from (182). The vector potential terms are found from (204), (205), and (206), and the scalar potentials from (208) and (209). When the loop is excited as an antenna, (173), (174), and (175) are readily specialized to the loop.

6.3. The Pulse Tested Normalized Radiated Far Field

The normalized radiated far field of a loop has only an azimuthal component E_ϕ. There is no polar component(θ-component in spherical coordinates) because the dot product between $\hat{U}_\theta$ and the current subsections is zero. The receiver geometry is shown in Figure 6.5.

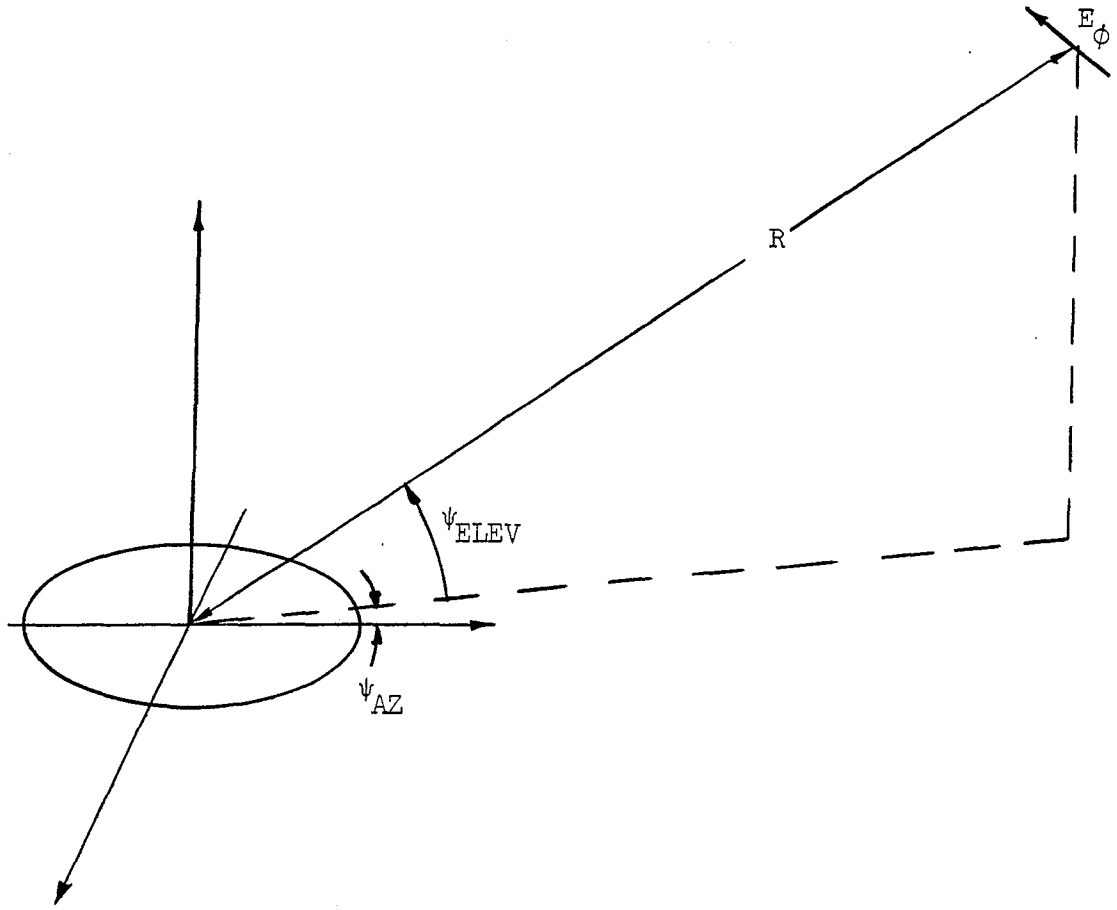

Loop-Receiver Geometry

Figure 6.5

The testing current at the far field point is an azimuthally directed dipole of the same type as considered in Chapter 4. The testing current radiates an impulsive electric field

$$\underset{\sim}{E}_2(t,R) = -\frac{\mu}{4\pi}\left(\frac{1}{R}\right)\left[\frac{\delta(t+t_0) - \delta(t+t_0+\Delta T)}{\Delta T}\right]\hat{U}_\phi \qquad (211)$$

where t_0 = time delay between the field point and any point at R, and

$\hat{U}_\phi$ is an azimuthally directed unit vector.

The field $\underset{\sim}{E}_2$ is the testing field in the reciprocity expression (107). The normalized electric field RE_ϕ radiated by the loop can be shown to be given by the expression

$$|\underset{\sim}{R}|E_\phi(t_j+|\underset{\sim}{R}|/v_p,\underset{\sim}{R}) = -\frac{\eta}{4\pi}\left(\frac{1}{\Delta\ell}\right)\sum_{i=1}^{N}\left(\cos(\psi_{AZ} - \left(\frac{2\pi}{N}\right)i)\right)$$
$$\left(\{DLC(\alpha,|i-k|)[\beta(j-\alpha,i)-\beta(j-1-\alpha,i)]\}\right.$$
$$\left.+\{DCC(\alpha,|i-k|)[\beta(j-1-\alpha,i)-\beta(j-z-\alpha,i)]\}\right) \qquad (212)$$

where

$$\alpha = \text{Fix}\left[\frac{N}{2\pi}(1-\cos(\psi_{AZ}-\left(\frac{2\pi}{N}\right)i)\cos\ \psi_{ELEV}\right]$$

$$DCC(\alpha,|i-k|) = \Delta\ell - DLC(\alpha,|i-k|)$$

η = free space wave impedance

ψ_{AZ} = the azimuthal position of the field point

ψ_{ELEV} = the elevation of the field point

and, $DLC(\alpha,|i-k|)$ is the part of the i-th subsection which is excited

by the testing field as it propagates over the loop. DLC(α, |i-k|) performs the same role as the geometry functions G(α, |i-k|), in the evaluation of the pulse tested far field. The form of the DLC's is simpler than the G's because R is a constant in (212) and may be extracted from the integral leaving simple linear integrals which are evaluated as DLC(α, |i-k|) and DCC(α, |i-k|).

6.4. Conclusions

It has been shown that the loop may be analyzed by use of the method of moments solution formulated for the arbitrarily bent wire. The algorithm that results is iterative in the time domain. The far field of the loop can be analyzed by a moments solution which is analogous to the straight wire far field formulation found in Chapter 4.

6.5. Computations for the Loop

Computations have been made for the current and scalar potential along a loop when the loop is excited as an antenna. The geometry is shown in Figure 6.6. The ratio of loop radius to wire diameter considered was 18.92. The exciting voltage was a unit step applied as shown. Two cases of source resistance were considered: $R_g = 0\ \Omega$ and $R_g = 100\ \Omega$ (the matched case).

Let us examine Figure 6.7 which shows plots of the spatial distribution of current and scalar potential at selected instants of time. As the current wave travels away from the source, the vector directions of the current are away from the plus (+) terminal and towards the minus (-) terminal of the source. This is indicated on the figure by + and -

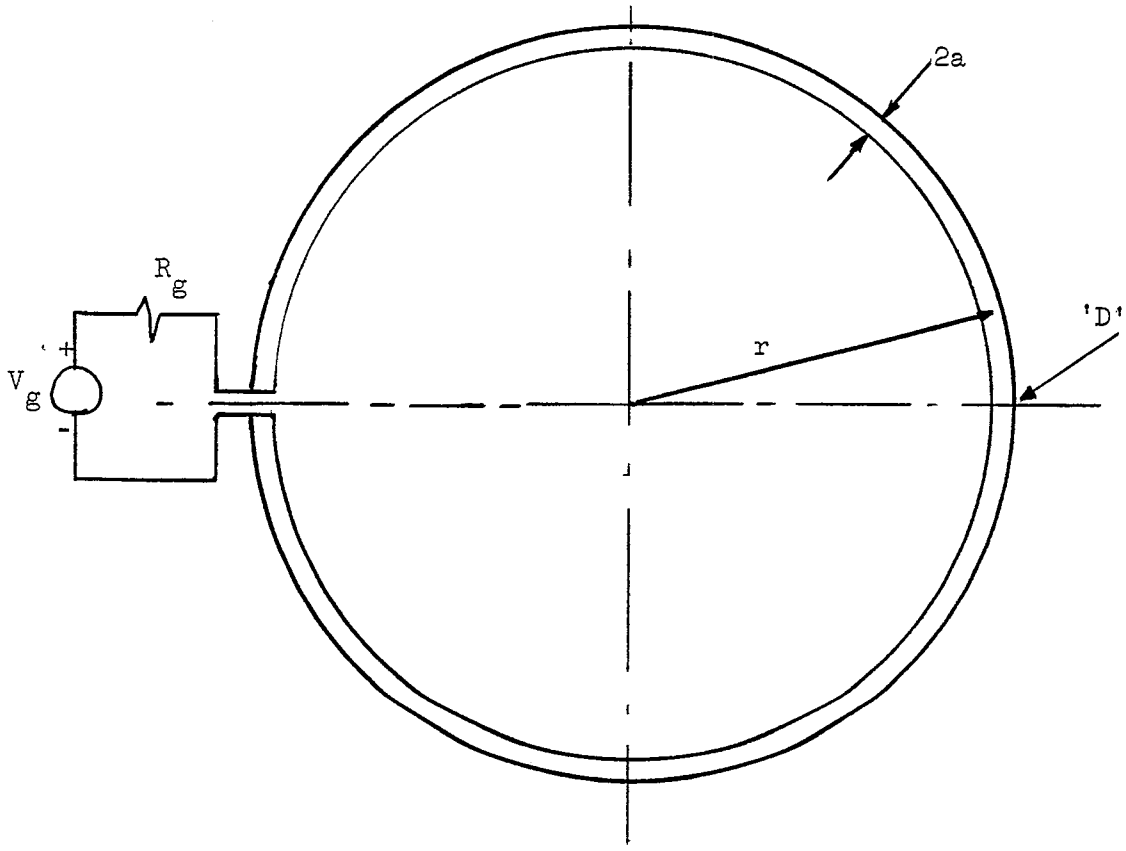

The Loop Excited as an Antenna

Figure 6.6

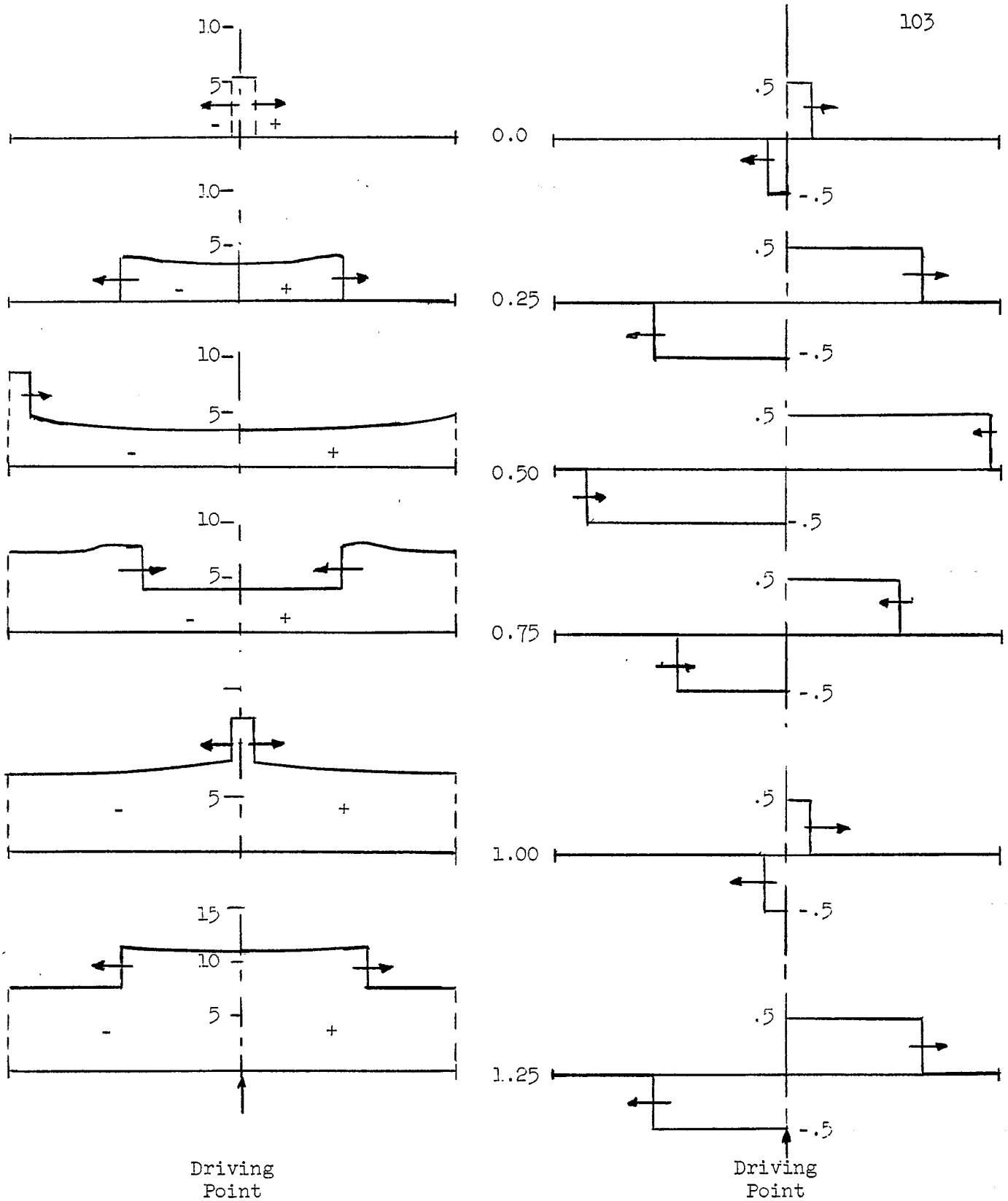

The Spatial Distribution of Current and Voltage for the Step Excited Loop at Selected Instants of Time for $R_g = 0.0$

Figure 6.7

respectively. When the current reaches a point opposite the source (marked as point "D" on Figure 6.6) at $t/\tau_L^* = 0.5$, the currents add as shown. Because of the shift of the time axis of the charge by $\Delta T/2$, the scalar potential is ahead of the current waveform in time (i.e., 0.5 corresponds to 0.55, etc.). The driving point current for $R_g = 0$, and $R_g = 100\ \Omega$ is shown in Figure 6.8. The behavior of the current for $R_g = 0.0$ is explained above. As expected as $t/\tau_L \longrightarrow \infty$, the current driven through the $R_g = 100\ \Omega$ approaches 10 ma. The current reaches 90% of its final value at $T/\tau_L \approx 3.0$. If an exponential fit to the data is made, the time constant is ≈ 1.3. Assuming the exponential behavior can be characterized by a series R-L circuit, the inductance is found to be

$$L \approx 130\ \tau_L \tag{213}$$

assuming the resistance $R = R_g$. For a loop $r = 0.5$ meters, $r/a = 18.92$, an equivalent inductance of

$$L = 1.35\mu \text{ henries} \tag{214}$$

is found. This agrees to within an order of magnitude with the inductance calculated from the susceptance curves found in Reference 1, page 93, for small b/λ, and in effect (213) can be taken as a rule of thumb.

---

*$\tau_L = 2\pi r/v_p$

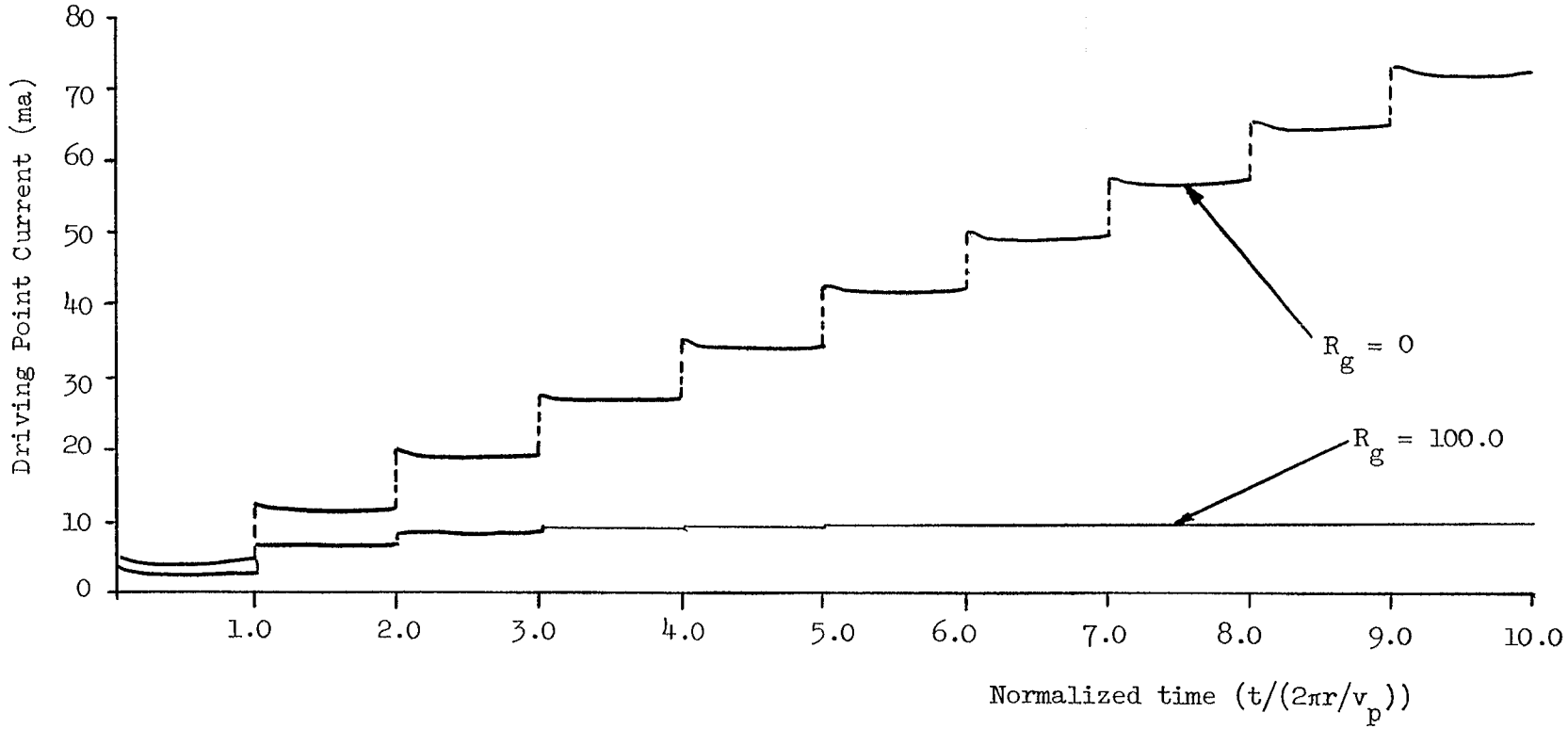

Circular Loop Driving Point Current for Step Excitation

Figure 6.8

Chapter 7

DISCUSSION

Additional results were computed for the straight wire scatterer, using the pulse tested formulation developed in Chapter 3. Figure 7.1 shows the normalized scattered field of a wire illuminated by a unit step electric field incident at 45°. Figure 7.2 illustrates the geometry. The scattered field is largest in the direction $\theta_R = \pi - \theta_{INC}$. Simple ray theory suffices for explanation. As the incident wave A propagates over the scatter, currents in each subsection are excited. These currents radiate a wave which is in time phase along the wavefront B. Hence, the radiation is largest in the direction $\theta_R = \pi - \theta_{INC}$.

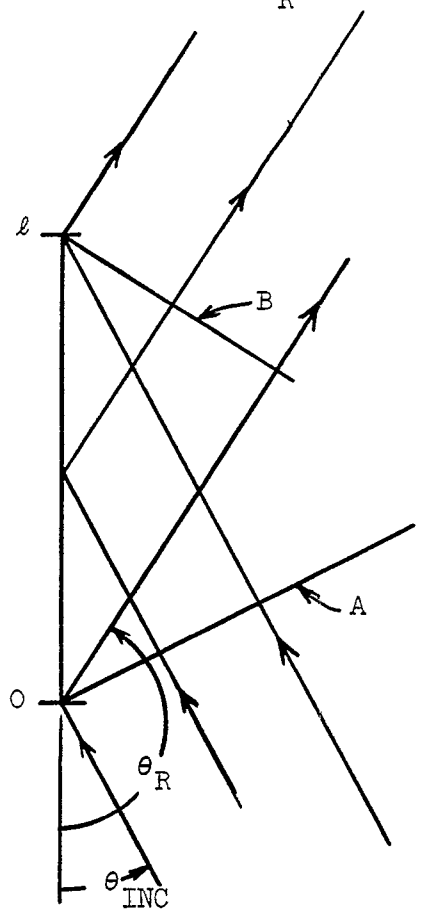

Scattering by a Straight Wire

Figure 7.2

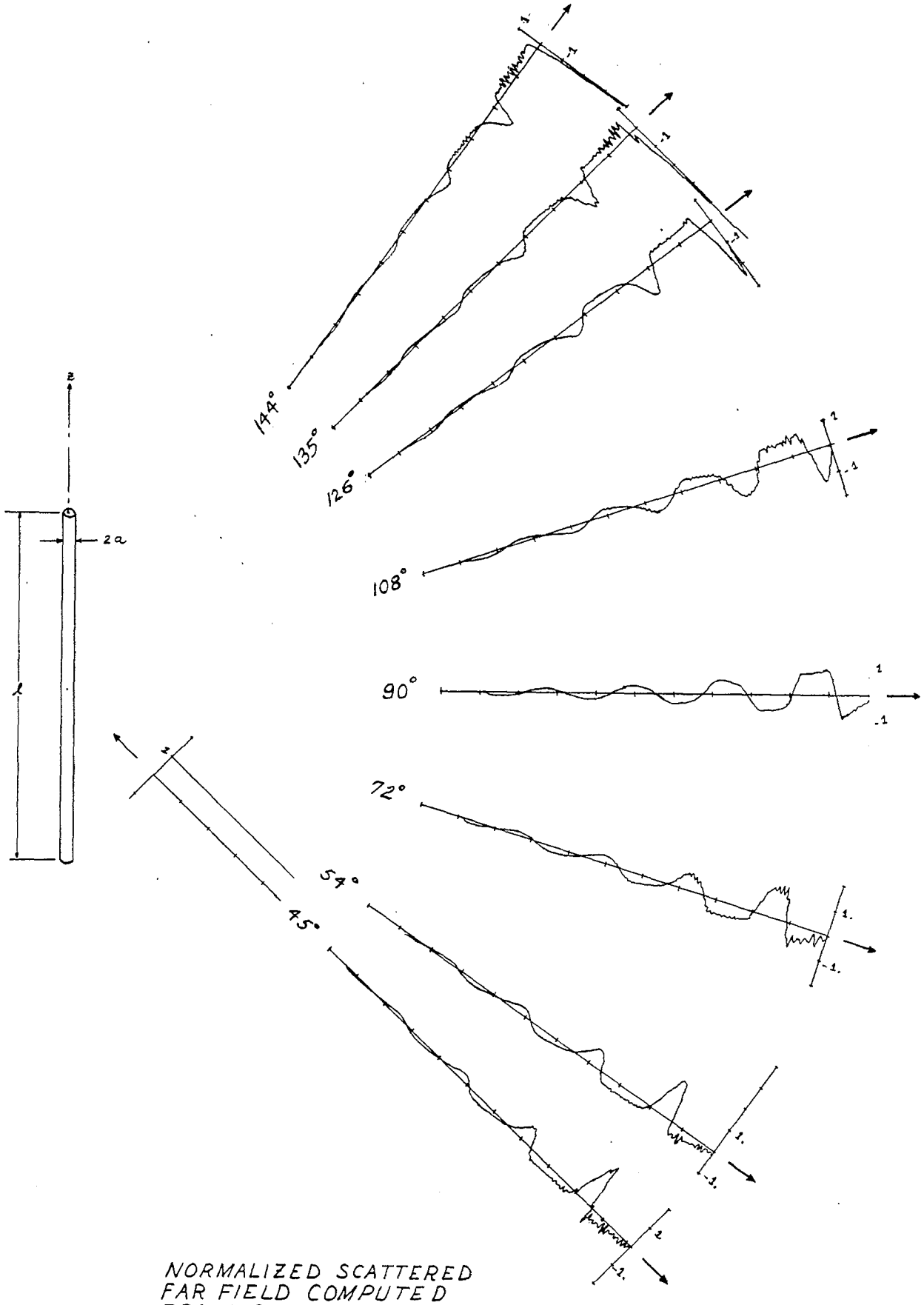

NORMALIZED SCATTERED FAR FIELD COMPUTED FROM PULSE TESTED CURRENT FOR $\theta_{INC} = 45°$

FIGURE 7-1

In the back scattered direction, no significant field is received until the time $t = \ell/v_p\ (1 + \cos \theta_{INC})$. This was experimentally verified by Hong, Borison and Ford.[26] The authors analyzed the results using an asymptotic ray theory developed by Ufimtsev.[27] The computations shown in Figures 4.4 and 7.1 agree with the results of these authors. The response at $\ell/v_p\ (1 + \cos \theta_{INC})$ was first analyzed by Peters.[28] He suggested that a traveling wave launched at the near end and then reflected at the far end is the source of the back scattered energy. The results presented in Figure 3.5 substantiate this suggestion. The current grows as it travels from the near end to the far end of the scatterer. When this current reaches $z' = \ell$, it is reflected, and simultaneously radiates a large field. It is this field contribution radiating in the back scattered direction which was noted by Peters.

The center driven straight wire antenna was investigated in Chapters 2 and 3 of this paper. The effect of changes in the source resistance R_g is shown in Figures 2.6, 2.7, and 3.3. (For $R_g = 0$, the value of the driving point current at $t = 0$ obtained by the pulse tested method of moments agrees with the exact value calculated by T. T. Wu[12] within 5%.) The effect of changes in the source resistance on the driving point current may be summarized. Increases in R_g cause the current to damp out faster, but do not materially affect the shape of the waveform. The effects of changes in the position of the feedpoint were also investigated. The feedpoint was moved from $z' = \ell/2$ to $z' = 3\ell/4$. The driving point current and the radiated far fields were calculated. The results are presented in Figures 7.3 and 7.4. In Figure 7.3, the driving point is $z' = 3\ell/4$.

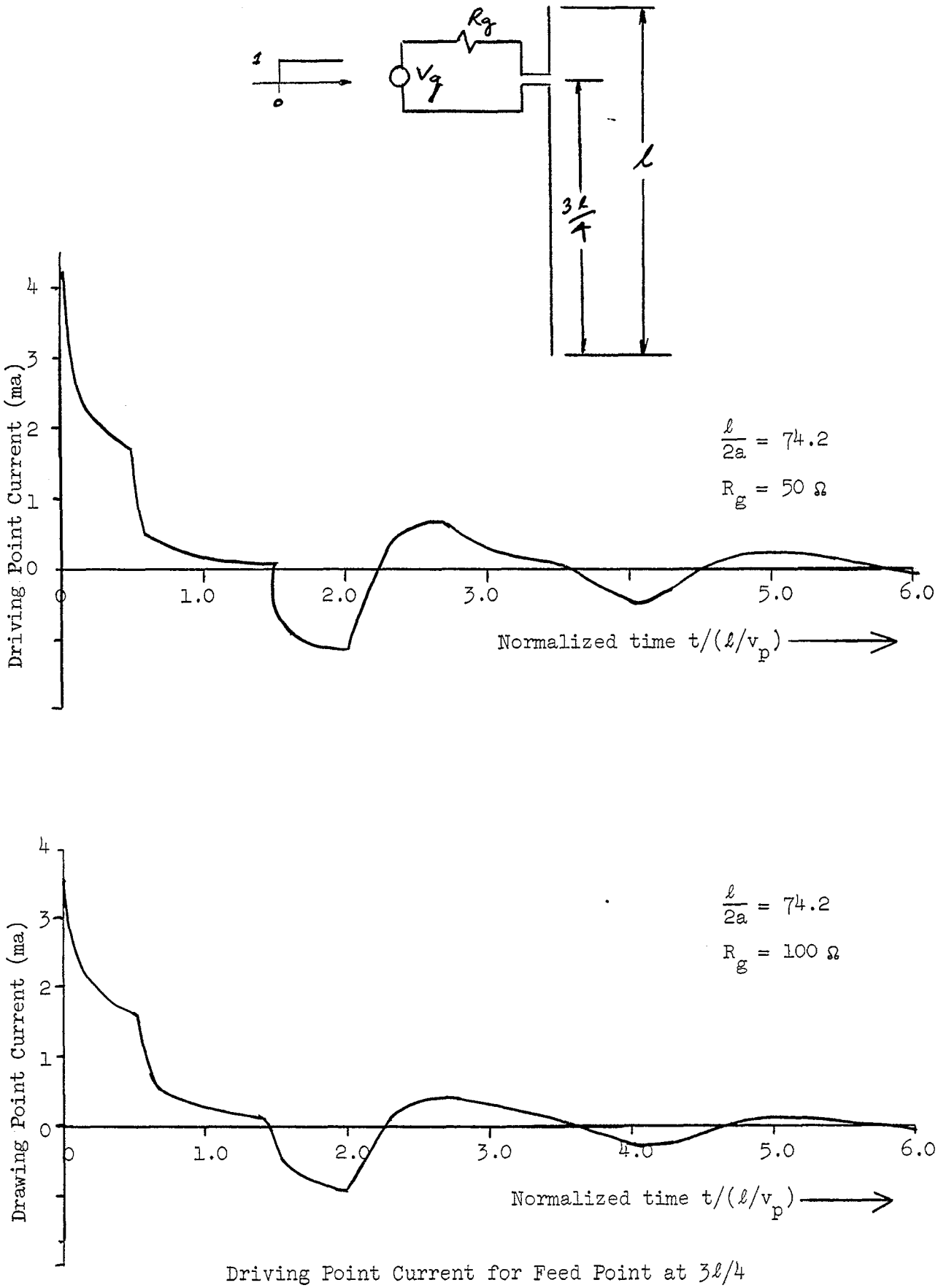

Driving Point Current for Feed Point at $3\ell/4$

Figure 7.3

The driving point current is shown for two different source resistances. It is interesting to compare Figure 7.3 with the results for the center driven antenna shown in Figures 3.2 and 3.3. The differences can be explained qualitatively by transmission line traveling wave theory. It was shown in Chapter 2 that a voltage source applied to the dipole excites two current waves traveling towards opposite ends of the wire. Let the wave traveling towards $z' = 0$ be denoted I_0 and the wave traveling towards $z' = \ell$ be denoted I_ℓ. Let the reflection coefficient of the wire end be denoted R. The center fed driving point current will be examined first. Between $0 \leq t/\tau_L < 1.0$*, neither I_0 nor I_ℓ has returned to the driving point. At $t/\tau_L \approx 1.0$, the two current waves reflected from the wire ends arrive at the driving point simultaneously and add, giving $-R(I_0 + I_\ell)$. The net current is driven to a negative value, since the driving point current has decreased from its value at $t = 0$ due to radiation. The waves proceed along the wire in this manner giving the entire time response.

Let the case for the wire driven at $z' = 3\ell/4$ be investigated similarly. Between $0 \leq t/\tau_L < 0.5$, neither I_0 nor I_ℓ has returned to the driving point. However, between $0.5 \leq t/\tau_L < 1.5$, the driving point current almost vanishes due to the return of the current $-RI_\ell$ from $z' = \ell$. At $t/\tau_L \approx 1.5$, the current $-RI_0$ returns from $z' = 0$ and causes the current to further decrease to negative values. The droop of the driving point current between $0 \leq t/\tau_L \leq 1.5$, is due to radiation at the source. Bulgakov[11] maintains that when R_g is matched, all current flow ceases after the two current waves reach the source. Figures 3.3 and 7.3 (for

---

*$\tau_L = \ell/v_p$

$R_g = 100\ \Omega$, the matched case) show this is not the case. Only when radiation from the source and wire ends is neglected is his conjecture true. It must be concluded that transmission line analysis without these effects is only qualitatively correct.

In the frequency domain, a paper by Shen, Wu and King[30] demonstrates that if the proper reflection coefficients are used for the ends of the wire, and the radiation is handled correctly, that transmission line-traveling wave theory can be used to analyze the dipole antenna. The effect of moving the feed from $z' = \ell/2$ to $z' = 3\ell/4$ on the dipole radiated far field is shown in Figure 7.4. In this figure the fields are plotted as a function of space at a fixed instant of time. The normalized far field RE_θ for the center fed dipole is shown on the left, and the field radiated by the dipole fed at $3\ell/4$ is shown on the right. The source resistance $R_g = 100\ \Omega$. As expected, the field radiated by the center fed dipole is symmetric about $\theta_R = 90^\circ$, but the far field for the antenna fed at $3\ell/4$ is shifted towards $\theta_R = 0$. This would indicate that the far field tends to shift towards the traveling wave as the feed is moved away from the center. In this case, the traveling wave propagates towards $z' = 0$. (The geometry shown in Figure 7.2 is applicable.)

It has been shown that the method of moments can be used to treat thin wire radiation and scattering in the time domain. Other problems can be treated by modifications or extensions of the theory. For example, the problem of scattering by bodies of revolution can be treated in a manner similar to that developed for the loop. Reactive loads can be treated by defining the proper operator on the current and charge for

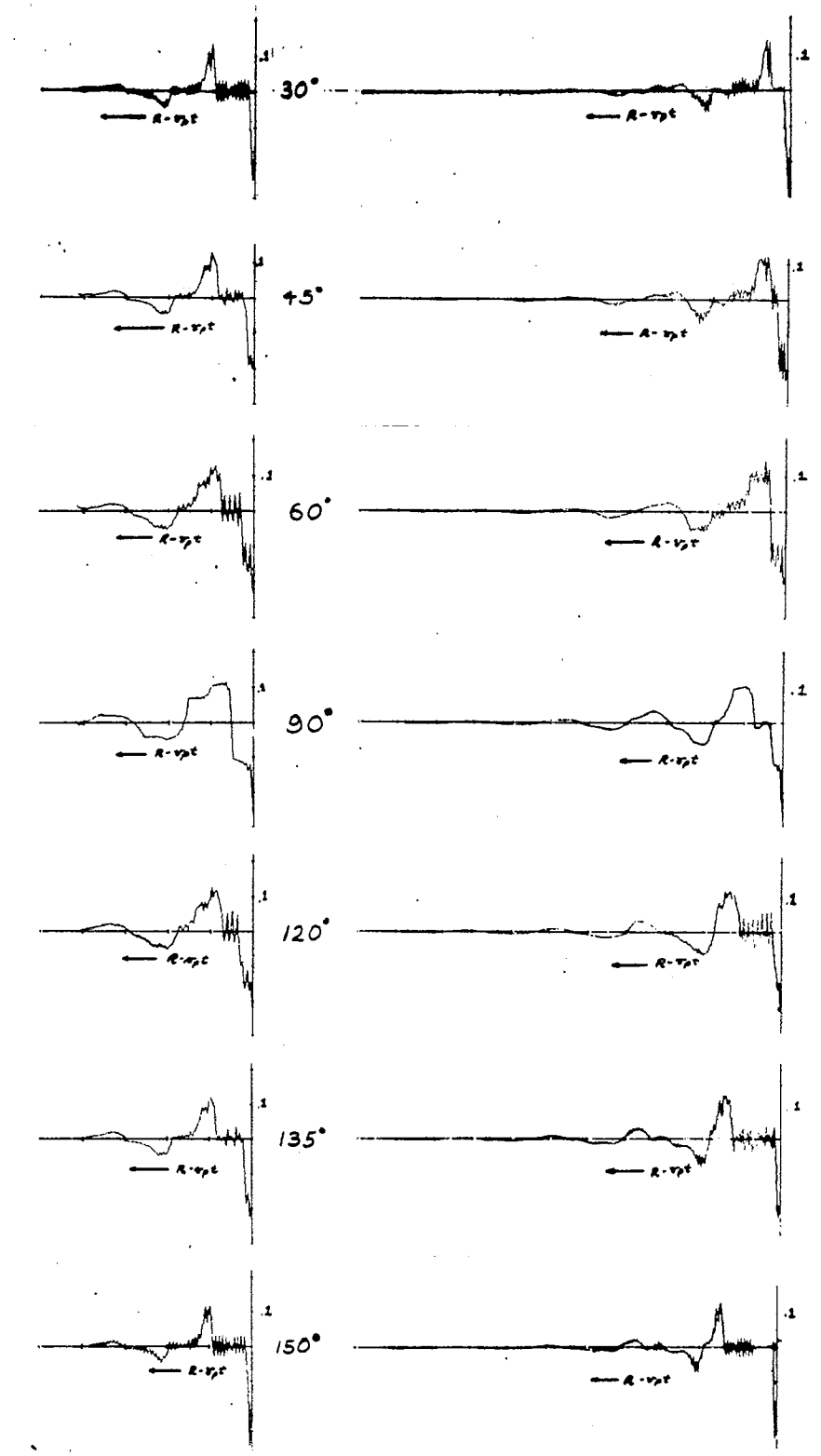

COMPARISON OF NORMALIZED RADIATED FIELD RE_ϕ AS FEED POINT IS CHANGED - $R_2 = 100$

FIGURE 7.4

these elements. The reflection coefficients at the ends of the wire can be determined by a careful evaluation of the fields in the vicinity of the wire ends.

Numerical errors which occurred in the results are due to the time delay approximation used in the evaluation of the retarded potential integrals. These errors can be substantially reduced by a more sophisticated handling of these integrations.

Appendix A

A TIME RECIPROCITY THEOREM FOR WIRE OBJECTS

A time reciprocity theorem which is the basis for the method of moments solutions for wire objects is developed in this appendix. The identification of the negative time domain with the adjoint time space is an integral part of the theorem.

Let the following functions be defined on the time and space domains:

$$\underset{\sim}{E}_1(t,\ell) = 0 \qquad t < 0 \tag{A.1}$$

$$\underset{\sim}{I}^{(1)}(t,\ell') = 0 \qquad t < 0 \tag{A.2}$$

$$\underset{\sim}{I}^{(2)}(t,\ell) = 0 \qquad t > 0 \tag{A.3}$$

$$q^{(1)}(t,\ell') = 0 \qquad t \leq 0 \tag{A.4}$$

$$q^{(2)}(t,\ell) = 0 \qquad t \geq 0 \tag{A.5}$$

The inner product $\left\langle \underset{\sim}{E}^{(1)}(t,\ell),\ \underset{\sim}{I}^{(2)}(-t,\ell) \right\rangle$ will be taken over the unprimed coordinates ℓ. (The notation $\hat{U}_k$ will be used to denote unit vector tangent to the subscript coordinate system.) Thus,

$$\left\langle \underset{\sim}{E}^{(1)}(t,\ell),\ \underset{\sim}{I}^{(2)}(t,\ell) \right\rangle = \int_0^\infty \int_\ell \left[\frac{\partial}{\partial t} \left(\frac{\mu}{4\pi} \int_{\ell'} \frac{\underset{\sim}{I}^{(1)}(t-\tau,\ell')}{R(\ell,\ell')}\, d\ell' \right) + \hat{U}_\ell \frac{\partial}{\partial \ell} \left(\frac{1}{4\pi\epsilon} \int_{\ell'} \frac{q^{(1)}(t-\tau,\ell')}{R(\ell,\ell')}\, d\ell' \right) \right] \cdot \underset{\sim}{I}^{(2)}(-t,\ell)\, d\ell\, dt \tag{A.6}$$

This integral is most conveniently investigated by considering the vector

and scalar potential terms separately. The vector potential term

$$\int_0^\infty \int_\ell \left[\frac{\partial}{\partial t} \left(\frac{\mu}{4\pi} \int_{\ell'} \frac{\underset{\sim}{I}^{(1)}(t-\tau,\ell')}{R(\ell,\ell')} \, d\ell' \right) \right] \cdot \underset{\sim}{I}^{(2)}(-t,\ell) d\ell dt \tag{A.7}$$

when integrated by parts with respect to the time variable results in the sum

$$\int_\ell \left[\frac{\mu}{4\pi} \int_{\ell'} \frac{\underset{\sim}{I}^{(1)}(t-\tau,\ell')d\ell'}{R(\ell,\ell')} \right] \cdot \underset{\sim}{I}^{(2)}(-t,\ell) d\ell \Bigg|_0^\infty$$

$$+ \int_0^\infty \int_\ell \left[\frac{\mu}{4\pi} \int_{\ell'} \frac{\underset{\sim}{I}^{(1)}(t-\tau,\ell')}{R(\ell,\ell')} \, d\ell' \right] \cdot \frac{\partial \underset{\sim}{I}^{(2)}(-t,\ell)}{\partial(-t)} \, d\ell dt \tag{A.8}$$

If the additional requirement that $\underset{\sim}{I}^{(2)}(t,\ell)$ vanish as $t \longrightarrow -\infty$, then only the second integral need be considered. If a new time variable t' is defined as

$$t' = t - \tau \tag{A.9}$$

and substituted into the remaining term of (A.7) the integral

$$\int_0^\infty \int_\ell \frac{\mu}{4\pi} \int_{\ell'} \frac{\underset{\sim}{I}^{(1)}(t',\ell')}{R(\ell,\ell')} \, d\ell' \cdot \frac{\partial \underset{\sim}{I}^{(2)}}{\partial(-t)} (-(t'+\tau)) d\ell dt' \tag{A.10}$$

results. The limits on the t' integration are as before since $t \geq 0$. An interchange of the spatial integrations

$$\int_0^\infty \int_{\ell'} \underset{\sim}{I}^{(1)}(t',\ell') \cdot \left[\frac{\partial}{\partial(-t)} \left(\frac{\mu}{4\pi} \int_\ell \frac{\underset{\sim}{I}^{(2)}(-(t'+\tau),\ell)}{R(\ell,\ell')} \, d\ell \right) \right] d\ell' dt' \tag{A.11}$$

gives an integral that is of the form

$$\left\langle \underset{\sim}{I}^{(1)}, L_1^a \underset{\sim}{I}^{(2)} \right\rangle \tag{A.12}$$

where

$$L_1^a F = \frac{\mu}{4\pi}\left(\frac{\partial}{\partial t}\int \frac{F(t+\tau,\ell)}{R(\ell,\ell')}\right)d\ell \tag{A.13}$$

and L_1^a is recognized as the adjoint operator to the retarded potential integral operator

$$L_1 G = \frac{\mu}{4\pi}\left(\frac{\partial}{\partial t}\int \frac{F(t-\tau)}{R(\ell,\ell')}\right) d\ell \tag{A.14}$$

and, by virtue of (A.7), (A.12), (A.13), and (A.14),

$$\left\langle L_1 \underset{\sim}{I}^{(1)}, \underset{\sim}{I}^{(2)} \right\rangle = \left\langle \underset{\sim}{I}^{(1)}, L_1^a \underset{\sim}{I}^{(2)} \right\rangle \tag{A.15}$$

The negative time domain is adjoint to the positive time domain and is the domain on which L_1^a operates.

The second term of (A.6)

$$\int_0^\infty \int_\ell \hat{U}_\ell \frac{\partial}{\partial \ell}\left[\frac{1}{4\pi\epsilon}\int_{\ell'} \frac{q^{(1)}(t-\tau,\ell')}{R(\ell,\ell')}\, d\ell'\right] \cdot \underset{\sim}{I}^{(2)}(-t,\ell)\, d\ell\, dt \tag{A.16}$$

is integrated by parts with respect to ℓ to get

$$\int_0^\infty \frac{\hat{U}_\ell}{4\pi\epsilon}\int_{\ell'} \frac{q^{(1)}(t-\tau,\ell')}{R(\ell,\ell')}\, d\ell' \cdot \underset{\sim}{I}^{(2)}(-t,\ell)\Big|_0^\ell dt$$

$$- \int_0^\infty \int_\ell \left[\frac{\hat{U}_\ell}{4\pi\epsilon}\int_{\ell'} \frac{q^{(1)}(t-\tau,\ell')}{R(\ell,\ell')}\, d\ell' \cdot \frac{\partial \underset{\sim}{I}^{(2)}}{\partial \ell}(-t,\ell)\right] d\ell\, dt \tag{A.17}$$

The imposition of either the open wire boundary condition

$$I(t,0) = I(t,\ell) = 0$$

or the closed wire periodic boundary conditions

$$\underset{\sim}{I}(t,0) = \underset{\sim}{I}(t,\ell)$$

$$q(t,0) = q(t,\ell)$$

causes the first term of (A.17) to vanish, leaving only the second term for consideration. The current $\underset{\sim}{I}^{(2)}(-t,\ell)$ satisfies the continuity equation,

$$\hat{U}_\ell \cdot \frac{\partial \underset{\sim}{I}^{(2)}}{\partial \ell}(-t,\ell) + \frac{\partial q^{(2)}}{\partial(-t)}(-t,\ell) = 0 \qquad \text{(A.18)}$$

which can be substituted into the remaining term of (A.17) to give

$$+\int_0^\infty \int_\ell \left[\frac{1}{4\pi\epsilon}\left(\int_{\ell'} \frac{q^{(1)}(t-\tau,\ell')}{R(\ell,\ell')}\, d\ell'\right) \frac{\partial q^{(2)}}{\partial(-t)}(-t,\ell)\right] d\ell dt \qquad \text{(A.19)}$$

If (A.19) is integrated by parts with respect to t, the sum

$$-\int_\ell \left(\frac{1}{4\pi\epsilon}\int_{\ell'} \frac{q^{(1)}(t-\tau,\ell')}{R(\ell,\ell')}\, d\ell'\right) q^{(2)}(-t,\ell) d\ell \Bigg|_0^\infty$$

$$+\int_0^\infty \int_\ell \left(\frac{\partial}{\partial t}\left[\frac{1}{4\pi\epsilon}\int_{\ell'} \frac{q^{(1)}(t-\tau,\ell')}{R(\ell,\ell')}\, d\ell'\right]\right) q^{(2)}(-t,\ell) d\ell dt \qquad \text{(A.20)}$$

results. If the additional requirement that $q^{(2)}(t,\ell)$ vanish as $t \longrightarrow -\infty$, then only the second integral contribution need be considered. A new time variable t' will be defined as

$$t' = t - \tau$$

and substituted into the remaining term of (A.20) to get

$$\int_0^\infty \int_\ell \left[\frac{\partial}{\partial t'}\left(\frac{1}{4\pi\epsilon}\int_{\ell'} \frac{q^{(1)}(t',\ell')}{R(\ell,\ell')}\, d\ell'\right) q^{(2)}(-(t'+\tau),\ell)\right] d\ell dt' \qquad \text{(A.21)}$$

The charge $q^{(1)}$ satisfies the continuity equation

$$\frac{\partial q^{(1)}}{\partial t'}(t',\ell') + \hat{U}_{\ell'} \cdot \frac{\partial \underset{\sim}{I}^{(1)}}{\partial \ell'}(t',\ell') = 0 \tag{A.22}$$

allowing (A.21) to be written in terms of $\underset{\sim}{I}^{(1)}$. An interchange of spatial integrations can also be made. The resulting integral is

$$-\int_0^\infty \int_{\ell'} \hat{U}_{\ell'} \cdot \frac{\partial \underset{\sim}{I}^{(1)}(t',\ell')}{\partial \ell'} \left(\frac{1}{4\pi\epsilon} \int_{\ell} \frac{q^{(2)}(-(t'+\tau),\ell)}{R(\ell,\ell')}\, d\ell \right) d\ell'\, dt' \tag{A.23}$$

which can be integrated by parts with respect to ℓ'. Thus

$$-\int_0^\infty \underset{\sim}{I}^{(1)}(t',\ell') \cdot \left(\frac{\hat{U}_{\ell'}}{4\pi\epsilon} \int_{\ell} \frac{q^{(2)}(-(t'+\tau),\ell)}{R(\ell,\ell')}\, d\ell \right) \Bigg|_0^{\ell'} dt'$$

$$+\int_0^\infty \int_{\ell'} \underset{\sim}{I}^{(1)}(t',\ell') \cdot \hat{U}_{\ell'} \frac{\partial}{\partial \ell'} \left(\frac{1}{4\pi\epsilon} \int_{\ell} \frac{q^{(2)}(-(t'+\tau),\ell)}{R(\ell,\ell')} d\ell \right) d\ell'\, dt' \tag{A.24}$$

The first term of (A.24) vanishes whether the wire is open or closed leaving the term

$$\int_0^\infty \int_{\ell'} \underset{\sim}{I}^{(1)}(t',\ell') \cdot \hat{U}_{\ell'} \frac{\partial}{\partial \ell'} \left(\frac{1}{4\pi\epsilon} \int_{\ell} \frac{q^{(2)}(-(t'+\tau),\ell)}{R(\ell,\ell')}\, d\ell \right) d\ell'\, dt' \tag{A.25}$$

which is recognized to be of the form

$$\langle \underset{\sim}{I}^{(1)}, L_2^a q^{(2)} \rangle \tag{A.26}$$

where

$$L_2^a F = \frac{\partial}{\partial \ell'} \frac{1}{4\pi\epsilon} \int_{\ell} \frac{F(t+\tau,\ell)}{R(\ell,\ell')}\, d\ell\, \hat{U}_{\ell'} \tag{A.27}$$

L_2^a is the adjoint operator to

$$L_2 F = \frac{\partial}{\partial \ell} \frac{1}{4\pi\epsilon} \int_{\ell'} \frac{F(t-\tau,\ell')}{R(\ell,\ell')} \, d\ell' \, \hat{U}_\ell \quad , \text{ and,} \tag{A.28}$$

by virtue of the definition of the adjoint operator

$$\langle L_2 \underset{\sim}{q}^{(1)}, \underset{\sim}{I}^{(2)} \rangle = \langle \underset{\sim}{I}^{(1)}, L_2^a q^{(2)} \rangle \tag{A.29}$$

Equation (A.6) can now be written,

$$\langle \underset{\sim}{E}^{(1)}(t,\ell), \underset{\sim}{I}^{(2)}(t,\ell) \rangle = \langle L_1 \underset{\sim}{I}^{(1)}, \underset{\sim}{I}^{(2)} \rangle + \langle L_2 q^{(1)}, \underset{\sim}{I}^{(2)} \rangle \tag{A.30}$$

and by virtue of (A.15) and (A.29), as

$$\langle \underset{\sim}{E}^{(1)}(t,\ell), \underset{\sim}{I}^{(2)}(t,\ell) \rangle = \langle \underset{\sim}{I}^{(1)}, L_1^a \underset{\sim}{I}^{(2)} \rangle + \langle \underset{\sim}{I}^{(1)}, L_2^a \underset{\sim}{q}^{(2)} \rangle \tag{A.31}$$

Finally, since

$$\underset{\sim}{E}^{(2)}(t,\ell') = L_1^a \underset{\sim}{I}^{(2)} + L_2^a q^{(2)} \tag{A.32}$$

the desired reciprocity relationship

$$\langle \underset{\sim}{E}^{(1)}(t,\ell), \underset{\sim}{I}^{(2)}(t,\ell) \rangle = \langle \underset{\sim}{I}^{(1)}(t,\ell'), \underset{\sim}{E}^{2}(t,\ell') \rangle \tag{A.33}$$

is obtained. When this theorem is used to compute far field quantities, the distance $R(\ell,\ell')$ is considered a constant with respect to the ℓ and ℓ' integrations. As a consequence, the requirement that $q^{(2)}(t,\ell) \longrightarrow 0$ as $t \longrightarrow -\infty$ may be relaxed since over the object no net charge accumulates and hence the first integral of (A.20) vanishes.

Appendix B

POINT AND PULSE TESTED GEOMETRY FUNCTIONS

B.1. Point Tested Geometry Functions

The point tested straight wire solution requires the evaluation of integrals of the form $\int \frac{1}{R}\, dz'$. These can be integrated analytically and are given by

$$\int_{(k-.5)\Delta z}^{(k+.5)\Delta z} \frac{dz'}{(i\Delta z - z')^2 + a^2} = \log_e \left(\frac{(i-k+.5)\Delta z + \sqrt{(i-k+.5)^2 \Delta z^2 + a^2}}{(i-k-.5)\Delta z + \sqrt{(i-k-.5)^2 \Delta z^2 + a^2}} \right) \qquad \text{(B.1-1)}$$

when $k > i$, this function suffers a loss of significance, but as noted by Harrison and Aronson[23], the identity

$$\log_e(-x + \sqrt{x^2+a^2}) = \log_e \left[\frac{a}{x + \sqrt{x^2+a^2}} \right] \qquad \text{(B.1-2)}$$

can be used to remove the difficulty. The identity is also useful to show that (B.1-1) is a function of $|i-k|$ only. Let $k > i$, then using (B.1-2), (B.1-1) is rewritten,

$$\log_e \left[\frac{(k-i+.5)\Delta z + \sqrt{(k-i+.5)^2 \Delta z^2 + a^2}}{(k-i-.5)\Delta z + \sqrt{(k-i-.5)^2 \Delta z^2 + a^2}} \right] \qquad \text{(B.1-3)}$$

If, in (B.1-1), the field points are denoted by the index i and the source points by k, when the field and source points are interchanged, (B.1-3) equals (B.1-1). The point tested geometry functions $F(|i-k|)$ are thus functions only of the absolute difference of (i-k) and are given by

$$F(P) = \log_e \left[\frac{(P+.5)\Delta z + \sqrt{(P+.5)^2 \Delta z^2 + a^2}}{(P-.5)\Delta z + \sqrt{(P-.5)^2 \Delta z^2 + a^2}} \right] \qquad P = |i-k| = 0, \ldots, N-1 \qquad \text{(B.1-4)}$$

B.2. The Pulse Tested Geometry Functions

The pulse tested straight wire formulation requires the evaluation of integrals of the form

$$\frac{1}{\Delta z}\int_{(\ell-.5)\Delta z}^{(\ell+.5)\Delta z} dz \int_{(k-.5)\Delta z}^{(k+.5)\Delta z} \frac{dz'}{\sqrt{a^2+(z-z')^2}} \qquad \text{(B.2-1)}$$

The holding of z fixed and the substitution $\eta = (z-z')$ allows (B.2-1) to be written

$$-\frac{1}{\Delta z}\int_{(\ell-.5)\Delta z}^{(\ell+.5)\Delta z} dz \int_{z-(k-.5)\Delta z}^{z-(k+.5)\Delta z} \frac{d\eta}{\sqrt{a^2+\eta^2}} \qquad \text{(B.2-2)}$$

The substitution of $z'' = z - (k-.5)\Delta z$ results in the final integral form

$$\frac{1}{\Delta z}\int_{(\ell-k)\Delta z}^{(\ell-k+1)\Delta z} dz'' \int_{z''-\Delta z}^{z''} \frac{d\eta}{\sqrt{a^2+\eta^2}} \qquad \text{(B.2-3)}$$

Equation (B.2-3) is evaluated using Dwight[25] (200.01) and 625).

$$G(P) = P\log_e\left[\frac{((P+1)\Delta z + \sqrt{a^2+(P+1)^2\Delta z^2})((P-1)\Delta z + \sqrt{a^2+(P-1)^2\Delta z^2})}{\left[P\Delta z + \sqrt{a^2+P^2\Delta z^2}\right]^2}\right]$$

$$+ \log_e\left[\frac{(P+1)\Delta z + \sqrt{a^2+(P+1)^2\Delta z^2}}{(P-1)\Delta z + \sqrt{a^2+(P-1)^2\Delta z^2}}\right]$$

$$+ \frac{1}{\Delta z}\left[2\sqrt{a^2+P^2\Delta z^2} - \sqrt{a^2+(P+1)^2\Delta z^2} - \sqrt{a^2+(P-1)^2\Delta z^2}\right] \qquad \text{(B.2-4)}$$

where $P = |\ell-k|$, $P = 0,1,\ldots,(N-1)$. Loss of significance[23] can occur in the calculation of G(0). Application of (B.1-2) allows G(0) to be written

$$G(0) = 2 \log_e \left[\frac{\Delta z + \sqrt{a^2+\Delta z^2}}{a} \right] - \frac{2\Delta z}{a + \sqrt{a^2+z^2}} \qquad \text{(B.2-5)}$$

The symmetry properties of G(P) were investigated by letting P' = -P, (this is equivalent to interchanging in field and source points) and applying (B.1-2). It can be shown that G(P) = G(-P), and hence (B.2-4) is valid for P = $|\ell-k|$.

An analytical comparison of the point and pulse tested geometry functions was not carried out due to the dissimilarity of functional forms.

B.3. Comparison of Point and Pulse Tested Geometry Functions

Computations have been made for $(\ell/2a) = 74.2$ for N = 20 and 26 of both the point and pulse tested geometry functions. The point tested functions are shown in Tables B-1 and B-2, with the pulse tested functions in Tables B-3 and B-4.

The point and pulse tested geometry functions only differ to any degree for $|i-k| = 0$ where the point tested functions are about 10% larger than the pulse tested functions. The difference can be explained on physical grounds. The geometry functions F(0) and G(0) have been shown to be proportional to the input resistance of the lossless wire and a measure of the self-reaction of a subsection on itself. In the point tested solution the current over an entire subsection has as its source a unit voltage applied across a small distance in the middle of a subsection (this is referred to as a slice generator). This induces a highly localized field which

opposes the slice generator voltage resulting in an input resistance which is higher than when the voltage source is applied across an entire subsection which is the case in the pulse tested solutions. The notion of the pulse tested solution as a local averaging operation with the average of the current being less than the value of the current at the midpoint of the subsection leads to a similar conclusion. A comparison of the geometry functions is shown in Figure B.3-1 for N = 26, $\ell/2a = 74.2$.

POINT TESTED
GEOMETRY FUNCTIONS

N = 20

1	4.0445	2	1.0829	3	0.5095	4	0.3361	5	0.2511
6	0.2005	7	0.1670	8	0.1430	9	0.1251	10	0.112
11	0.1000	12	0.0909	13	0.0833	14	0.0769	15	0.0714
16	0.0666	17	0.0625	18	0.0588	19	0.0555	20	0.0526

Table B-1

N = 26

1	3.5423	2	1.0726	3	0.5086	4	0.3358	5	0.2510
6	0.2005	7	0.1669	8	0.1430	9	0.1251	10	0.1112
11	0.1000	12	0.0909	13	0.0833	14	0.0769	15	0.0714
16	0.0666	17	0.0625	18	0.0588	19	0.0555	20	0.0526
21	0.0500	22	0.0476	23	0.0454	24	0.0434	25	0.0416
26	0.0400								

Table B-2

PULSE TESTED
GEOMETRY FUNCTIONS

N = 20

1	3.6551	2	1.2583	3	0.5217	4	0.3394	5	0.2525
6	0.2012	7	0.1673	8	0.1433	9	0.1253	10	0.113
11	0.1001	12	0.0910	13	0.0834	14	0.0769	15	0.0714
16	0.0667	17	0.0625	18	0.0588	19	0.0555	20	0.0526

Table B-3

N = 26

1	3.2050	2	1.2225	3	0.5207	4	0.3391	5	0.2524
6	0.2012	7	0.1673	8	0.1432	9	0.1252	10	0.1113
11	0.1001	12	0.0910	13	0.0834	14	0.0769	15	0.0714
16	0.0667	17	0.0625	18	0.0588	19	0.0535	20	0.0526
21	0.0500	22	0.0476	23	0.0454	24	0.0435	25	0.0416
26	0.0400								

Table B-4

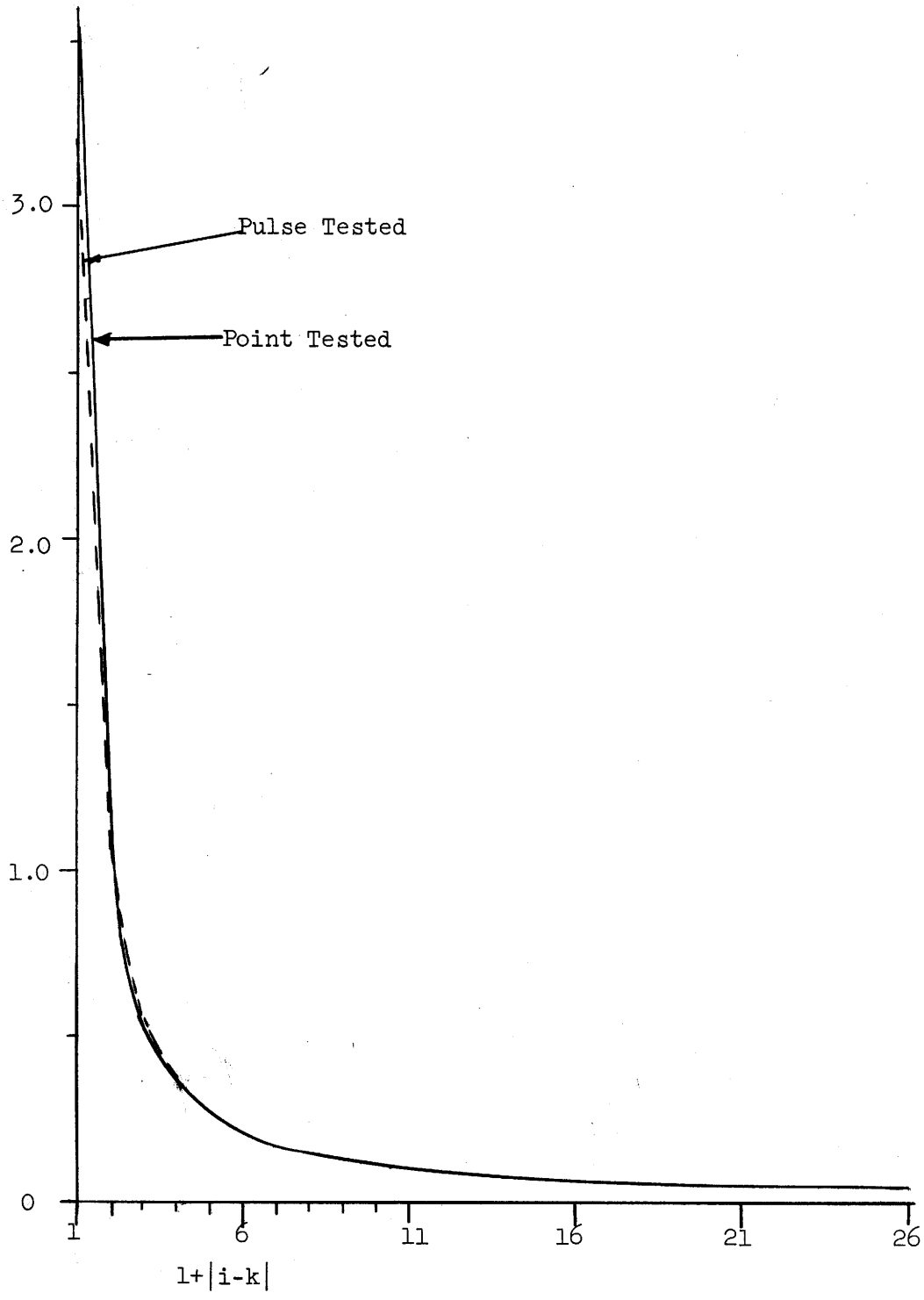

Comparison of Point and Pulse Tested
Geometry Functions ($\ell/2a = 74.2$)
N = 26

Figure B.3-1

Appendix C

PROGRAMMING INSTRUCTIONS AND PROGRAMS

A sample program will be examined in detail in this Appendix. Since the programs are largely similar, and differ only in the subroutines specialized to the function of the object (antenna or scatterer) and type (straight wire, loop, etc.), only the main program and subroutines for the pulse tested straight wire scatterer will be examined in detail. The main program is shown in Figure C.1.

Between (1)* and (2), the variables are declared and physical qualities are read in. The following variables are used:

B(J,K)	current coefficient
A(J,K)	vector potential
POT(J,K)	scalar potential
G(J,K)	charge coefficient
VA(J,K)	the tangential component of the incident field
RL(K)	resistive load
F(K)	geometry function
TI(J)	an array to store the normalized time values
ER(J,M)	the array which stores the normalized far fields
R THETA(M)	array which stores the angles for far field computation

The J subscript is the time iterate, K the space iterate on the wire, and M the far field angle iterate.

The following integer quantities are read in:

N	number of subsections
MT	number of transit times to be examined
KTH	number of far field angles $\leq$ 10

*Circled numbers refer to the source quantities found in Figure C.1.

```
C     ****************************************************************
C
C
C     THIS PROGRAM CALCULATES THE INDUCED CURRENT ON A STRAIGHT WIRE
C     SCATTERER FOR AN INCIDENT PLANE WAVE UNIT STEP ELECTRIC FIELD
C     WHOSE INCIDENCE ANGLE IS ARBITRARY.
C     ALSO CALCULATED IS THE TIME DEPENDENT NORMALIZED FOR FIELD FOR A
C     DISCRETE NUMBER OF ANGLES.    KTH- NUMBER OF FAR FIELD ANGLES  )11
C
C     N-NUMBER OF WIRE SUBSECTIONS  MT-NUMBER OF TRANSIT TIMES
C     AL-ANTENNA LENGTH IN METERS D-ANTENNA DIAMETER IN METERS
C     THETA - INCIDENCE ANGLE      DRTH-SPACING OF FAR FIELD ANGLES
C     UM-RELATIVE PERMEABILITY   RTHETA-REFLECTION ANGLE
C     EP-RELATIVE PERMITTIVITY      UM-RELATIVE PERMEABILITY
C     RTHETA-ARRAY CONTAINING THE FAR FIELD ANGLES
C
C     ****************************************************************
      REAL*4 B(52,26),A(52,26),POT(52,26),G(52,26),VA(52,26),F(26),  <-- (1)
     1TI(500),ER(50,1C1,RTHETA(10),RL(26)
      COMMON UP(4,EPI4,A,MF,NMM,DT,DZ,C
      READ 101,N,MT,KTH,AL,OMEGA,EP,UM,PL,DRTH
  101 FORMAT(3I5,6F10.5)
      NMM=N-1
      READ 104,(RL(K),K=1,NMM)
  104 FORMAT(10E8.1)                                          <-- (2)
      MF=N*MT
      D=AL/OMEGA
      DZ=AL/N
      UUM=UP
      EPP=EP
      UM=UM*1.25664E-6
      EP=EP*8.85525E-12
      LP=PL/DZ
      R=D/2
      C=SQRT(1/(EP*UM))
      DT=DZ/C
      UP(4=UM/(4.*3.14159265)
      EPI4=1/(4.*3.141593*EP)
      CALL GEO*(F,R)
      DO 16002 I=1,2
      GO TO 1,THETA
 1001 RL(M)=F(1..1)                                           <-- (3)
      PRINT103
  103 FORMAT(1H1,1X,'UNIT STEP PLANE WAVE EXCITATION AT ARBITRARY ANGLES
     1OF A STRAIGHT WIRE SCATTERER WITH RESISTIVE BOUNDARY CONDITIONS',/
     2///)
      PRINT 102,AL,D,OMEGA,THETA,N,MF,KTH,EPP,UUM

  102 FORMAT(1H ,'DIPOLE LENGTH (METERS) =',F9.3,'  DIPOLE DIAMETER (MET
     1ERS) =',F9.3,'  LENGTH TO DIAM. RATIO =',F9.5,//
     2,1H ,'INCIDENCE ANGLE (DEG) =',F7.3,'  NUMBER OF SUBSECTIONS =',I3
     3,'  NUMBER OF TRANSIT TIMES(L/C) =',I3,
     3'  NUMBER OF FAR FIELD ANGLES =',I3,
     4///,1H ,20X,'MEDIUM CONSTITUTIVE PARAMETERS',///,1H ,'RELATIVE DIEL
     5ECTRIC CONSTANT =',F8.5,'  RELATIVE PERMEABILITY =',F8.5,////)
      THETA=THETA*3.14159265/180.
      PRINT 602
  602 FORMAT(1H ,50X,'GEOMETRY PARAMETERS F(K)',//)
      PRINT 500,(I,F(I),I=1,N)
  500 FORMAT(5(1H ,I5,6X,F10.8))
      PRINT 502
  502 FORMAT(1H ,////)
      PRINT 501,(I,RL(I),I=1,NMM)
  501 FORMAT(1H ,50X,'RESISTIVE LOADS (OHMS/METER)',//,5(1H ,'SUBSECTION
     1   LOAD     '),//,5(1H ,I5,E17.2))
      PRINT 503
  503 FORMAT(1H1)                                             <-- (4)
```

```
C***************PUT DATA IS IN MACHINE AND PARAMETERS HAVE BEEN CALCULATE   <-- (4)
      KOUNT=1
  500 CONTINUE
      IF(KOUNT-MF)2,2,5
C***************STATEMENT 5 SIGNIFIES THAT TIME ITERATION IS COMPLETE
    2 CONTINUE
      TI(KOUNT)=(KOUNT-1.)/NMM
      IF(KOUNT-2*N-1) 3,4,555
C***************BRANCH 3 SIGNIFIES INITIAL ARRAYS BEING FILLED
    3 CONTINUE
      CALL VOLTI(KOUNT,VA,THETA,KOUNT)
      CALL CURRI(RL,F,VA,B,A,POT,KOUNT)
      CALL CGPOT(F,P,G,POT,KOUNT)
      KOUNT=KOUNT+1
      GO TO 500
C***************BRANCH 4 SIGNIFIES KOUNT=2*N+1 AND THE FIRST N NORMALIZED   <-- (5)
C***************FAR FIELD COMPONENTS MUST BE CALCULATED.
    4 CONTINUE
      DO 301 J=1,N
      CALL RFRLD(R,J,RTHETA,ER,MPF,KTH,DRTH,J,THETA)
  301 CONTINUE                                                <-- (6)
  555 CONTINUE
      AK=KOUNT-1
      P=AK/(2*N)
      KP=P
      AK=KP
      IF(AK-P)6,7,6
    7 CALL OTPT(2*N,1,A,B,G,POT,VA,KOUNT,TI)                  <-- (7)
    6 CONTINUE
      CALL SHIFT(B,G,A,POT,VA)
      LZ=2*N
      CALL VOLTI(Z,VA,THETA,KOUNT)
      CALL CURR(RL,F,VA,B,A,POT,LZ)
      CALL CGPOT(F,P,G,POT,LZ)
      CALL RFRLD(B,N,RTHETA,ER,MPF,KTH,DRTH,KOUNT-N,THETA)
      KOUNT=KOUNT+1
      GO TO 30(                                               <-- (8)
    1 CONTINUE
      MA=MT/2.
      IF(MT-2.*MA) 222,223,222
  223 CALL OTPT(2*N,1,A,B,G,POT,VA,KOUNT,TI)
      GO TO 224
  222 CALL OTPT(2*N,N+1,A,B,G,POT,VA,KOUNT,TI)
  224 CONTINUE
      LZ=MF-N+1
      DO10I=LZ,MF
      J=2*N-(MF-I)
   10 CALL RFRLD(C,J,RTHETA,ER,MPF,KTH,DRTH,I,THETA)          <-- (9)
      AR=MPF/1..
      EPP=AR
      AD=EPP
      IF(AD.EQ.AR) GO TO 304
      EPP=EPP+1
  304 CONTINUE
      DO 900 J=1,KTH
  900 RTHETA(J)=RTHETA(J)/0.017453
      PRINT 503
      DO 308 I=1,EPP
      PPP=10*I
      PPE=10*(I-1)+1
      IF(I.LO.EPP) PPE=PPP
      PRINT 804
  804 FORMAT(1H ,///,1H ,50X,'NORMALIZED FAR FIELD')
      PRINT307,(I,(K),K=PPE,PPP)
  307 FORMAT(1H ,///,1H ,6HTIME =,10(2X,F7.2,2X),//)
      DO 406 J=1,KTH
      PRINT 801,RTHETA(J),(ER(M,J),M=PPE,PPP)
  801 FORMAT(1H ,F6.2,10(1X,E1..3))
  406 CONTINUE
  308 CONTINUE
      DO 1002 J=1,KTH
      PUNCH 1003,RTHETA(J)
 1003 FORMAT(F10.3)
      PUNCH 1003,(I,(M),ER(M,J),M=1,MPF)
 1003 FORMAT(8(E10.3))
 1002 CONTINUE
 1002 CONTINUE                                                <-- (10)
      STOP
      END
```

Pulse Tested Straight Wire Scatterer

Main Program

Figure C.1

and then the following floating point variables are read in:

AL	straight wire length
OMEGA	ratio of length to diameter
EP	relative permittivity of the surrounding medium
UM	relative permeability of the surrounding medium
PL	the driving point if wire is an antenna
DRTH	increment in far field angles
RL(K)	the resistive and/or generator loads

Between (2) and (3) quantities are calculated which are derived from the basic quantities just read in. Some additional data are read in as well. The quantities calculated are:

MF	number of time iterations to be performed
R,D	the antenna radius and diameter
DZ	the subsection length
LP	the driven subsection (if wire is antenna)
C	speed of light of surrounding medium
DT	transit time of subsection and basic time iterate

The geometry functions are calculated from the statement CALL GEOM (F,R), and returned to the main program for printing later. The subroutine GEOM is shown as C-2.a.

Between (3) and (4), the program is identified and the quantities just calculated are outputted by the printer.

Before the remainder of the program is described, the general philosophy of the program will be discussed. In general, the retarded potential formulation requires at most the N previous currents and charges. The far field evaluation needs at most N current coefficients previous to the time J and

```
      SUBROUTINE GEOM (F,R)
      REAL*4 F(20)
      COMMON UPI4,EPI4,N,MF,NMM,DT,DZ,C
      F(1)=2.*ALOG((DZ+SQRT(R*R+DZ*DZ))/R)-2.*DZ/(R+SQRT(R*R+DZ*DZ))
      DO 1 K=2,N
      PP1=K*DZ+SQRT(R*R+(K*DZ)**2)
      PM1=(K-2)*DZ+SQRT(R*R+((K-2)*DZ)**2)
      PP=(K-1)*DZ+SQRT(R*R+((K-1)*DZ)**2)
      F(K)=(K-1)*ALOG(PP1*PM1/(PP**2))
      F(K)=F(K)+ALOG(PP1/PM1)
      F(K)=F(K)+(2.*PP-PP1-PM1)/DZ
    1 CONTINUE
      RETURN
      END
```

C.2-a

```
      SUBROUTINE VOLT(J,VA,THETA,JJ)
      REAL*4 VA(52,26)
      COMMON UPI4,EPI4,N,MF,NMM,DT,DZ,C
      SR=SIN(THETA)
      CR=COS(THETA)
      IF(CR) 5,4,4
    4 DO 1 K=1,NMM
      MTT=(K+.5)*CR
      MF=(K-.5)*CR
      IF((JJ-MTT).GT.MF) GOTO 21
      IF((MTT-MF-1)) 2,3,3
    2 TK1=JJ-K*CR
      VA(J,K)=SR*EXCT(TK1)
      IF((.5-TK1).GE.0.0) VA(J,K)=VA(J,K)/2.
      GO TO 1
    3 DZC=MTT/CR-K+.5
      DCC=1-DZC
      TK1=JJ-((K-.5)+DZC/2.)*CR
      TK2=JJ-((K+.5)-DCC/2.)*CR
      VA(J,K)=SR*(DZC*EXCT(TK1)+DCC*EXCT(TK2))
      IF((.5-TK1).GE.0.0) VA(J,K)=VA(J,K)/2.
    1 CONTINUE
      GO TO 21
    5 DO 7 K=1,NMM
      KK=K-N
      MTT=(KK-.5)*CR
      MF=(KK+.5)*CR
      IF((JJ-MTT).GT.MF) GO TO 21
      IF(MTT-MF-1) 9,8,8
    9 TK1=JJ-KK*CR
      VA(J,K)=SR*EXCT(TK1)
      IF((.5-TK1).GE.0.0) VA(J,K)=VA(J,K)/2.
      GO TO 7
    8 DZC=-(MTT/CR-KK-.5)
      DCC=1-DZC
      TK1=JJ-((KK+.5)-DZC/2.)*CR
      TK2=JJ-((KK-.5)+DCC/2.)*CR
      VA(J,K)=SR*(DZC*EXCT(TK1)+DCC*EXCT(TK2))
      IF((.5-TK1).GE.0.0 ) VA(J,K)=VA(J,K)/2.
    7 CONTINUE
   21 RETURN
      END
```

C.2-b

```
      FUNCTION EXCT(X)
      IF(X.LT.0.0) GO TO 1
      EXCT=1.0
      GO TO 2
    1 EXCT=0.0
    2 CONTINUE
      RETURN
      END
```

C.2-c

```
      SUBROUTINE CURR   (RL,F,VA,B,A,POT,J)
      REAL*4 RL(26),F(26),VA(52,26),B(52,26),A(52,26),POT(52,26)
      COMMON UPI4,EPI4,N,MF,NMM,DT,DZ,C
      DO1K=1,NMM
      IF(J.EQ.1) GO TO 2
      SUM1=0.
      SUM2=0.
      LK=K-1
      IF(LK.EQ.0)GO TO 16
      DO205 M=1,LK
      IF(J-M)16,16,18
   18 CONTINUE
      SUM1=SUM1+F(M+1)*B(J-M,K-M)
  205 CONTINUE
   16 CONTINUE
      LK=K+1
      IF(LK.EQ.N)GO TO 19
      DO206M=LK,NMM
      IF(J-M+K)19,19,21
   21 CONTINUE
      SUM2=SUM2+B(J-M+K,M)*F(M+1-K)
  206 CONTINUE
   19 CONTINUE
      DPOT=(POT(J-1,K)-POT(J-1,K+1))/DZ
      B(J,K)=(VA(J,K)-B(J-1,K)*RL(K)/2.+DPOT+(A(J-1,K)-(SUM1+SUM2)*UPI
     1/DT)/(RL(K)/2.+UPI4*F(1)/DT)
      A(J,K)=(B(J,K)*F(1)+SUM1+SUM2)*UPI4
      GO TO 1
    2 B(J,K)=VA(J,K)/(RL(K)/2.+UPI4*F(1)/DT)
      A(J,K)=B(J,K)*F(1)*UPI4
    1 CONTINUE
      RETURN
      END
```

C-2-d

```
      SUBROUTINE CGPOT(F,B,G,POT,J)
      REAL*4 F(26),B(52,26),G(52,26),POT(52,26)
      COMMON UPI4,EPI4,N,MF,NMM,DT,DZ,C
      DO1K=1,N
      IF(J.EQ.1) GO TO 2
  708 IF(K-1)23,22,23
   22 G(J,K)=-B(J,1)/C+G(J-1,1)
      GO TO 1
   23 IF(K-N)25,24,25
   24 G(J,K)=B(J,N-1)/C+G(J-1,N)
      GO TO 1
   25 G(J,K)=G(J-1,K)+(B(J,K-1)-B(J,K))/C
      GO TO 1
    2 CONTINUE
      IF(K-1)9,8,9
    8 G(1,1)=-B(1,1)/C
      GO TO 203
    9 IF(K-N)11,10,11
   10 G(1,N)=B(1,N-1)/C
      GO TO 203
   11 G(1,K)=(B(1,K-1)-B(1,K))/C
  203 CONTINUE
      POT(J,K)=EPI4*F(1)*G(J,K)
    1 CONTINUE
      IF(J.EQ.1) GO TO 3
      DO 208K=1,N
      SUM2=0.
      SUM1=0.
      LK=K-1
      IF(LK.EQ.0)GO TO 26
      DO209M=1,LK
      IF(J-M)26,26,28
   28 CONTINUE
      SUM1=SUM1+F(M+1)*G(J-M,K-M)
  209 CONTINUE
   26 CONTINUE
      LK=K+1
      IF(LK.EQ.N+1)GO TO 29
      DO210M=LK,N
      IF(J-M+K)29,29,31
   31 CONTINUE
      SUM2=SUM2+F(M+1-K)*G(J-M+K,M)
  210 CONTINUE
   29 CONTINUE
      POT(J,K)=EPI4*(F(1)*G(J,K)+SUM1+SUM2)
  208 CONTINUE
    3 RETURN
      END
```

C.2-e

Pulse Tested Straight Wire Subroutines

Figure C.2

N currents after, making a total of 2N coefficients which must be known before far field evaluations must be made. In view of this, at any time only 2N × N currents and charges must be stored together with at least 2N vector and scalar potentials. The program actually stores 2N × N vector and scalar potentials for ease in outputting the quantities. The program meets these requirements by shifting coefficients in their arrays and outputting desired quantities every 2N time iterates. If MF is not an integer multiple of 2N, provision is made at the end of the program to output the remaining quantities in storage.

Between (4) and (5) the first 2N × N currents, charges and potentials are calculated. The calculation begins with

KOUNT = 1

This quantity is incremented by unity until it exceeds MF, when the program goes into its exit routine. The normalized time is calculated and stored in TI(J).

If KOUNT < 2N+1, the program calculates the first 2N currents, charges and potentials. The calculation begins with the statement

CALL VOLT (KOUNT, VA, THETA, KOUNT)

This subroutine calculates the excitation (in this case the pulse tested tangential electric field for the straight wire). This subroutine is found on Figure C-2 as (C-2b) along with a function statement used in VOLT and termed EXCT-(C-2c). EXCT is a functional description of the incident electric field as a function of time, and in this case describes a unit step function. The call to VOLT returns the excitation in the array VA, which is used in the next subroutine. The statement

CALL CURR (RL, F, VA, B, A, POT, KOUNT)

causes the arrays RL, F, VA, B, A, POT to be available to this subroutine found as (C-2d). In this subroutine the current is found in terms of the retarded integrals described in Chapter 3. The most recent coefficients are returned as B(KOUNT,K) K = 1,N-1.* The next call statement

CALL CG POT(F, B, G, POT, KOUNT)

results in the set of charge coefficients G(KOUNT,K) K = 1,N to be found, and from these charges and those found previously, the set of potentials POT(KOUNT,K) K = 1,N is also found and returned along with the G's to the main program. This program is labeled C-2d. The time iterate KOUNT is advanced by unity and tested again. When KOUNT = 2N+1, the first far field quantities ER(J,M), J = 1,N; M = 1,KTH are computed by the call

CALL RFRLD(B, J, RTHETA, ER, MPF, KTH, DRTH, J, THETA)

This subroutine is labeled (C-3a). The program header describes the purpose and method of computation performed by the subroutine.

Between (5) and (6), the program checks whether KOUNT-1 is a multiple of 2N. If it is, then the subroutine OTPT is called to output the data in the arrays VA, B, G, A, POT. In the version labeled (C-3b) only VA, B and G are outputted. The call is

CALL OTPT(2*N, 1, A, B, G, POT, VA, KOUNT, TI) .

The subroutine PROUT called in OTPT is a standard array format to be used for each outputted array variable. The subroutine is shown in (C-3c). If (a), KOUNT-1 is not a multiple of 2N, or (b) the outputting is completed, the program proceeds to the steps between (7) and (8). The call

*The notation K = 1, N-1 implies K takes all integer values from 1 up to and including N-1.

```
      SUBROUTINE RFRLD (B,JJ,RTHETA,ER,MPF,KTH,DRTH,J,THETA)
C*****************************************************************************
C
C
C     THIS PROGRAM COMPUTES THE NORMALIZED FAR FIELD OF A LINEAR DIPOLE FOR A
C     GIVEN REFLECTION ANGLE. THE METHOD IS EQUIVALENT TO PULSE MATCHING IN THE
C     TIME AND SPACE DOMAINS. THE BASIS SPACE FOR THE CURRENT EXPANSION IS A SET
C     OF TWO DIMENSIONAL PULSE FUNCTIONS. THE PARTIAL DERIVATIVES IN TIME ARE
C     APPROXIMATED BY THE DIFFERENCE OPERATOR. BECAUSE OF THE BASIS SPACE FOR
C     THE CURRENT, THE INTEGRAL OPERATIONS ARE REPLACED BY FINITE SUMS WHICH
C     TAKE INTO ACCOUNT THE TIME DELAY OPERATOR WHICH IS A FUNCTION OF THE
C     REFLECTION ANGLE.
C
C**********NOTE. KTH MUST NOT BE LARGER THAN 10.**********
C
C
C
C*****************************************************************************
      REAL*4 B(52,26),ER(500,10),RTHETA(10)
      COMMON UPI4,EPI4,N,MF,NMM,DT,DZ,C
      IF(KTH.GT.10) KTH=10
      CGR=COS(THETA)
      DO 4KN=1,KTH
      RTHETA(KN)=KN*DRTH*3.14159265/180.0
      CR=COS(RTHETA(KN))
      SR=SIN(RTHETA(KN))
      IF(CR.LT.0.0) GO TO 22
      SUM1=0.
      DO 1KK=1,NMM
      MTT=(KK+.5)*CR
      MT=(KK-.5)*CR
      IF((JJ-MTT).GT.MF) GO TO 22
      IF(MTT-MT-1) 2,3,3
C     BRANCH 2 INDICATES ENTIRE SUBSECTION IS EXCITED
    2 CONTINUE
      KT=KK*CR
      IF(CGR) 20,21,21
   20 KT=JJ+KT
      K=N-KK
      GO TO 23
   21 KT=JJ-KT
      K=KK
   23 CONTINUE
      IF(KT-1) 1,6,7
    6 SUM1=SUM1+B(KT,K)*2.
      GO TO 1
    7 SUM1=SUM1+B(KT,K)-B(KT-1,K)
      GO TO 1
    3 DZC=MTT/CR-KK+.5
      DCC=1-DZC
      K1=((KK-.5)+DZC/2.)*CR
      K2=((KK+.5)-DCC/2.)*CR
      IF(CGR) 24,25,25
   24 K1=JJ+K1
      K2=JJ+K2
      K=N-KK
      GO TO 26
   25 K1=JJ-K1
      K2=JJ-K2
      K=KK
   26 CONTINUE
      IF(K1-1) 1,12,13
   12 SUM1=SUM1+DZC*B(K1,K)*2.
      GO TO 8
   13 SUM1=SUM1+DZC*(B(K1,K)-B(K1-1,K))
    8 CONTINUE
      IF(K2-1) 1,9,10
    9 SUM1=SUM1+DCC*B(K2,K)*2.
      GO TO 1
   10 SUM1=SUM1+DCC*(B(K2,K)-B(K2-1,K))
    1 CONTINUE
      ER(J,KN)=-SR*SUM1*UPI4/DT
   22 MPF=J
    4 CONTINUE
      RETURN
      END
```

C.3-a

```
      SUBROUTINE DIPT(KF,KI,A,B,G,POT,VA,KOUNT,TI)
      REAL*4A(52,26),B(52,26),G(52,26),A(52,26),POT(52,26),VA(52,26) ,TI(500)
      COMMON UPI4,EPI4,N,MF,NMM,DT,DZ,C
      PF=(KF-KI)/10.
      MPF=PF
      PPF=MPF
      IF(PPF.EQ.PF) GO TO 1
      MPF=MPF+1
    1 CONTINUE
      DO302I=1,MPF
      MPE=10*I+KI-1
      MFE=10*(+KOUNT-1-KF+KI-1
      MPI=10*(I-1)+KI
      MFI=10*(I-1)+KOUNT-KF+KI-1
      IF(I.EQ.MPF) GO TO 11
      GO TO 12
   11 CONTINUE
      MPE=KF
      MFE=KOUNT-1
   12 CONTINUE
      PRINT 411
  411 FORMAT(1H ,50X,23HINCIDENT ELECTRIC FIELD)
      CALL PROUT(TI,VA,NMM,MFI,MFE,MPE,MPI)
      PRINT 311
  311 FORMAT(1H ,50X,20HCURRENT COEFFICIENTS)
      CALL PROUT(TI, B,NMM,MFI,MFE,MPE,MPI)
      PRINT 312
  312 FORMAT(1H ,50X,19HCHARGE COEFFICIENTS)
      CALL PROUT(TI, G,N  ,MFI,MFE,MPE,MPI)
  302 CONTINUE
      RETURN
      END
```

C.3-b

```
      SUBROUTINE PROUT(TI,X,KN,MFI,MFE,MPE,MPI)
      REAL*4 X(52,26),TI(500)
      PRINT307,(TI(K),K=MFI,MFE)
      DO406J=1,KN
      PRINT301,J,(X(P,J),P=MPI,MPE)
  406 CONTINUE
      PRINT 305
  307 FORMAT(1H ,///,1H ,6HTIME =,10(2X,F7.2,2X),//)
  305 FORMAT(1H ,//////)
  301 FORMAT(1H ,2X,I3,1X,10(1X,E10.3))
      RETURN
      END
```

C.3-c

```
      SUBROUTINE SHIFT(B,G,A,POT,VA)
      REAL*4B(52,26),G(52,26),A(52,26),POT(52,26),VA(52,26)
      COMMON UPI4,EPI4,N,MF,NMM,DT,DZ,C
      LZ=2*N-1
      DO1 K=1,NMM
      DO2J=1,LZ
      B(J,K)=B(J+1,K)
      A(J,K)=A(J+1,K)
      VA(J,K)=VA(J+1,K)
    2 CONTINUE
      B(2*N,K)=0.0
      A(2*N,K)=0.0
      VA(2*N,K)=0.0
    1 CONTINUE
      DO3K=1,N
      DO4J=1,LZ
      G(J,K)=G(J+1,K)
      POT(J,K)=POT(J+1,K)
    4 CONTINUE
      G(2*N,K)=0.0
      POT(2*N,K)=0.0
    3 CONTINUE
      RETURN
      END
```

C.3.d

Straight Wire Subroutines

Figure C.3

statement

```
CALL SHIFT(B, G, A, POT, VA).
```

causes all the elements of the arguments to be shifted one place back in their storage locations and the most recent location to be initialized to zero. As an example, the following occurs:

$$B(J,K) = B(J+1,K)$$

for J = 1,(2*N-1); K = 1,N-1. The most recent location B(2*N,K) is set to zero preparatory to the new value of B which will be stored in that location by CURR. Subroutine SHIFT is shown as C-3d. The subroutines VA, CURR, CGPOT, RFRLD operate as previously described, each time inserting their results in the (2N,K), K = 1,N or N-1 locations in the proper arrays.

Branching to statement 1 signifies that the program has begun its exit procedures. Between (8) and (9) the last far field quantitites are calculated and the arrays are outputted by OTPT so that no data remain which have not been outputted. Between (9) and (10), the far field quantities are arranged for convenient printing and are printed out as a function of angle and time. In addition, the time and far field are punched out on cards by the instructions

```
      DO 1002 J = 1,KTH
      PUNCH 1003, (TI(M), ER(M,J), M = 1,MPF)
1003  FORMAT (8(E10.3))
1002  CONTINUE
```

The program stops and exits.

Note that all routines on Figure C-3 are common to all straight wire problems. SHIFT, OTPT and PROUT are common to all time domain moment problems solved using the algorithms of this paper.

REFERENCES

1. R. F. Harrington, Field Computation by Moment Methods, New York, The Macmillan Company, 1968, Chapter 4.

2. C. Manneback, "Radiation from Transmission Lines", AIEE Journal, V. 42 (1923), pp. 95-105.

3. H. J. Schmitt, "Transients in Cylindrical Antennas", Technical Report No. 296, Cruft Laboratory, Harvard University, 1959.

4. H. J. Schmitt, "Transients in Cylindrical Antennae", IEE Monograph No. 377E, April 1960.

5. R. W. P. King, H. J. Schmitt, "The Transient Response of Linear Antennas and Loops", IRE Trans., Vol. AP-9, (1962).

6. T. T. Wu, R. W. P. King, "Transient Response of Linear Antennas Driven from a Coaxial Line", IEEE Trans., Vol. AP-11, (1963).

7. C. W. Harrison, Jr., C. S. Williams, Jr., "Transients in Wide-Angle Connical Antennas", IEE Trans., Vol. AP-13, (1965).

8. H. J. Schmitt, C. W. Harrison, Jr., C. S. Williams, Jr., "Calculated and Experimental Response of Thin Cylindrical Antennas to Pulse Excitation", IEEE Trans., Vol. AP-14, (1966).

9. E. A. Lewis, "Radiation from Idealized Shock Excitation Currents in a Straight Conductor Rising from a Perfect Earth at an Arbitrary Angle", Electromagnetic Wave Propagation. Edited by M. Diserant and J. L. Michiels, New York, Academic Press (1960).

10. D. M. Bolle, I. Jacobs, "The Radiation Pattern of Long Thin Antennas for Short-Pulse Excitation", IRE Trans., Vol. AP-9 (1962), pp. 787-788.

11. A. K. Bulgakov, N. I. Busev, V. M. Rysakov, "Transients in Linear Antennas, Izvestiya VUZ Radiofizeka, Vol. 8, No. 6, pp. 1187-1195 (1965).

12. T. T. Wu, "Transient Response of a Dipole Antenna", J. Math. Physics, Vol. 2, No. 6 (1961).

13. W. J. Welch, "Reciprocity Theorems for Electromagnetic Fields whose Time Dependence is Arbitrary", IEEE Trans., AP-8, January, 1960.

14. B. Ru-Shao Cheo, "A Reciprocity Theorem for Electromagnetic Fields with General Time Dependence", IEEE Trans., AP-13, March, 1965.

15. B. A. Friedman, Principles and Techniques of Applied Mathematics, John Wiley and Sons, 1960, Chapter 1.

16. R. F. Harrington, Field Computation by Moment Methods, New York, The Macmillan Company, 1968, Chapter 1, Section 3.

17. F. B. Hildebrand, Methods of Applied Mathematics, Prentice-Hall, Second Edition, Chapter 3, Section 3.18.

18. L. Kantorovich and G. Akilov, Functional Analysis in Normed Spaces, translated by D. E. Brown, Pergamon Press, Oxford, 1964, pp. 586-587.

19. E. P. Sayre, "Transient Response of Conducting Straight Wire Scatterers and Antennas", Technical Memorandum 68-2, Electrical Engineering Department, Syracuse University, Syracuse, New York.

20. T. T. Wu, "Transient Response of a Dipole Antenna", J. Math. Physics, 1961, Figures 2 and 3.

21. V. H. Rumsey, "Reaction Concept in Electromagnetic Theory", Physical Review, Vol. 94, No. 6.

22. C. R. Wylie, Jr., Advanced Engineering Mechanics, McGraw-Hill Book Company, New York, New York, 1951.

23. C. W. Harrison, E. A. Aronson, "On the Evaluation of Potential Integrals Occurring in Antenna Theory Using Digital Computers", IEEE Trans., PGAP-15, No. 4, July 1967, p. 576.

24. R. F. Harrington, Time Harmonic Fields, McGraw Hill Book Company, New York, New York, 1961 Appendix A.

25. H. B. Dwight, Tables of Integrals and Other Mathematical Data, The Macmillan Company, New York, 1947.

26. S. Hong, S. L. Borison and D. P. Ford, "Short Pulse Scattering by a Long Wire", IEEE Trans., AP-16, May 1968.

27. P. Ya. Ufimtsev, "Diffraction of Plane Electromagnetic Waves by a Thin Cylindrical Conductor", Radio Engrg. Electron Phys., Vol. 7, 1962.

28. L. Peters, Jr., "End-fire Echo Area of Long Thin Bodies", IRE Trans., AP-6, January 1958.

29. R. J. Palcianskas, R. E. Beam, "Transient Fields of Cylindrical Antennas", Symposium Record, 1968 PGAP International Antennas and Propagation Symposium, paper V-2.

30. L. C. Shen, T. T. Wu, R. W. P. King, "A Simple Formula of Current in Dipole Antennas", IEEE Trans., AP-16, September 1968.